博士論文

Organic Structure-Directing Agent-Free Synthesis of Zeolites through a Seed-Directed Approach

（種結晶添加法による有機構造規定剤を用いないゼオライト合成）

Kenta IYOKI

伊與木健太

Department of Chemical System Engineering,
The University of Tokyo

A Dissertation Submitted in Partial Fulfillment of

the Requirements for the Degree of Doctor of Philosophy

Dissertation Committee:

Tatsuya Okubo, Professor (Supervisor)
Department of Chemical System Engineering
The University of Tokyo

Kazunari Domen, Professor
Department of Chemical System Engineering
The University of Tokyo

Atsuo Yamada, Professor
Department of Chemical System Engineering
The University of Tokyo

Ryuji Kikuchi, Associate Professor
Department of Chemical System Engineering
The University of Tokyo

Masaru Ogura, Associate Professor
Department of Applied Chemistry
The University of Tokyo

Toru Wakihara, Associate Professor
Department of Chemical System Engineering
The University of Tokyo

List of abbreviations

IZA-SC: the Structure Commission of the International Zeolite Association

FTC: framework type code

OSDA: organic structure-directing agent

CBU: composite building unit

SBU: secondary building unit

MR: membered ring

TMAOH: tetramethylammonium hydroxide

TEAOH: tetraethylammonium hydroxide

Table of contents

Chapter 1. General Introduction

1.1. Porous materials

Porous materials have enabled us to control atoms, ions, molecules, and clusters because of the unique “spaces” that exist in their interiors.[1] As a result, they have attracted much interest in both scientific and industrial fields. Not only are they well-known porous industrial materials such as adsorbents, ion-exchangers, and catalysts; porous materials are also being investigated for the use in new applications such as low-*k* and low-*n* materials, drug delivery carriers, and chemical sensors.[1–9] Porous materials are generally categorized by their pore size. According to the definition of the International Union of Pure and Applied Chemistry (IUPAC), pores with diameters greater than 50 nm, from 2 to 50 nm, and less than 2 nm are classified as macropores, mesopores, and micropores, respectively.[10] Moreover, the distributions of the sizes, shapes, and volumes of their pores are directly related to the potential applications of porous materials. A uniform pore structure can enable precise control of adsorbates, for example, materials with well-defined micropores such as zeolites and metal-organic frameworks (MOFs) can be used to separate molecules with sizes of the order of angstroms.

To date, many types of porous materials constructed from various components have been developed as shown in Figure 1.1. One of the well-known porous materials is activated carbon, which has been used for over a thousand years. At present, surface-modified[11] and structure-controlled[12–14] carbon materials with high specific surface areas (*ca.* 2000–4000 m^2 g^{-1}) have been reported,[15] and carbon nanotubes can also be considered an example of porous carbon.[16,17] Moreover, porous organic polymers[18–20] and porous crystalline covalent organic frameworks (COFs)[21–23] are also known as carbon-based porous materials. These organic-based materials comprising light elements such as C, H, and O possess extremely high specific surface areas due to the presence of these light elements.

On the other hand, porous structures can also be constructed of inorganic bodies such as metals[24–26] and metal oxides.[27–29] Among these inorganic porous materials, silica-based materials are promising due to the abundance of this natural resource and the wide variety of possible structures and functionalities. Zeolites are very important silicate materials and are discussed separately in the following section 1.2. Mesoporous silica, including FSM-16[30,31] and MCM-41,[32,33] were first synthesized in the 1990s using amphiphilic organic molecules by Kuroda group and a research group at Mobil Corp., respectively. Their discoveries have opened up a new class of ordered porous materials with diameters greater than 2 nm that can interact with complex molecules, molecular complexes, and even biomolecules.[34,35]

In addition, periodic mesoporous organosilica can be synthesized via surfactant-directed polycondensation of organic-bridged trialkoxysilane ($(R'O)_3Si$–R–$Si(OR')_3$) precursors.[36–38] These novel inorganic–organic hybrid materials are expected to have numerous applications as functional materials such as fluorescent systems, sensors, charge-transporting materials, and solid-state catalysts.[39] Numerous types of inorganic–organic hybrid porous materials, including porous coordination polymers (PCPs)[40–42] and MOFs[43–45], have been synthesized from metal ions or clusters and organic linkers that are connected by coordinating bonds. The pore sizes of PCPs and

MOFs are now almost designable and tunable using reticular strategies,[44,46,47] and these systems are expected to find applications as gas storage materials and sensors[48,49] due to their “soft” pore characteristics,[50,51] extremely high surface areas, and large pore volumes.[52,53]

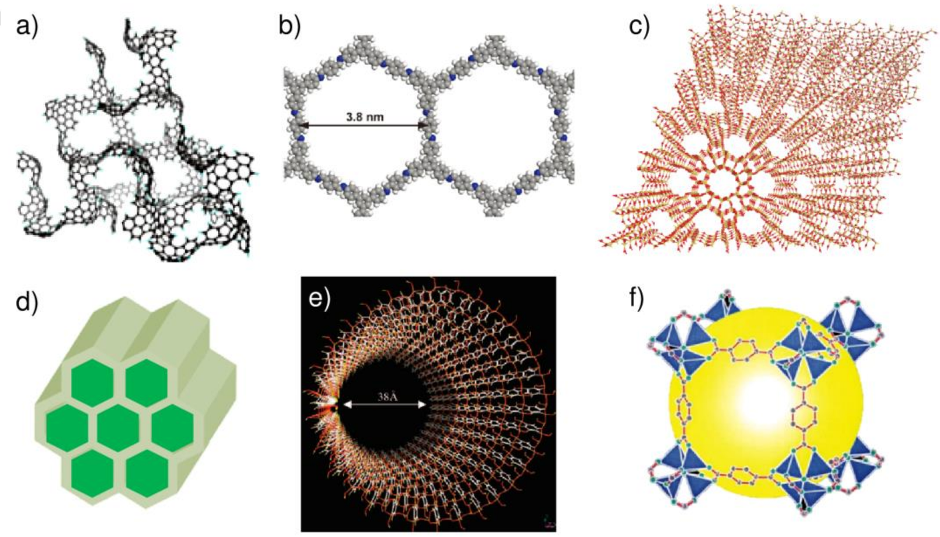

Figure 1.1 Illustrations of representative ordered porous materials: a) crosslinked-fullerene-like framework[14], b) covalent organic framework[23], c) zeolite, d) mesoporous silica, e) periodic mesoporous organosilica[38], and f) metal-organic framework[43].

1.2. Zeolites

Zeolites are crystalline microporous inorganic materials constructed from tetrahedral $TO_{4/2}$ (T = Si, Al, Zn, P, etc.) primary building units (Figure 1.2).[54,55] They have found widespread application in many fundamental industrial processes concerning catalysis, adsorption, ion-exchange, and so on.[56,57] The first zeolite was discovered in 1756 by Cronstedt, a Swedish mineralogist.[54] In the 1940s, Barrer and Milton studied the synthesis of zeolites and are regarded as the founders of science of zeolite synthesis.[58–61] To date, 213 types of zeolite structures have been identified and given three-letter Framework Type Codes (FTCs) such as LTA, MFI, *BEA, and -CLO by the Structure Commission of the International Zeolite Association (IZA-SC),[62] and the number of structures is still increasing. The FTCs with asterisks and hyphens correspond to frameworks with polymorphs and interruptions, respectively. These codes contain only topological information; therefore, zeolites with different material names sometimes have the same FTCs. For instance, the silicalite-1 and ZSM-5 frameworks are identical, and an FTC code of MFI has been assigned to each of these two zeolites, although they have different compositions (pure silica and aluminosilicate, respectively).

The replacement of framework Si atoms with other elements such as Al, Ga, and Zn leads to zeolite frameworks that are negatively charged. Because of this charge, these zeolites have counter cations in their frameworks that can also be exchanged with other cations. Typical counter cations are alkaline metals, e.g., Na^+, K^+, and alkaline earth metals, e.g., $Ca^{2+,}$ Mg^{2+}. In fact, zeolites are widely used as builders in laundry detergents to take up Ca^{2+} and Mg^{2+} in exchange for Na^+, thereby softening the washing water.[63] Importantly, ion-exchanged zeolites have also been good candidates for specific applications. For example, recently, zeolites containing Ag^+ and Cu^{2+} have been utilized

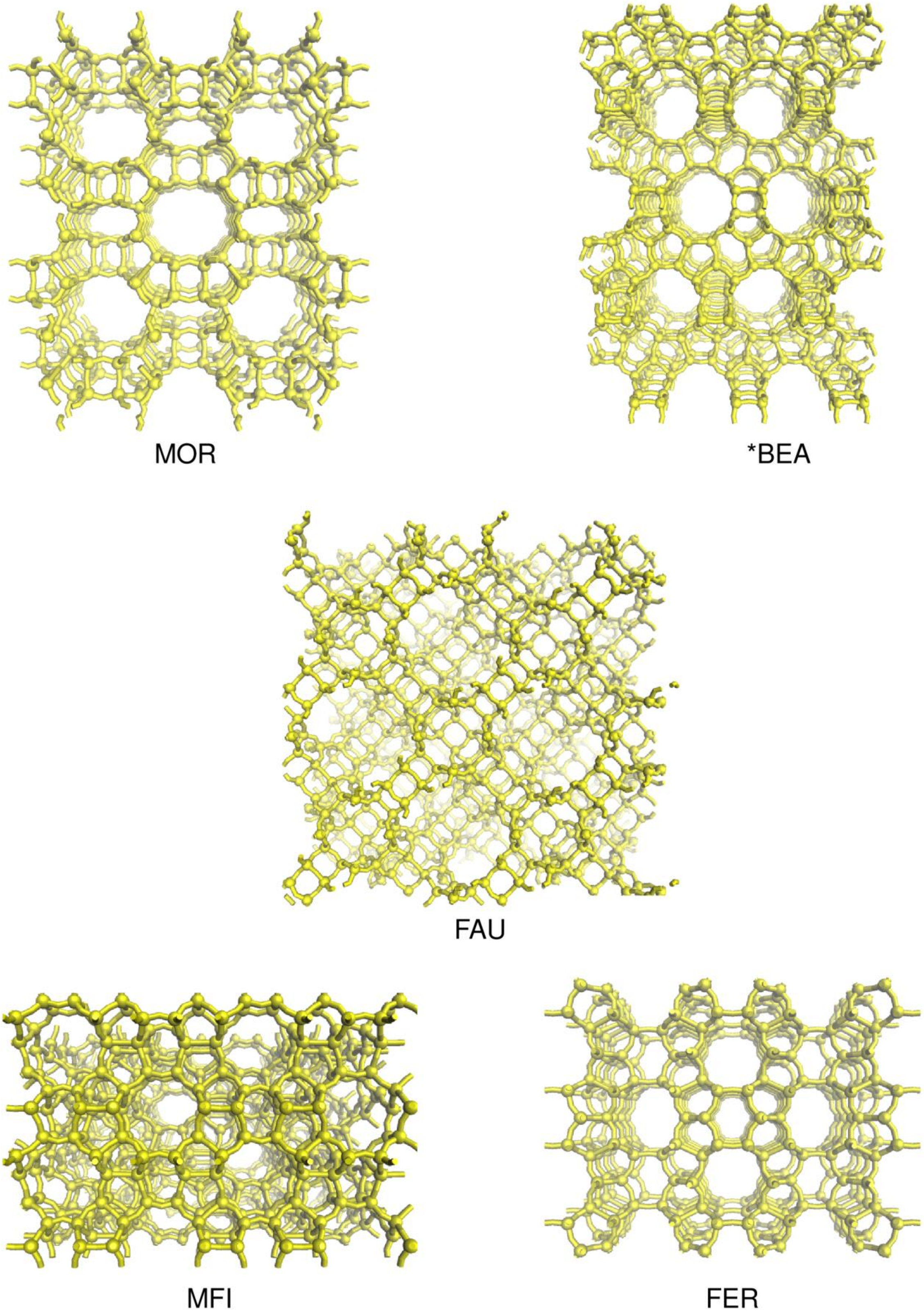

MOR

*BEA

FAU

MFI

FER

Figure 1.2 Framework topologies of industrially important "Big 5" zeolite catalysts.

as antimicrobial agents[64] and automotive catalysts,[65–68] respectively. Brønsted acidic sites in zeolites, which can be generated by introducing ammonium ions followed by heat treatment to convert $NH4^+$ to NH_3 and H^+, play a key role in many catalytic applications. In fact, the fluid catalytic cracking of heavy petroleum distillates using ultra-stable zeolite Y is one of the most important chemical processes in the world.[69] Zeolites are also known to have Lewis acidic properties,[70] and zeolites with transition metal ions isomorphously-substituted for Si^{4+} show remarkable catalytic activity in redox reactions.[71–74] Moreover, very recently, Davis and co-workers showed that hydrophobic zeolites with Lewis acidic centers such as tin can catalyze the isomerization of aldoses.[75,76]

Zeolites are typically synthesized using hydrothermal techniques performed in the presence of high-temperature and high-pressure water.[77] In addition to the raw materials such as silica and alumina, mineralizing agents such as hydroxide and fluoride anions are required. Organic molecules and inorganic cations mainly influence the crystallization process and phase selectivity of zeolites. Because these additives are not true “templates” of pore formation, they are referred to as structure-directing agents. Numerous studies have been reported on the structure-directing effects of both organic[78–80] and inorganic[77,81–85] compounds. However, the synthesis conditions for zeolites are rather complex, and many other factors should be considered such as the initial gel composition, temperature, water content, and aging procedure.[87–89] Moreover, zeolites are typically obtained as metastable phases that are readily converted to more stable phases according to the Ostwald step rule.[90] Therefore, not only thermodynamic but also kinetic analyses and considerations are required to reveal the crystallization mechanisms of zeolites.[91,92] Recently, Maldonado et al. carefully investigated six synthesis conditions for Na-aluminosilicate systems and identified multiple stages of zeolite phase transformations, involving the framework types FAU, LTA, EMT, GIS, SOD, ANA, CAN, and JBW (Figure 1.3).[89]

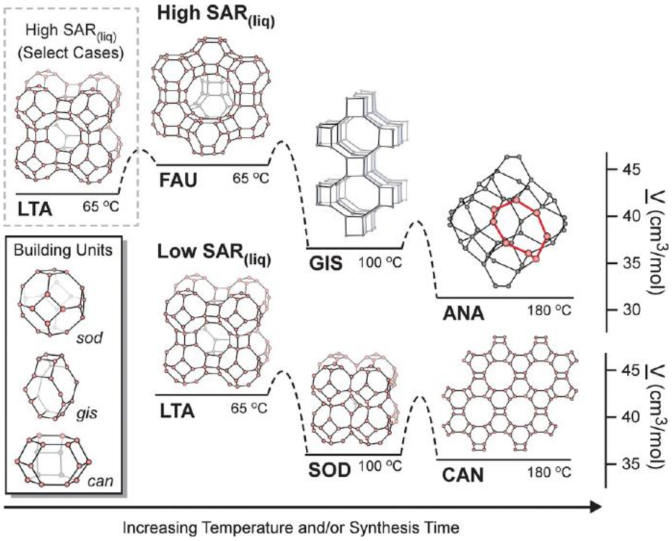

Figure 1.3 Stages of Na-zeolite phase transformation with increasing synthesis temperature and/or time. These transitions are consistent with Ostwald step rule wherein metastable structures progressively transform to more thermodynamically stable structures. The relative enthalpy of formation, $\Delta H_f - \Delta H_o$, for anhydrous zeolite structures is assumed to be proportional to its molar volume, $\underline{V}$. The sequence of stages progresses from low to high density structures (i.e., increasing thermodynamic stability).[89]

Cundy and Cox reviewed the mechanistic studies of zeolite crystallization and described the most probable mechanistic pathways involved in zeolite formation: the induction period, nucleation, and crystal growth.[77] The induction period is the time between the notional start of the reaction and the point where the crystalline product is first observed (typically, X-ray diffraction techniques are used to detect the crystalline phases). During the induction period, the nonequilibrium *primary amorphous phase* is considered to be converted into a pseudo-steady-state intermediate, or the *secondary amorphous phase*.[93–94] Next, as a result of reversible condensation reactions that constantly make and break T–O–T bonds, the nuclei in the secondary amorphous phase increase in size. Naturally, to initiate crystallization, the solution must be supersaturated.[95] Cation-mediated (see Figure 1.4) and heterogeneous nucleation mechanisms have been proposed, and generally, these nucleation processes are considered to require high activation energies.[77,96–98] Finally, crystals grow via the repeated cation-mediated addition of growth units (small silicates). In this period, the activation energy may be different (estimated to be low) from those in the former stages.[99] Although a great deal of attention has been devoted to this topic, the mechanisms are not fully understood yet on the molecular-scale.[100–102] Each of the steps mentioned above involves a large number of reactive species with varying roles. Notably, in addition to the conventional hydrothermal treatment, other synthesis techniques such as dry gel conversion,[103–105] solvothermal synthesis,[106,107] and ionothermal synthesis[108,109] methods have been developed.

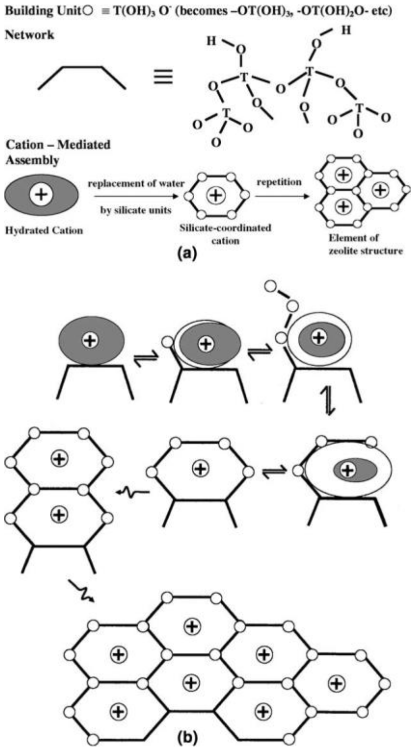

Figure 1.4 The basic mechanism for the cation-mediated assembly of ordered regions: (a) nomenclature and symbolism; (b) details of in-situ construction process by addition of solution units to a surface site.[77]

The synthesis of novel zeolite structures largely relies on the use of various organic structure-directing agents (OSDAs), fluoride ions, and the introduction of metal atoms other than aluminum to the framework.[110–117] From a historical perspective, zeolites such as A (LTA), X, Y (FAU), L (LTL), and mordenite (MOR) have been synthesized without the use of OSDAs and have played important roles in industrial processes.[118,119] On the other hand, most zeolites synthesized in recent years have been carried out using bulky OSDAs such as tetraalkylammonium cations.[110,111] These new zeolites have unique features such as a high silica content[113,116] and extra-large (greater than 12-membered ring (MR)) pore channels,[120,121] and are expected to be used for new applications.[1] Burkett and Davis studied the structure-directing mechanism of OSDAs in the synthesis of pure-silica zeolites and proposed a hydrophobic hydration model as shown in Figure 1.5.[122–125]

However, the cost of OSDAs accounts for a large portion of the total cost of the starting materials. In addition, for zeolites synthesized with OSDAs, thermal calcination (or alternative processes[126–132]) is indispensable; thus, processing/treatment of the waste gas and water produced by these processes is also necessary, which further increases the production costs. Moreover, using fluoride ion or metals other than aluminum is also unfavorable for industrial production. Therefore, the synthesis of aluminosilicate zeolites without using OSDAs has been one of the most important topics for the commercialization of zeolites.[133–135]

Recently, interesting results have been reported; several zeolites that were believed to require the use of OSDAs were synthesized without the addition of organic matter but with seed crystals (Figure 1.6). This new seed-directed approach is expected to reduce the cost and enable the development of environmentally friendly production

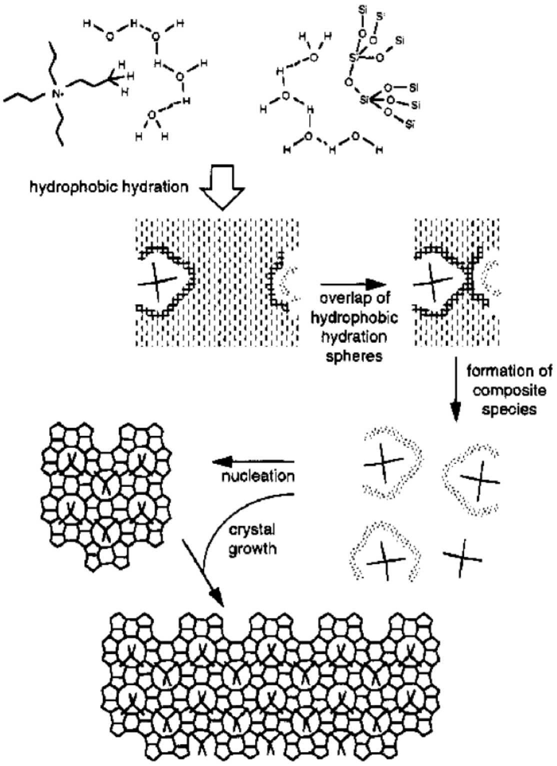

Figure 1.5 Proposed mechanism of structure direction in the TPA-mediated synthesis of silicalite-1.[124]

processes for useful zeolites. In this dissertation, the word "seed-directed" is used to distinguish this novel method from the conventional "seed-assisted" method, reflecting the fact that target zeolites have never been obtained without seed crystals in seed-directed syntheses. Historically, seed crystals have been used mainly for the reduction of the synthesis time, elimination of impurities, control of the particle size, and for the preparation of membranes.[61] In these cases, seed crystals have been added to a system that yields the same zeolite even without the seed crystals. Thus, while the seed-assisted synthesis of zeolites has been well known as a production technique, recent progress in the seed-directed approach has opened the door to the OSDA-free synthesis of zeolites.

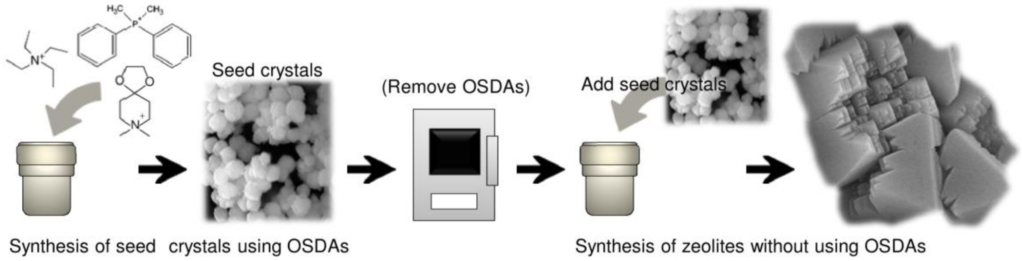

Figure 1.6 Schematic illustration of the seed-directed, OSDA-free synthesis of zeolites.[136]

1.3. Synthesis of zeolites using seed crystals

1.3.1. Conventional seed-assisted synthesis of zeolites

Seed-assisted synthesis of zeolites has been mainly used to increase the crystallization rate or control the purity and properties (e.g., the crystal size) of the products. In the 1960s, Kerr investigated the factors affecting the formation of zeolites (A, B, and X) and showed that the presence of zeolite seed crystals eliminated the induction period.[137,138] A mechanism involving liquid-mediated supply of the dissolved (alumino)silicate species to the surface of the seed zeolite crystals was also claimed in these and following papers.[139,140] Ueda et al. subsequently reported that the crystallization of zeolites from clear, homogenous, aqueous solutions, and seed crystals was also effective in these crystallizations, which supported the concept of a liquid-mediated crystallization formation mechanism.[141–143] In addition to increasing the crystallization rate, the presence of seed crystals also prevents the formation of other byproducts. Kasahara et al. investigated a synthesis system for the preparation of zeolite Y, in which impurities such as chabazite and philipsite were readily formed, and found that the size of the seed crystals affected the maximum yield of Y (see Table 1.1).[144] Secondary nucleation via the initial breeding mechanism caused by microcrystalline dust washed out from seed surfaces has been investigated.[145–153] It was claimed that the size of the seeds significantly influenced the formation of secondary nuclei; that is, large zeolite A crystals (40 μm) promoted nucleation of a new population of zeolite crystals, while small seed crystals (approximately 1–3 μm) did not promote such a population.[151] Small seed crystals will provide large surfaces for the newly growing crystals, and they effectively act in many cases; however, not always small crystals are effective. On the other hand, polycrystalline breeding formed over seed crystals has been reported in a hydroxysodalite seed system.[146] In addition, Valtchev et al. reported the effect of tribochemical pretreatment of seeds for rapid crystallization of zeolite Y,[154] and very recently, seed-assisted methods were applied for fluoride media to synthesize nanosized zeolite beta.[155] Analytical and theoretical investigations have also been reported on the synthesis of MFI-type zeolites (silicalite-1 or ZSM-5).[156–158] Although these mechanisms have not been fully understood and some conflicting results have been obtained, this study has been summarized in reviews. [77,159] It should be noted that in these conventional methods, the addition of zeolite seeds to the reactant mixture yields the same zeolites that are obtained even when no seed crystals are used. In most cases, the presence of seeds with different crystal structures does not promote the crystallization of the target phases.[160,161]

Table 1.1 Maximum yield for zeolite Y crystallization using seed crystals. Data are from Ref. 144.

	Crystal sizes of seeds	SiO_2/Al_2O_3 ratios of seeds	Maximum yield of zeolite Y (%)
Without seeds	-	-	20
Zeolite X seeds	2–3 μm	2.5	25
Zeolite Y seeds	0.4 μm	5.5	30
Zeolite X seeds	0.05 μm	2.0	50

The secondary growth of zeolites from seed crystals has also been used for other applications, such as the preparation of zeolite membranes. In addition to an increase in the crystallization rate and improvement in the purity level, the seeding approach is advantageous for the highly reproducible preparation of dense and stable membranes with oriented crystal growth of the zeolite layer.[162–172] Lovallo et al. first demonstrated the preparation of zeolite L membrane by the secondary growth of zeolite L seeds on the porous substrate.[164] Matsukata and co-workers reported that ZSM-5 and mordenite membranes prepared via in situ hydrothermal synthesis using seed crystals in

OSDA-free media (shown in Figure 1.7) showed a very high separation factor for a water–isopropyl alcohol mixture compared to membranes prepared without seeding.[173–175] The synthesis conditions were optimized for controllable growth of the seed crystals by adjusting the water content in the reaction mixture.[174,175] Notably, both mordenite and ZSM-5 seed crystals grow in the same synthesis mixture under the same hydrothermal conditions,[174] as do zeolites A and Y. [176] Lai et al reported that controlled secondary crystal growth of silicalite-1 using OSDAs also results in improved membranes with high permeance and selectivity in xylene isomer separation.[177]

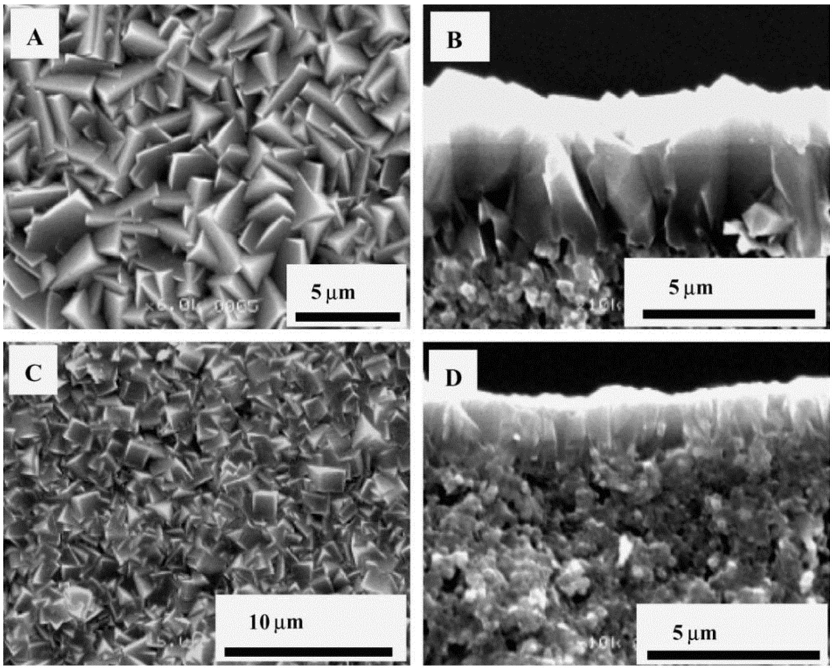

Figure 1.7 Typical SEM images: (A) top surface and (B) cross section of a mordenite membrane, (C) top surface, and (D) cross section of a ZSM-5 membrane. The membranes were prepared on a porous α-Al_2O_3 plate at 180 °C for 12 h using a synthesis mixture with the molar composition Na_2O: Al_2O_3: SiO_2: H_2O = 10: 0.15: 36: 960.[174]

Moreover, secondary growth of nano-seed crystals are also used for the preparation of macro-structured zeolite materials. Zeolite seeds can be deposited on various supports such as polystyrene beads, carbon fibers, and biological templates. The successive hydrothermal treatment and template removal by calcination result zeolite replicas of these templates. This topic has been reviewed by Tosheva and Valtchev.[178,179]

1.3.2. Recent seed-directed, OSDA-free syntheses of zeolites

A pioneering work of the recent OSDA-free synthesis was reported by Xie et al. in 2008.[180] They demonstrated that zeolite beta (*BEA) could be synthesized without using OSDAs but with the addition of zeolite beta seeds (10 wt.% to silica). A seed supplied from Sinopec Catalyst Co. was added to an aluminosilicate gel with a molar ratio of 0.25 Na_2O: 0.025 Al_2O_3: SiO_2: 14.25 H_2O. Because zeolite beta is one of the most industrially important materials in petrochemical production, waste gas treatment of automobile, and so on, this study had a significant impact on people working in the concerned field. Xie et al. also claimed that this novel route is quite fast (140 °C for 17–19 h) compared to the conventional crystallization of beta using OSDAs such as tetraethylammonium (TEA). Although the initial gel compositions were limited, details on the seed were not disclosed, and reproduction was not easy in the early stage; the reaction conditions have been improved by other researchers including us.[181–185] Majano et al. independently showed that zeolite beta synthesized by the seed-directed method had a low SiO_2/Al_2O_3 ratio of 7.8 (the SiO_2/Al_2O_3 ratio of the seeds was 52) when using an initial gel with the following composition: 0.3 Na_2O: aAl$_2$O3: SiO_2: 15 H_2O, where a = 0.01, 0.02, or 0.03.[181] They also determined that crystallization of zeolite beta with a lower number of seeds (≤2.5 wt.% to silica) can be achieved at lower temperatures (<125 °C); higher temperatures often induce the formation of mordenite as a byproduct. The influence of the synthesis conditions on the products were carefully investigated and identified a broader set of appropriate synthesis conditions in Okubo-laboratory. Moreover, zeolite beta can be synthesized using recycled seeds for the production of further generations of zeolite beta without using an OSDA. This zeolite beta was named "Green Beta."[182] This result provides the basis for a completely OSDA-free synthesis of zeolite beta under economically favorable conditions. The gel compositions used in this study for both first generation beta and Green Beta were x Na_2O: y Al_2O_3: SiO_2: z H_2O, where $x = 0.225–0.35$, $y = 0.01–0.025$, and $z = 20–25$, while the SiO_2/Al_2O_3 ratios of the seeds were 14–24 and 11–13, respectively (Figure 1.8). The crystal growth mechanism for beta was also investigated by Xie et al.[183] and Kamimura et al.[184] Xie et al. proposed a core−shell growth mechanism for the seed-directed synthesis of beta on the basis of SEM and TEM observations and EDX and XPS analyses.[183] On the other hand, research results from Okubo laboratory showed that the beta seeds were partially dissolved during the initial stage of the hydrothermal treatment, and new beta crystallized on the surface of the residual beta seeds after the seeds were exposed to the liquid (Figure 1.9). The Raman spectroscopy, solid-state ^{27}Al and ^{23}Na MAS NMR, and high-energy XRD analyses of the seeded and unseeded amorphous reactant mixtures revealed that the beta seeds induced no structural change in the amorphous aluminosilicate gels during the hydrothermal treatment.[184] Honda et al. reported the OSDA-free synthesis of zeolite beta using zeolite Y ($SiO_2/Al_2O_3 = 44$) as the starting material and beta as the seeds (9.1–33.3 wt.%).[185] More recently, the OSDA-free synthesis of zeolite beta was extended to Fe-containing beta[186] and aluminosilicate zeolite beta with a hollow structure using zincosilicate zeolite seeds with *BEA-type topology (known as CIT-6 and described in Chapter 5).[187]

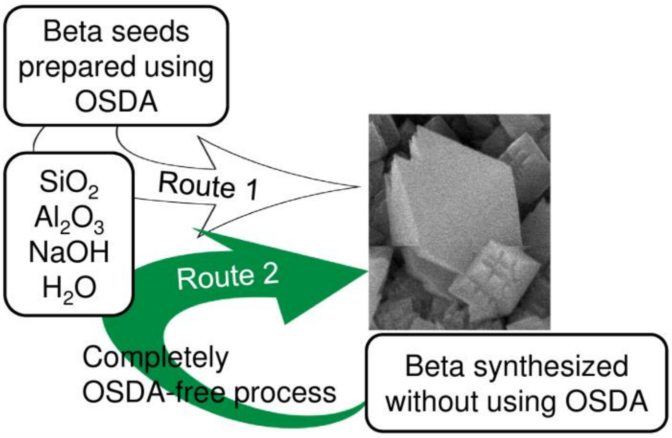

Figure 1.8 Concept of Green Beta.[136]

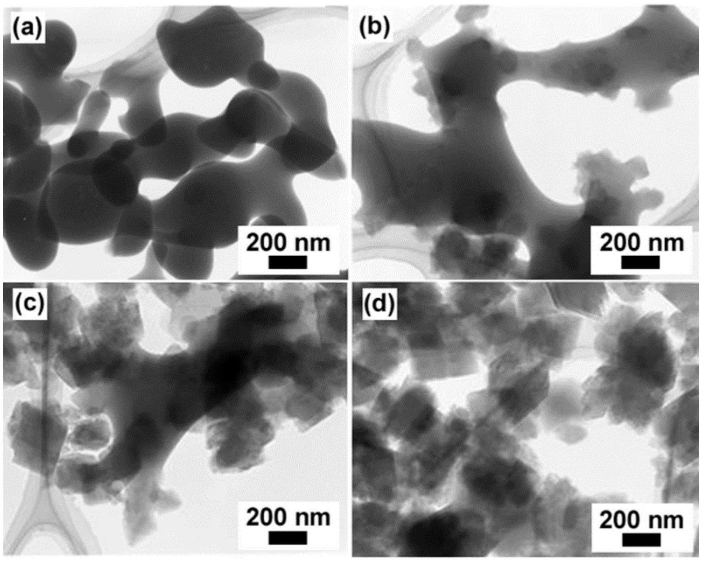

Figure 1.9 TEM images of the solid aluminosilicate products obtained after (a) 5 h, (b) 20 h, (c) 30 h, and (d) 40 h of hydrothermal treatment.[184]

Not only beta but also other various zeolites can be synthesized by the seed-directed method without OSDAs, although it was previously believed that OSDAs were essential for their synthesis. Yokoi et al.[188] and Yoshioka et al.[189] reported the OSDA-free synthesis of TTZ-1 (RTH) with various compositions (bolo, alumino, and gallosilicates) using the seed-directed approach. They concluded that the key factors for the successful seed-directed synthesis of TTZ-1 are the addition of sodium hydroxide and calcined [B]-RUB-13 crystals as the seeds and the use of 0.1 Na_2O: 0.125 B_2O_3: SiO_2: 200 H_2O as the optimum molar composition of the reactant mixture. Subsequently, Nukaga et al. reproduced the synthesis of TTZ-1, investigated details, and showed existence of ITE-type zeolite in TTZ-1.[190] The important features of these synthesis conditions are the low alkalinity (Na_2O/SiO_2 = 0.1) and very dilute conditions (H_2O/SiO_2 = 200). TTZ-1 may be a good candidate for the selective synthesis of propene in the methanol to olefin reaction (Table 1.2), although the catalytic properties of RTH-type zeolites have not yet been thoroughly investigated owing to the difficulty in synthesizing them by conventional methods. Notably, the SiO_2/Al_2O_3 ratio of [Al]-TTZ-1 is exceptionally high (SiO_2/Al_2O_3 = 82) considering that low-silica zeolites tend to be obtained from the OSDA-free system due to high charge densities of the alkaline cations (details are discussed in a following chapter). Unfortunately, the reason why TTZ-1 has such a high SiO_2/Al_2O_3 ratio has not yet been fully elucidated. We have been able to reproduce the synthesis, but still the reproducibility is not 100%. The details are under investigation.

Table 1.2 Results of MTO reactions after 90 min at 400 °C[a]. Data are from Ref. 188.

	SiO_2/Al_2O_3	Conv. (%)	Selectivity (%)					
			C1	C2=	C3=	C2+C3	C4-C6	DME
[Al]-TTZ-1	82	78	0.8	22.6	44.8	0.8	27.7	3.5
[Al, B]-TTZ-1	216	97	0	26.7	43.7	0	21.2	0
[Al, B]-RUB-13	180	100	0	26.4	46.9	1.3	25.4	0
SAPO-34	no data	100	0.8	41.8	41.2	0.5	15.6	0
ZSM-5	100	100	0.8	19	32.9	4.3	42.9	0

[a]: Reaction conditions: catalyst, 100 mg; temperature, 400 °C; W/F, 34 gcat.h$(molMeOH)^{-1}$; weight hourly space velocity (WHSV) of methanol, 1.0 h^{-1}; partial pressure of MeOH, 5.0 kPa. W/F = weight/flow.

Levyne (LEV) was recently synthesized via a seed-directed method.[183,191,192] Yashiki et al. used zeolite Y with various SiO_2/Al_2O_3 ratios (8–74) as the starting materials and gel compositions of aM$_2$O: bAl$_2$O$_3$:SiO$_2$: cH$_2$O, where a = 0.2–0.4, M = Li, Na, K, Rb, Cs, b = 0.0135–0.125, and c = 15–30,[191] while Zhang et al. used starting gels with compositions aNa$_2$O: bAl$_2$O$_3$: SiO$_2$: 35 H$_2$O: c alcohol, where a = 0.35–0.38, b = 0.022–0.025, c = 1–2, and the alcohols were methanol, ethanol, n-propanol, and n-butanol.[192] The synthesis of levyne from zeolite Y as the starting material utilizes the difference in the solubility of Y and the levyne seed crystals; therefore, it can be concluded that levyne is more stable than Y under these hydrothermal conditions. The core−shell structure of the obtained levyne crystals was also confirmed by TEM-EDX analysis as shown in Figure 1.10.[191] Notably, “2nd generation” levyne, designated as Na-LEV-SDS-2nd, was synthesized using levyne seeds synthesized without using OSDAs. More importantly, compared with conventional H-ZSM-5 and H-SAPO-34 catalysts in the MTO reaction, the H-form of the LEV-SDS zeolite exhibited higher selectivity for light olefins, particularly for ethylene.[192]

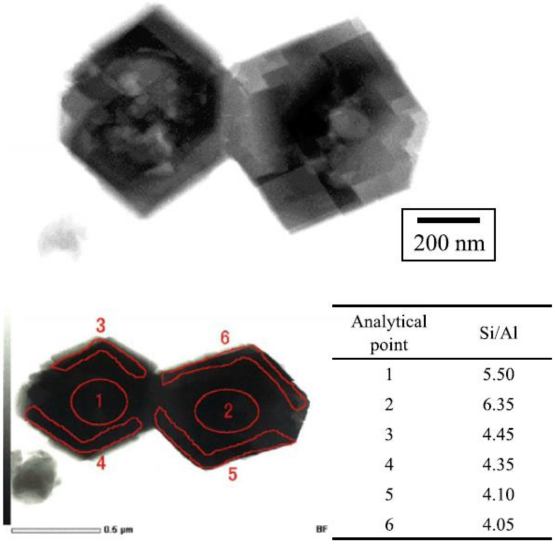

Analytical point	Si/Al
1	5.50
2	6.35
3	4.45
4	4.35
5	4.10
6	4.05

Figure 1.10 TEM-EDX analysis of LEV zeolite crystals obtained from FAU zeolite.[191]

The OSDA-free synthesis of ZSM-12 (MTW) was reported by us,[193–195] and the details are discussed in the following Chapter 3. Zhang et al.[196] and Wu et al.[197] also found that SUZ-4 (SZR) and ZJM-6 (MTT) could be synthesized under OSDA-free conditions, respectively. In addition, some zeolites with unique features that have been difficult to synthesize without OSDAs have been prepared in recent years by the seed-directed method. For example, nanosized ZSM-5 (MFI)[198] and high-silica ferrierite (FER, $SiO_2/Al_2O_3 = 29$)[199] were synthesized using ZSM-5 and RUB-37 (CDO) seeds, respectively. The zeolite structures recently synthesized by seed-directed OSDA-free methods are summarized in Table 1.3. However, zeolite types (both structure and composition) are still limited and enough mechanistic studies have not been reported.

Table 1.3 Summary of zeolites synthesized using seed-directed, OSDA-free methods.

Seed				Product		Note	Ref.
Material name	FTC	SiO_2/Al_2O_3 ratio	Amount (wt.% to silica)	FTC	SiO_2/Al_2O_3 ratio		
Beta	*BEA	no data	10	*BEA	no data		180
Beta	*BEA	52	0.5–2.5	*BEA	7.8–9.0	Al-rich	181
Beta	*BEA	14–24	1–10	*BEA	10.4–13.2		182
Beta	*BEA	20.4, 23.2	10.3	*BEA	core:26.6, shell:10.6		183
Beta	*BEA	50	9.1–33.3	*BEA	14.6–22		185
Beta	*BEA	no data	5	*BEA	9.8 $SiO_2/Fe_2O_3 = 100$	Fe-Beta	186
CIT-6	*BEA	SiO_2/ZnO = 13,	10	*BEA	10.9–21.4	Hollow	187
RUB-13	RTH	∞ SiO_2/B_2O_3 = 46, ∞	2	RTH	82, 216[a] SiO_2/B_2O_3 = 42–54 SiO_2/Ga_2O_3 = 504		188, 189
RUB-50	LEV	19.4	4.6	LEV	no data		183
	LEV	21.4	5–17	LEV	9.2–12		191
RUB-50	LEV	19.5	1.5–5	LEV	8.1		192
ZSM-12	MTW	101	10	MTW	no data		193
ZSM-12	MTW	94.6	1–10	MTW	23.4–32.4		194
Beta	*BEA	24	10	MTW	31.8–46.4		195
SUZ-4	SZR	no data	1	SZR	no data		196
Silicalite-1	MFI	∞	0.1–3	MFI	19.2–20.4	Nanosized	198
RUB-37	CDO	∞	5	FER	14.6–29.0	High-silica	199
ZSM-11	MEL	66.0	10	MEL	17.6		200
ECR-18	PAU	no data	10	PAU	no data		200

[a] 82 for [Al]-TTZ-1 and 216 for [Al, B]-TTZ-1.

1.4. Scope and overview of this dissertation

This dissertation describes the OSDA-free synthesis of various zeolites using a seed-directed approach and aims to broaden the applicable zeolite types, clarify the requirements, and investigate the mechanisms of seed-directed synthesis. Moreover, the characteristics of this process and the unique features of the obtained zeolites are described. An important concept is *"divide it into small jobs,"* namely, understanding zeolite synthesis systematically dividing into separate nucleation and crystal growth steps. Generally, adding seed crystals means skipping the nucleation process involving a higher activation energy, and the OSDA-free synthesis of zeolites using the seed-directed method means that OSDAs are not necessary for the crystal growth of zeolites. Therefore, requirements and mechanisms for this zeolite synthesis method are related to crystal growth, and the unique features of these zeolite products can be explained as a result of crystal growth-dominated synthesis. Although the seed-directed method has been utilized for half a century, OSDA-free synthesis is a novel achievement that may enable the elucidation of the crystal growth mechanisms of zeolites.

The structure of this doctoral dissertation is shown in Figure 1.11. For clarity, material names and FTCs for zeolites are used properly for conventional zeolites and zeolites synthesized using the seed-directed and OSDA-free method, respectively. In this chapter, a general background on porous materials, particularly zeolites, is described, followed by a brief review of the seed-assisted synthesis of zeolites and a summary of recent advances in OSDA-free synthesis. Chapter 2 presents a discussion on two aluminosilicate zeolites with the FTCs PAU and MAZ synthesized by applying the seed-directed method based on the "CBU hypothesis." These two zeolites have cage-based topologies and even-membered ring-rich ring distributions. In Chapter 3, the synthesis of MTW-type aluminosilicate zeolites using two types of seed crystals is presented. The differences in the pore characteristics of the obtained MTW-type zeolites compared to those of seed crystals are evaluated. In Chapter 4, the expansion of the seed-directed method to a VET-type zincosilicate system is described. The VET-type structure is unique, and its crystal growth mechanism is worth investigating. In Chapter 5, the use of an easy-to-dissolve zincosilicate seed crystal with a *BEA-type structure referred to as CIT-6 for the synthesis of a *BEA-type aluminosilicate zeolite to clarify the requirement for seed crystals is reviewed. In situ dissolution of seed crystals enables the synthesis of characteristic *BEA-type zeolites with hollow interiors. The general conclusions of this dissertation and a future perspective on the field of OSDA-free zeolite synthesis are described in Chapter 6.

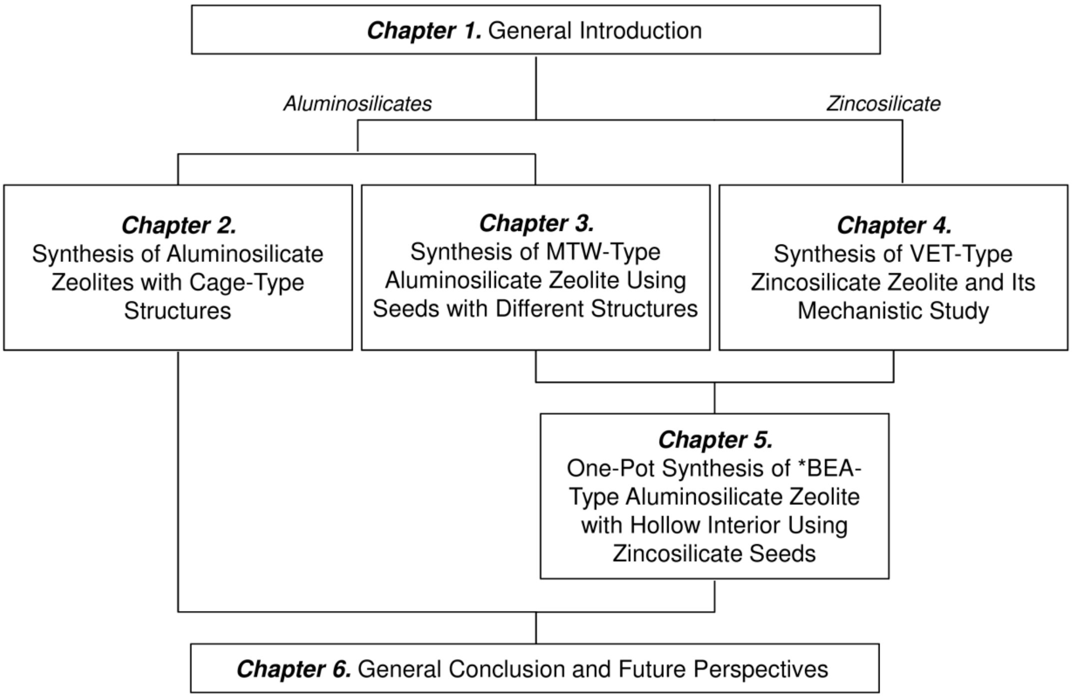

Figure 1.11 Structure of this dissertation.

Chapter 2. Synthesis of Aluminosilicate Zeolites with Cage-Type Structures

2.1. Introduction

2.1.1. “CBU hypothesis” and its applicability

It was confirmed that zeolite beta crystallized only when beta seeds were added; alternatively, mordenite was obtained from gels without the seeds after a long hydrothermal treatment and typically from gels with a composition of 0.3 Na_2O: 0.01 Al_2O_3: SiO_2: 20 H_2O (ref. 184 and point A in ref. 200). Why does the crystal growth of beta proceed only when beta seeds are added to a gel that yields mordenite without seed addition? The answer to this question should indicate the crucial difference between the recent seed-directed methods and the conventional one. To answer this question and to broaden the zeolite types by this synthesis method, the effect of seeds with different framework structures was examined using a Na−aluminosilicate gel with the same chemical composition as that used in the OSDA-free synthesis of beta (point A in ref. 200).

The addition of mordenite seeds at 140 °C resulted in evident crystal growth of mordenite only after 1 h of heating. The maximum peak intensities for mordenite were observed in the XRD pattern after 12 h of heating, which is in contrast with the slow crystallization of mordenite from an unseeded gel with the same chemical composition

(7 days). Ferrierite was also crystallized at a considerably rapid growth rate at 150 °C, and the peak intensities in XRD reached to maximum after 24 h. These results indicate that some nutrient species coexisting in the liquid phase that remains after heating of the Na−aluminosilicate gel can contribute to the crystal growth of beta, mordenite, and ferrierite zeolites. On the basis of the above results, we assumed that beta, mordenite, and ferrierite may have common key precursors for crystal growth and that these three zeolites should have common structural units in their frameworks.

The three-dimensional framework structures of zeolites consist of secondary building units (SBUs) and/or composite building units (CBUs), as summarized in the database of the IZA-SC.[62] First, the ring distributions of beta, mordenite, and ferrierite were compared, and the common units turned out to be 5 and 12-MR, which can also be seen in many other zeolites. This result indicates that the common unit among the three zeolites should be considered at the level of the higher units; that is, the CBUs. Currently, the number of approved CBUs in the IZA-SC is 47, and those contained in each framework structure type are summarized in the IZA-SC database.[62] It is easily understood that beta (*BEA) contains the *bea*, *mtw*, and *mor* CBUs, whereas mordenite (MOR) and ferrierite (FER) contain only the *mor* unit and the *fer* unit, respectively, in their frameworks. Apparently, there is no common CBU among these three zeolites; however, the *fer* unit consists of 13 T (T for tetrahedral = Si or Al) atoms and is decomposed into the *mor* unit and 5MR, which consist of 8 and 5 T atoms, respectively, as illustrated in Figure 2.1. Consequently, the *mor* unit is elucidated as the common CBU of beta, mordenite, and ferrierite zeolites.

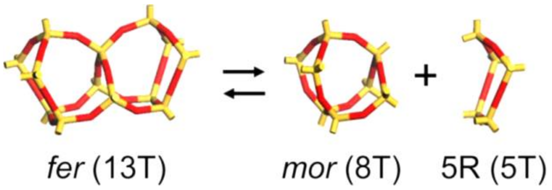

Figure 2.1 Structural correlation of the CBUs between *fer* and *mor*.[200]

On the basis of the discussion on the common CBUs in seed zeolites and considering that the zeolites ultimately crystallized from corresponding seed-free gels, the following working hypothesis was proposed to understand the effect of the seeds with different framework structures. For OSDA-free synthesis, the target zeolite should be added as seeds to a gel that yields a zeolite containing the common CBU when the gel is heated without seeds. This hypothesis does not claim the presence of the silicate and/or aluminosilicate molecules or ions with the same structure as common CBUs but can provide guidelines for exploring synthesis conditions.

If the hypothesis is applicable for the synthesis of other zeolites, ZSM-5 (MFI) and ZSM-11 (MEL), containing the *mor* building unit should be synthesized with the addition of these seeds into a reactant gel that otherwise yields mordenite. The correlation of the CBU among ZSM-5, ZSM-11, and mordenite is shown in Figure 2.2. The seed-directed, OSDA-free syntheses of ZSM-5 and ZSM-11 were performed at 160 and 140 °C for 20 and 15 h, respectively. The results indicate that similar to the case of beta, the crystal growth of ZSM-5 and ZSM-11 with the addition of the corresponding seeds is highly accelerated compared to the spontaneous nucleation of mordenite.

However, all of these zeolites synthesized by seed-directed method are classified into the pentasil-type zeolites, so far, and the successful expansion of the applicability of the hypotheses to the synthesis of additional zeolites is necessary in order to enhance its usefulness. In this chapter, two other zeolites with PAU and

MAZ-type structures, which have even-membered rings and cage-type structure, were studied.

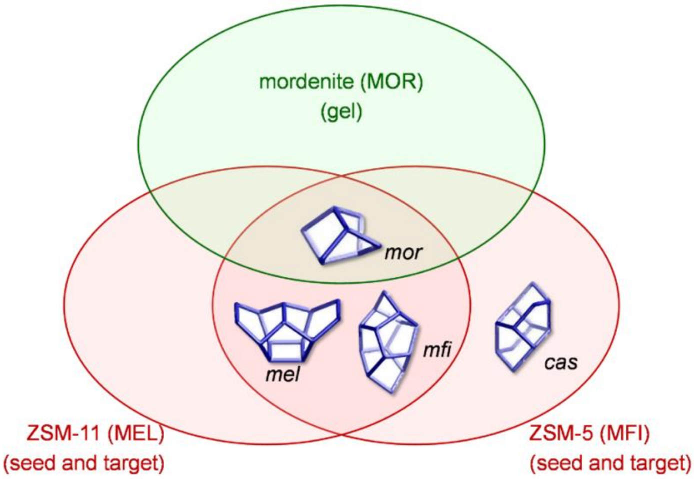

Figure 2.2 Correlation of the common CBUs in MOR, MFI, and MEL.[136]

2.1.2. Zeolite ECR-18 (PAU) and zeolite Linde W (MER)

Zeolite ECR-18 was first synthesized by Vaunghan and Strohmaier in 1999 as the counter part of a natural zeolite paulingite, which was discovered in 1960.[201,202] Both ECR-18 and paulingite have PAU-type structure, which possess three-dimensional pore channels composed of 8-MRs (3.6 × 3.6 Å). The unit cell of PAU-type structure is constructed from 672 T-atoms, and according to the report from Krivovichev, PAU-type structure is the most second complex structure of all zeolite structures (201 types were known up to the report).[203] According to the IZA-SC, CBUs of PAU-type structure are *d8r*, *gis*, *lta*, and *pau*.[62] Other description of this structure also exist owing to the fact that this structure has been attracted many crystallographers. This structure can be described as a result of linkage of bipyramidal (octahedral) complexes constructed from 4-MR chains (Figure 2.3) as well as packing of small building units.[205,206] In the conventional synthesis of ECR-18, the tetraethylammonium cation (TEA^+) has been essential as OSDA in addition to the two alkaline cations, sodium and potassium. This complex three cation system has made synthesis of ECR-18 difficult as well as long synthesis time (over 2 weeks) and an aging process.[207–209]

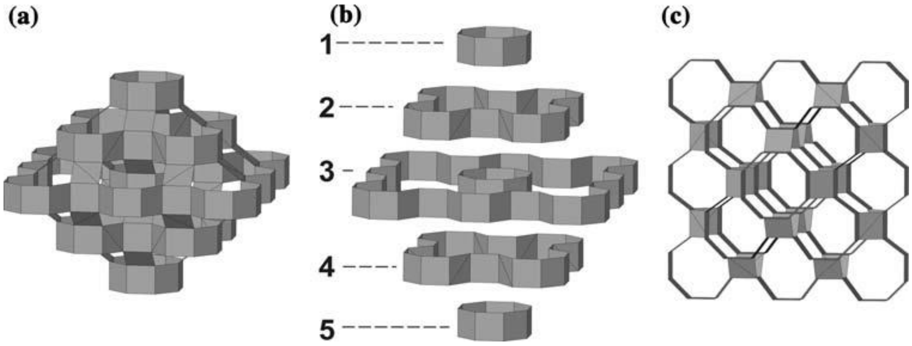

Figure 2.3 Bipyramidal nanocomplex as construction of 4-MRs (shown as squares): (a) side view, (b) stratified structure, (c) top view.[204]

Zeolite Linde W is a well-known zeolite with MER-type structure synthesized from K-aluminosilicate gels without using OSDAs.[210–212] MER-type structure is composed of *d8r* and *pau* as CBUs, which is common to PAU-type structure (Figure 2.4). Therefore, according to the CBU hypothesis, when zeolite ECR-18 is added as seeds to the gel from which zeolite Linde W is synthesized without any seeds, PAU-type zeolite should be obtained by hydrothermal treatment.

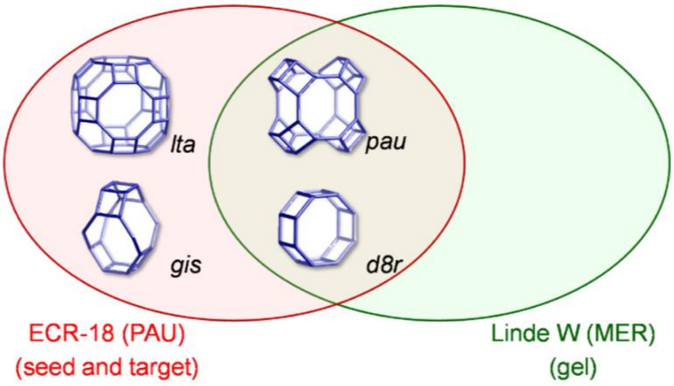

Figure 2.4 Correlation of the common CBUs for MER and PAU.[136]

2.1.3. Zeolite omega (MAZ) and zeolite T (OFF/ERI)

Zeolite omega (FTC: MAZ) has one-dimensional channels composed of 12-MRs (7.4 × 7.4 Å) and gmelinite cages (CBU: *gme*) in its framework.[62] Owing to its large micropores and strong solid acidity,[213] zeolite omega is expected to be useful as adsorbents and catalysts.[214,215] In the conventional synthesis of zeolite omega, the tetramethylammonium cation (TMA^+) is used as the OSDA,[216–218] but the use of *p*-dioxane[219] and piperazine[220] has also been reported. Moreover, at least 4–7 days of hydrothermal treatment is required to obtain zeolite omega using these OSDAs.[217–220] In this chapter, the OSDA-free synthesis of a MAZ-type zeolite according to the CBU hypothesis was explored using a (Na, K)-aluminosilicate gel system. Zeolite T, which is typically synthesized from (Na, K)-aluminosilicate gel systems without the addition of an OSDA, consists of offretite (OFF) as a major component of the intergrowth structure and erionite (ERI) as a minor component. OFF-type structure is composed of *gme*, *can*, and *d6r* CBUs, while ERI-type structure consists of *can* and *d6r* CBUs. As a result, *gme* is the CBU common to both zeolite omega and zeolite T, as illustrated in Figure 2.5. Therefore, according to the CBU hypothesis, when zeolite omega is added as seeds to the gel from which zeolite T is synthesized without any seeds, MAZ-type zeolite should be obtained by hydrothermal treatment.

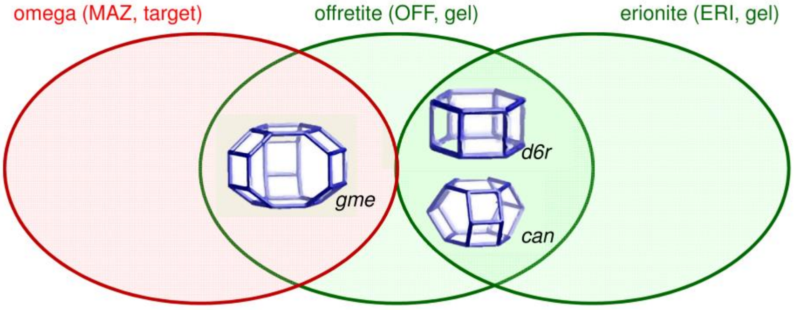

Figure 2.5 Correlation of the common CBU in OFF, ERI, and MAZ.[221]

2.2. Experimental

2.2.1. Chemicals

For the synthesis of the zeolite ECR-18 seed crystals, Ludox® HS-40 (40 wt.% silica in water, Sigma-Aldrich Co.) as the silica source, TEAOH (35 wt.% in water, Aldrich) as the OSDA, aluminum hydroxide ($Al(OH)_3$, Wako Pure Chemical Industries, Ltd.) and aluminum sulfate ($Al_2(SO_4)_3 \cdot 16H_2O$, Wako) as aluminum sources, and sodium hydroxide solution (NaOH, 50 w/v% in water, Wako) and potassium hydroxide solution (KOH, 50 wt.% in water, Wako) as the alkali sources were used as provided. For the OSDA-free synthesis of PAU-type zeolite, aluminum powder (Al, 99.5%, Wako) was used as the aluminum source.

For the synthesis of the zeolite omega seed crystals, Ludox® HS-40 as the silica source, TMAOH (25 wt.% in water, Aldrich) as the OSDA, and NaOH pellets (Wako) as the alkali source were used as provided. For the OSDA-free synthesis of MAZ-type zeolite, the following materials were used as provided: Cab-O-Sil® (Grade M5, Cabot Co.) as the silica source, sodium aluminate ($NaAlO_2$, Wako) as the aluminum source, and NaOH solution (50 w/v% in water, Wako) and KOH solution (50 wt.%, in water, Wako) as the alkali sources.

2.2.2. Preparation of ECR-18 and omega seed crystals

ECR-18 for seed crystals were prepared by already reported procedure.[207–209] The initial gel composition was 0.4 K_2O: 1.4 $(TEA)_2O$: 0.8 Na_2O: Al_2O_3: 9 SiO_2: 140 H_2O, and the hydrothermal treatment was carried out at 120 °C for 14 days at 20 rpm in a Teflon®-lined stainless autoclave (#4749, Parr Instrument Co.). As-synthesized ECR-18 was calcined at 550 °C for 10 hours in air to remove organic compounds in the obtained zeolite.

Zeolite omega seed crystals were prepared according to the previously reported procedure via hydrothermal treatment of a sodium aluminosilicate gel in the presence of TMAOH with the following chemical composition: 0.24 Na_2O: 0.024 TMA_2O: 0.l Al_2O_3: SiO_2: 110 H_2O.[218] The reactant mixture was statically aged at room temperature for 72 h, and then the mixture was transferred into a Teflon®-lined stainless autoclave (#4749, Parr) and subjected to hydrothermal treatment at 100 °C for 7 days in a convection oven under autogeneous pressure and static conditions. Thereafter, the obtained product was recovered by filtration, washed thoroughly with hot distilled water, and dried at 60 °C overnight. Prior to their use as seeds, all of the omega seed crystals used in the present study were calcined at 550 °C for 20 h in a stream of dry air.

2.2.3. OSDA-free synthesis of PAU and MAZ-type zeolites

As a typical run for the OSDA-free synthesis of PAU-type zeolite, aluminum powder was dissolved in aqueous solution of potassium hydroxide followed by addition of 10 wt.% relative to the silica source of ECR-18 seeds prepared by above mentioned method and colloidal silica solution. The initial gel with composition of 0.5–0.55 K_2O: 0.1 Al_2O_3: SiO_2: 20 H_2O was transferred into a Teflon®-lined stainless autoclave (#4749, Parr) and heated at 135 °C for 3 days under autogeneous pressure and static conditions. The product was collected by filtration, washed with distilled water until pH of filtrate was decreased to 8, and dried at 60 °C. For comparison, the same initial gel without any seeds was prepared and hydrothermally treated by the same conditions.

The OSDA-free synthesis of MAZ-type zeolites was performed via the addition of calcined zeolite omega seeds to (Na, K)-aluminosilicate gels with the following chemical compositions: x Na_2O: y K_2O: z Al_2O_3: SiO_2: 20 H_2O, where $x = 0.23–0.33$, $y = 0.075–0.11$, $x/(x+y) = 0.75$, and $z = 0.01–0.036$. In a typical procedure, sodium aluminate, sodium hydroxide, and potassium hydroxide solutions were mixed with distilled water to obtain a clear solution. The pre-mixed omega seeds and silica source were then slowly added together to the clear solution, and the resulting mixture was homogenized using a mortar and pestle to obtain a homogeneous pasty gel. The amount of added omega seeds was set at 10 or 20 wt.% relative to the silica source, and the total weight of all of the (Na, K)-aluminosilicate gels was adjusted to 10 g. Subsequently, the seeded gel was transferred into a Teflon®-lined stainless autoclave and subjected to hydrothermal treatment at 100 °C and 140 °C for different periods under autogenous pressure and static conditions. The synthesis procedure with intermediate addition of omega seeds is as follows. Unseeded (Na, K)-aluminosilicate gels with the same chemical compositions as those used for the initial addition method were prepared according to the procedure described above and then preheated at 140 °C for 5 h in an autoclave under static conditions, followed by rapid quenching of the autoclave with flowing water. After cooling, the autoclave was opened, and the omega seeds (20 wt.% relative to the silica source) were added to the cooled gel, followed by homogeneously mixing the gel with a spatula. Next, the autoclave was sealed and again subjected to hydrothermal treatment at 140 °C for 24 h under autogenous pressure and static conditions. After this treatment, the product was recovered by filtration, washed thoroughly with hot distilled water, and dried at 60 °C overnight.

The solid yield of the obtained product was defined as the weight ratio percentage (g/g × 100) of the dried solid product to the sum of the dry silica, alumina, and calcined seeds in the starting gel.

2.2.4. Characterizations

Both the as-synthesized and calcined forms of the seeds were characterized, whereas the products of the seed-directed, OSDA-free synthesis were characterized in their as-synthesized forms unless otherwise noted. The powder X-ray diffraction (XRD) patterns of the seeds and solid products were collected using a powder X-ray diffractometer (Mac Science MO3XHF22) with Cu Kα radiation (λ = 0.15406 nm, 40 kV, 30 mA) from 2θ = 5 to 40° with scanning steps of 0.02° at a scanning speed of 4°/min. Elemental analysis of the zeolite seeds and products were performed via inductively coupled plasma atomic emission spectroscopy (ICP-AES, Varian Liberty Series II) after dissolving them in a potassium hydroxide solution. The crystal sizes and morphologies of the solid products were observed using a field emission scanning electron microscope (FE-SEM, Hitachi S-900). Nitrogen adsorption–desorption measurements for the zeolite products were performed on a Quantachrome Autosorb-iQ2-MP at −196 °C. Prior to the measurements, all samples were degassed at 400 °C for 6 h under a vacuum. Solid-state ^{29}Si magic angle spinning nuclear magnetic resonance (MAS NMR) spectra were obtained at 59.7 MHz with a pulse width of 2.0 μs and a pulse delay of 100 s, while ^{27}Al MAS NMR spectra were recorded at 78.3 MHz, a pulse width of 1.0 μs, and a recycle delay of 5 s on a spectrometer (Chemagnetics CMS-300). The analysis of the temperature-programmed desorption of ammonia (NH_3-TPD) was performed using a BEL-CAT instrument (BEL Japan Inc.) in order to compare the acidic properties of the zeolite products. Each sample was allowed to adsorb NH_3 at 100 °C (5% NH_3 in He) for 10 min after pre-treatment at 500 °C in a He stream. The desorption behavior was then monitored using a thermal conductivity detector (TCD) while heating the sample to 550 °C at a heating rate of 10 K min^{-1}. The two-fold ammonium-exchange of the calcined seed crystals and as-synthesized product was carried out using 1 M ammonium chloride solution at 80 °C with stirring for about 12 h. The H-form sample was subsequently obtained via calcination of the NH_4^+-form product at 500 °C for 4 h.

2.3. Results and discussion

2.3.1. OSDA-free synthesis and characterization of PAU-type zeolite

The synthesis conditions and results for the OSDA-free synthesis of PAU-type zeolite are listed in Table 2.1. Figure 2.6 (a)–(d) show powder XRD patterns of simulated PAU-type zeolite, as-synthesized ECR-18 seed crystals, calcined seed crystals, and obtained PAU-type zeolite (sample No. 2.6 in Table 2.1), respectively. Clearly, PAU-type zeolite was obtained by the seed-directed approach using OSDA-free K-aluminosilicate gels without any impurities. The XRD pattern of obtained product is similar to that of calcined seed crystals suggesting that the occupied OSDA affects the structure of as-synthesized seed crystals. The SiO_2/Al_2O_3 ratios of the calcined seed crystals, sample Nos. 2.6 and 2.7 are 7.5, 4.8, and 4.5, respectively. In contrast, PAU-type zeolite was not obtained without seed crystals, but other zeolites, Linde W and L with FTC of MER and LTL, respectively were obtained as shown in Figure 2.7. These zeolites were also obtained as by-product as shown in Table 2.1 and optimal gel compositions were quite narrow for the successful OSDA-free synthesis of pure PAU-type zeolite in this time. Linde W was formed at the lower SiO_2/Al_2O_3 ratios and the higher K_2O/SiO_2 ratios as can be seen from the sample Nos. 2.1, 2.2, and 2.8. On the other hand, higher siliceous composition and lower alkalinity result the contamination of zeolite L as can be seen from the sample Nos. 2.3, 2.4, 2.9, and 2.10. Hydrothermal duration time is also important and the crystallinity of the sample No. 2.5 is lower than that of the sample No. 2.6 suggesting that about 72 h of heating is needed to complete crystallization of PAU-type zeolite. However, this duration time is extremely short compare to the previous reports on the synthesis of ECR-18 using OSDAs, which needed over 12 days.[207–209] Rapid synthesis of zeolites by seed-directed method is largely relies on skipping nucleation steps, and details will be discussed following section combined with the results for OSDA-free synthesis of MAZ-type zeolites. Further characterization of obtained PAU-type zeolite was performed using sample No. 2.6.

Table 2.1 Initial gel compositions, reaction times, and results for PAU-type zeolite from K-aluminosilicate gels.

	Initial gel[a]		Condition[b]	Product		
Sample	SiO_2/Al_2O_3	K_2O/SiO_2	Time [h]	Yield (%)[c]	Phase	SiO_2/Al_2O_3
2.1	6	0.50	48	-	MER	-
2.2	6	0.55	48	-	MER	-
2.3	10	0.40	48	-	PAU+LTL	-
2.4	10	0.45	72	-	LTL+MER+PAU	-
2.5	10	0.50	48	82.1	PAU (low crystalinity)	-
2.6	10	0.50	72	83.2	PAU	4.8
2.7	10	0.55	72	80.5	PAU	4.5
2.8	10	0.60	24	-	PAU+MER	-
2.9	15	0.50	72	-	PAU+LTL	-
2.10	20	0.50	72	-	PAU+LTL	-

[a] $H_2O/SiO_2 = 20$, seeds: 10wt% to SiO_2, [b] Static, temperature:135 °C, [c] Solid yield

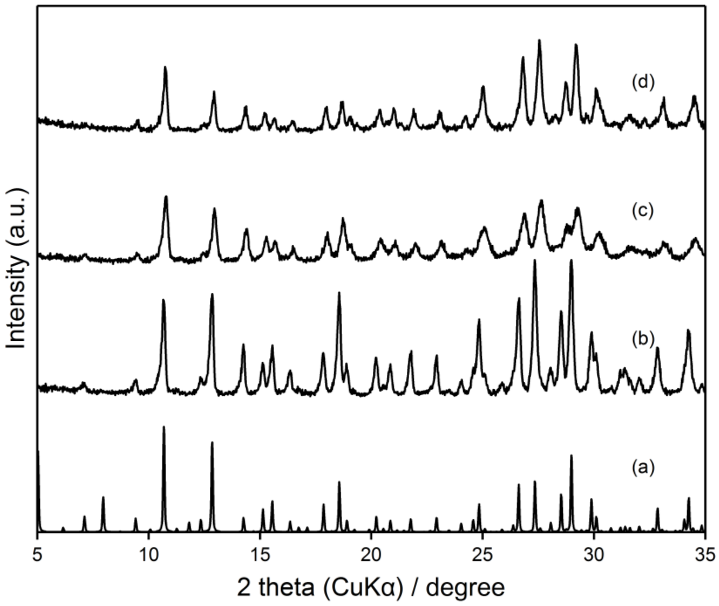

Figure 2.6 Powder XRD patterns of (a) simulated PAU, (b) as-synthesized ECR-18 seed crystals, (c) calcined ECR-18, and (d) obtained PAU-type zeolite (sample No. 2.6).

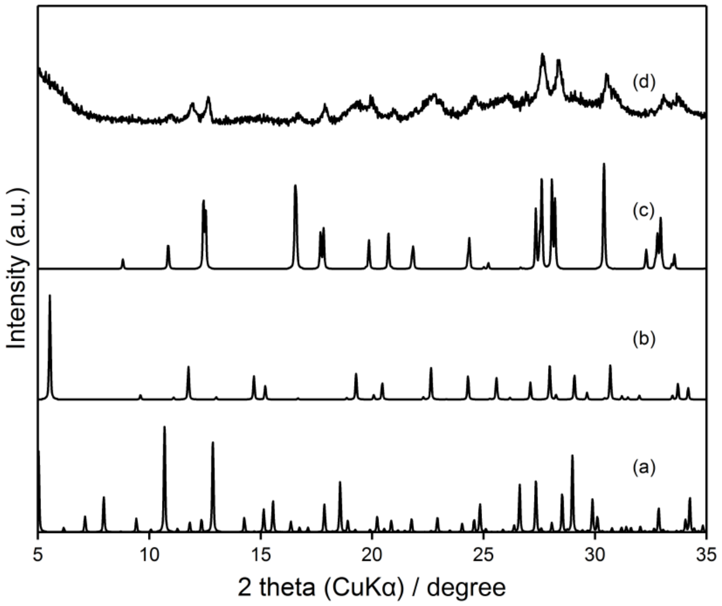

Figure 2.7 Simulated XRD patterns of (a) PAU-, (b) LTL-, and (c) MER-type zeolites and (d) powder XRD pattern of the product synthesized without seed crystals using same initial gel with product No. 2.6.

The solid-state ^{27}Al and ^{29}Si MAS NMR spectra of the product were shown in Figure 2.8 (a) and (b), respectively. It can be confirmed that all of aluminum species are incorporated into the zeolite framework (δ = *ca.* 58 ppm), and extra-framework aluminum species (δ = *ca.* 0 ppm) are hardly detected in the ^{27}Al MAS NMR spectrum. The ^{29}Si MAS NMR spectrum shows four main signals at –105, –100, –95, and –90 ppm that can be assigned to silicon atoms surrounded by 1, 2, 3, and 4 aluminum atoms, respectively. The SiO_2/Al_2O_3 ratio calculated from the integrated intensity ratios of the ^{29}Si MAS NMR spectrum is 3.7 with good agreement with the values obtained from the chemical analysis of 4.5. The products have aluminum-rich composition compare to the seed crystals (7.5 by chemical analysis), therefore, the hydrophilic properties of the products are expected. The water adsorption–desorption isotherms of the product and the seed crystals are shown in Figure 2.9. As expected, the product showed superior water uptake to the seed crystals suggesting good porosity and higher hydrophilicity of the product. Pore characteristics of PAU-type zeolites can be investigated only by water adsorption–desorption measurements, because, owing to its small pore sizes, PAU-type zeolites do not adsorb nitrogen at –196 °C (data not shown).

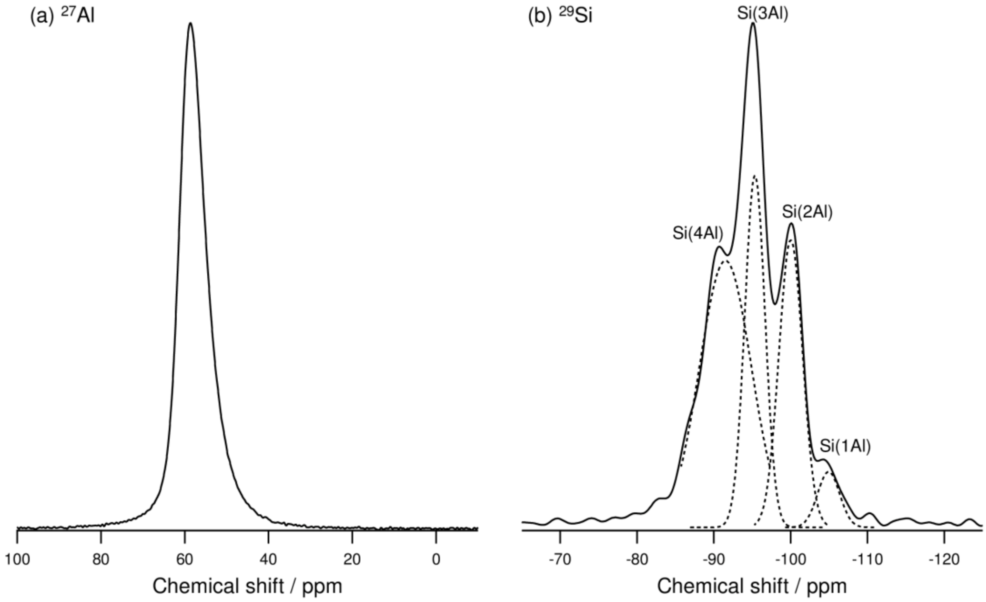

Figure 2.8 Solid-state (a) ^{27}Al and (b) ^{29}Si MAS NMR spectra of the product.

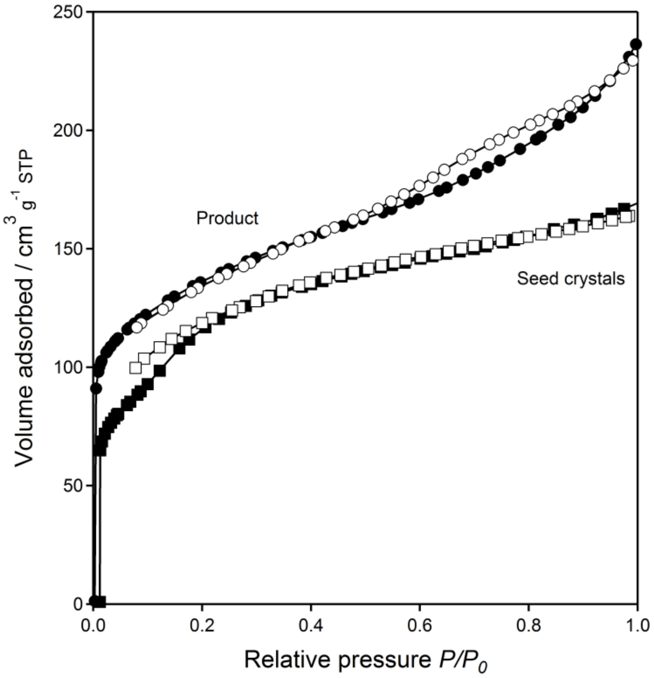

Figure 2.9 Water adsorption–desorption isotherms of the product (cuircle) and the seed crystals (square). Solid and Open simbols indicate adsorption and desorption brunch, respectively.

The SEM images of the product and the seed crystals are shown in Figure 2.10. Clearly, the particle sizes of the obtained product are larger than those of seed crystals suggesting that new zeolites were grown on the surfaces of seed crystals. The morphologies of these particles are similar reflecting the space group of PAU-type zeolite, $Im\bar{3}m$.

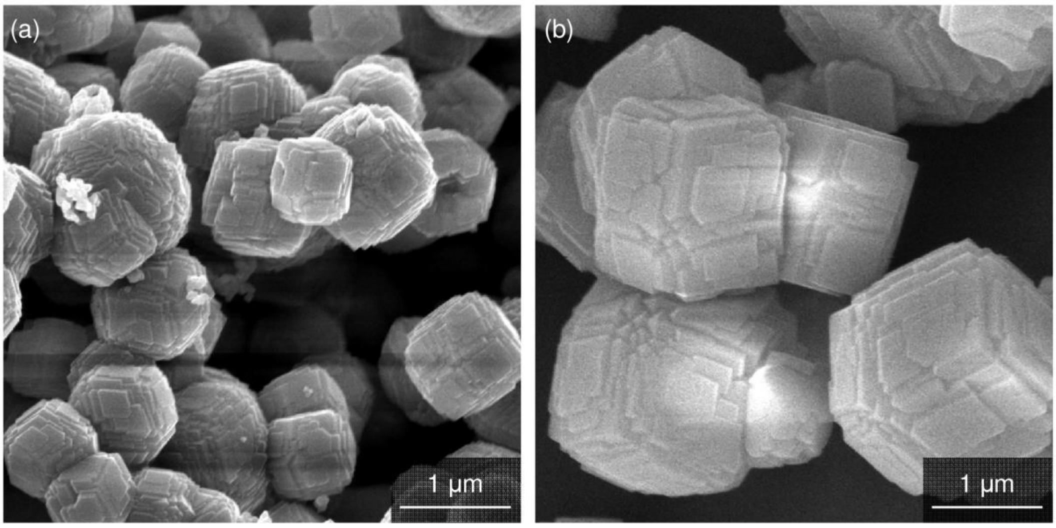

Figure 2.10 SEM images of (a) calcined seed crystals and (b) obtained PAU-type zeolite.

2.3.2. OSDA-free synthesis and characterization of MAZ-type zeolite

The chemical compositions of the initial gels, the reaction conditions, and the products obtained from different attempts to synthesize MAZ-type zeolite are summarized in Table 2.2. Zeolite T was obtained without seed crystals in all cases (see sample Nos. 2.11, 2.13, 2.14, 2.18, 2.20, 2.22, and 2.24 in Table 2.2), as confirmed by the XRD analysis. However, when the gels with relatively higher SiO_2/Al_2O_3 ratios were used, zeolite L was crystallized as a byproduct (sample Nos. 2.20 and 2.24) along with zeolite T. Figure 2.11 shows the XRD patterns for sample No. 2.15 at different times during the hydrothermal treatment at 100 °C. After 96 h, the obtained product was identified as amorphous, and the omega seed crystals remained undissolved; after 144 h, the amount of amorphous matter slightly decreased, but the growth of MAZ-type zeolite crystals did not proceed judging from the solid yield (only 19.7 wt.%), which was much lower than the solid yield obtained at 96 and 192 h (43.7 and 39.2 wt.%, respectively). If the MAZ-type zeolite had crystallized after 144 h of hydrothermal treatment, the solid yield would have been higher than the same obtained at 96 h. On the basis of the XRD patterns and the solid yields, however, it was concluded that the amorphous matter was dissolved in the liquid phase after 144 h. After 192 h of hydrothermal treatment, zeolite T was predominantly formed, while only a relatively small amount of seed crystals remained. Judging from these results and SEM image shown in Figure 2.12, the seed crystals may have been covered by the amorphous material for a long time in the reaction at 100 °C. Liquid-mediated crystal growth mechanism has been proposed for the seed-directed synthesis of zeolite beta, and contact between seed crystals and liquid phase is considered to be important.[184,222] In the present system, the amorphous materials covering seed crystals may prevent contact between them. Therefore, more rapid dissolution of the amorphous materials was required in order to expose and/or disperse the seeds at the interface of the amorphous material and the liquid phase. Although some previous reports claimed that a seeding method is effective even in steam-assisted crystallization systems, the amount of seed crystals required in these reports are quite small and secondary nucleation is estimated to occur.[223,224]

Table 2.2 Conditions for the synthesis of MAZ-type zeolite via initial and intermediate addition of seeds, along with the products obtained for each.[221]

	Initial gel[a]		Seed crystals		Condition[b]		
Sample	SiO_2/Al_2O_3	$(Na_2O+K_2O)/SiO_2$	Amount (wt.%)	Timing	Temp. [°C]	Time [h]	Phase
2.11	28	0.30	0	-	140	72	T+am
2.12	28	0.30	20	Intermediate	140	24	MAZ
2.13	28	0.35	0	-	100	168	T
2.14	28	0.35	0	-	140	120	T
2.15	28	0.35	10	Initial	100	144	am+omega
2.16	28	0.35	20	Initial	140	48	T+MAZ
2.17	28	0.35	20	Intermediate	140	24	MAZ+T
2.18	40	0.40	0	-	140	25	T
2.19	40	0.40	20	Intermediate	140	24	MAZ+T
2.20	40	0.43	0	-	140	25	T+L
2.21	40	0.43	20	Intermediate	140	24	MAZ+T
2.22	50	0.35	0	-	140	25	T
2.23	50	0.35	20	Intermediate	140	24	MAZ
2.24	50	0.40	0	-	140	25	T+L
2.25	50	0.40	20	Intermediate	140	24	MAZ

[a]$H_2O/SiO_2 = 20$, [b]Static

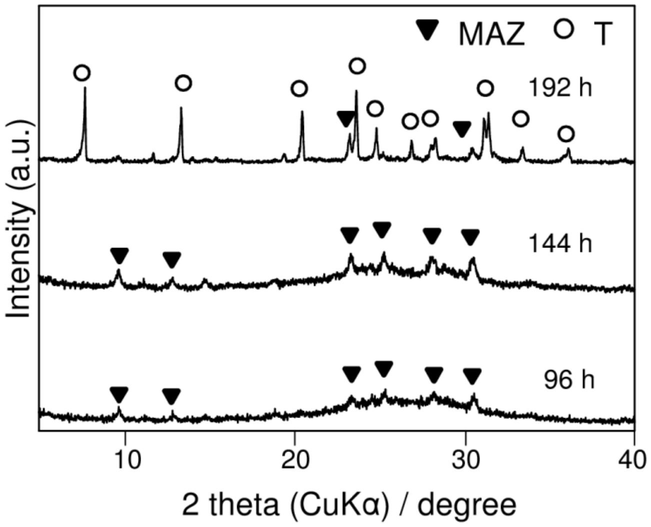

Figure 2.11 Evolution of the XRD patterns of sample No. 2.15.[221]

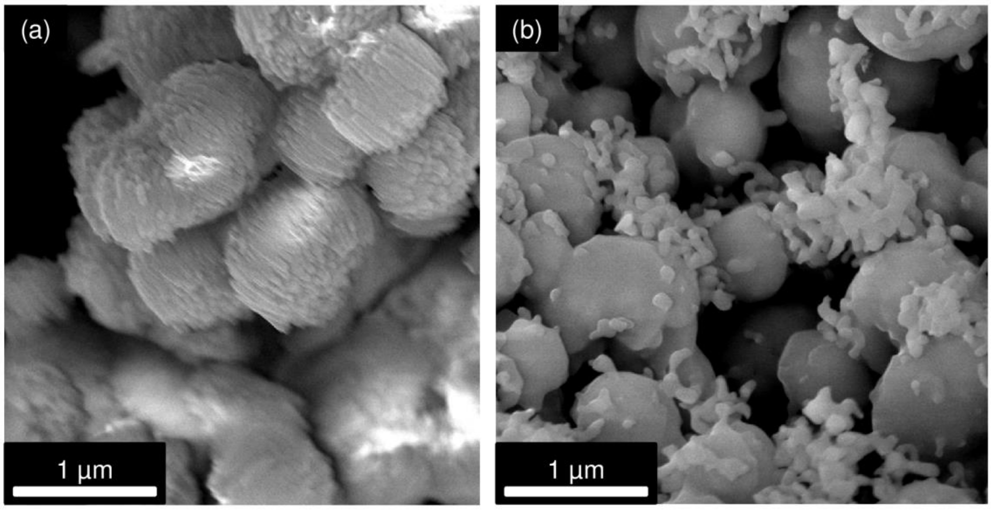

Figure 2.12 SEM images of (a) omega seed crystals[221] and (b) sample No. 2.15.

To address this issue, the reaction temperature was raised to 140 °C and the amount of seeds added to the gel was increased to 20 wt.% using the same gel composition as that of sample No. 2.15 (sample No. 2.16 in Table 2.2). XRD patterns of sample No. 2.16 over time and SEM images of the sample No. 2.16 product after 48 h of hydrothermal treatment are shown in Figure 2.13 (a) and (b), respectively. The XRD pattern of sample No. 2.16 after 48 h of hydrothermal treatment indicated that the product was a mixture of zeolite T and a MAZ-type zeolite; this result was also supported by the SEM images, in which two different morphologies, spherical and rod-like, can be attributed to two zeolites MAZ and T, respectively. It is worth mentioning here that even shorter duration of hydrothermal treatment (e.g. 28 h) of sample No. 2.16 was identified as mainly zeolite T with MAZ-type zeolite as a by-product suggesting that a fast nucleation of zeolite T occurs before the crystal growth of MAZ-type zeolite. The higher synthesis temperature was assumed to accelerate both the dissolution of the amorphous matter and the crystal growth of the MAZ-type zeolite; however, it should also be noted that the spontaneous nucleation of zeolite T occurred simultaneously. Therefore, to obtain pure MAZ-type zeolite, it is necessary to preferentially grow the MAZ-type zeolite prior to spontaneous nucleation and crystal growth of zeolite T with the use of increased amount of seeds (20 wt.% relative to the silica source).

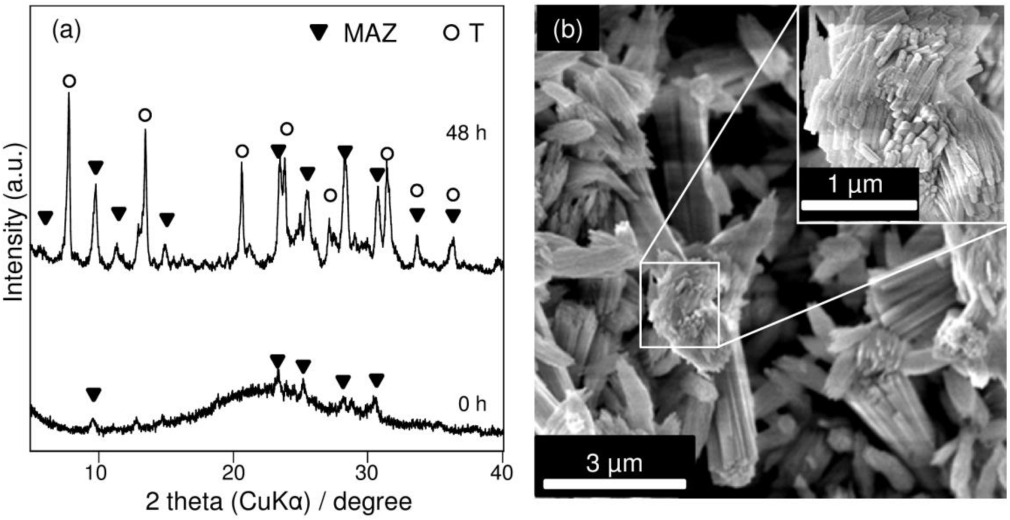

Figure 2.13 (a) Evolution of the XRD patterns of sample No. 2.16 and (b) FE-SEM images of the same sample after 48 h at different magnifications.[221]

Previously, it was confirmed that the intermediate addition of zeolite beta seeds after preheating of the seed-free gel significantly enhanced the crystallization rate of beta.[184] The addition of seeds to partially dissolved gel after preheating leads to immediate contact between liquid phase and the seeds, which provides an active surface for crystal growth. As a result, new crystals grow on the surface of the seeds by consuming the silicate and aluminosilicate precursors in the liquid phase. Thus, applying the technique of intermediate seed addition was expected to enable completion of crystal growth of the pure MAZ-type zeolite prior to crystal growth of other undesired phases. Therefore, reactions were performed using this method with the same gel compositions in which the zeolite T was synthesized at 140 °C, as summarized in

Table 2.2 (sample Nos. 2.12, 2.17, 2.19, 2.21, 2.23, and 2.25). The unseeded gels were first preheated at 140 °C for 5 h and then seeded. Figure 2.14 shows the evolution of XRD patterns of the products for sample No. 2.17 (Table 2.2) from 0–24 h of crystallization time (after seeding). More rapid crystal growth of the MAZ-type zeolite was achieved, and as the crystallization time was prolonged, the intensities of the MAZ-type zeolite peaks in the XRD pattern gradually increased. However, the spontaneous nucleation of zeolite T occurred after 4 h of hydrothermal treatment, and subsequently, slow crystal growth of the undesired zeolite was observed. Similar results were obtained for sample Nos. 2.19 and 2.21 (Table 2.2). On the other hand, for sample Nos. 2.12, 2.23, and 2.25, which were prepared using gels with different chemical compositions from those used to prepare sample Nos. 2.17, 2.19, and 2.21, nearly pure MAZ-type zeolite was successfully obtained. The representative XRD pattern and SEM images for sample No. 2.23 are shown in Figure 2.15 (a) and (b), respectively. The peak intensity in the XRD pattern of sample No. 2.23 was slightly lower than that of the seeds, and a trace amount of impurity attributed to zeolite T was observed both in the XRD pattern and the SEM images. It is also worth noting, however, that the required time for hydrothermal treatment was found to be much shorter than that in previous reports.[217–220] Furthermore, the gel compositions used to produce the MAZ-type zeolites (sample Nos. 2.12, 2.17, 2.19, 2.21, 2.23, and 2.25 in Table 2.2) were the same as those used for the synthesis of zeolite T (sample Nos. 2.11, 2.14, 2.18, 2.20, 2.22, and 2.24 in Table 2.2); that is, the crystal growth of MAZ-type zeolites in this study follows the CBU hypothesis (Figure 2.5).

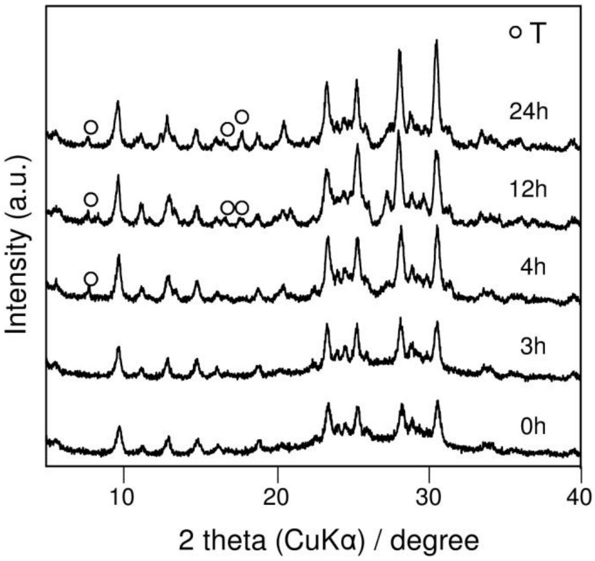

Figure 2.14 Evolution of the XRD patterns of sample No. 2.17.[221]

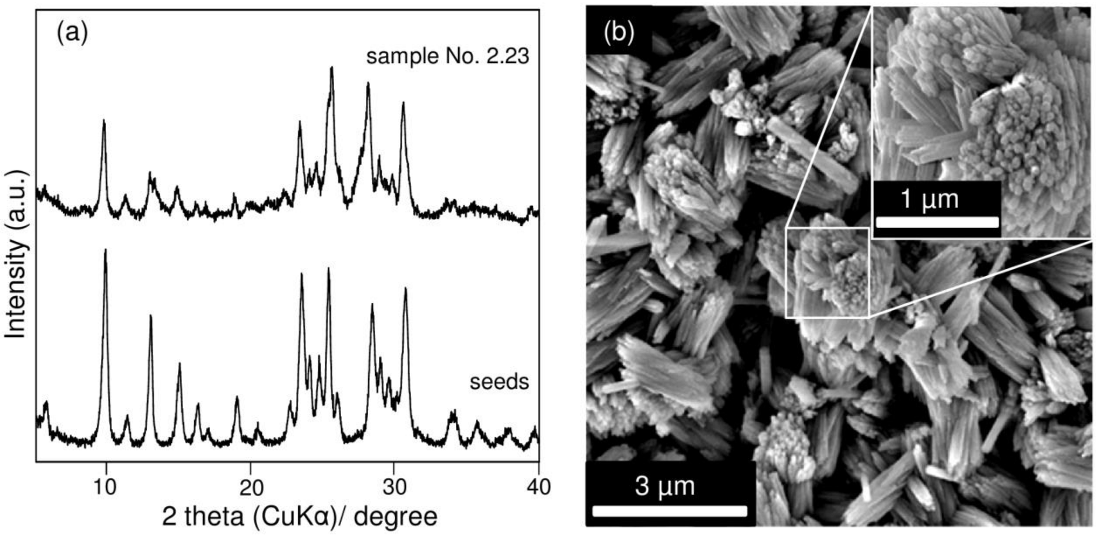

Figure 2.15 (a) XRD patterns of the seed crystals and sample No. 2.23, and (b) FE-SEM images of sample No. 2.23 at different magnifications.[221]

Detailed characterization of sample No. 2.23 and the omega seed crystals was then accomplished by obtaining their ^{27}Al and ^{29}Si MAS NMR spectra, N_2 adsorption–desorption isotherms, and NH_3-TPD measurements. The solid-state ^{27}Al and ^{29}Si MAS NMR spectra for these materials are shown in Figure 2.17 (a) and (b), respectively. Owing to the presence of two different T-sites in the framework of MAZ-type zeolite (see Figure 2.16),[225] both ^{27}Al MAS NMR spectra exhibited two signals attributed to the framework aluminum in T_1 (~60 ppm) and T_2 (~55 ppm) sites. In addition, extra-framework aluminum species (~0 ppm) were hardly detected in both samples. The integrated intensity ratios of these two signals are slightly different between sample No. 2.23 and the seed crystals, suggesting that aluminum is selectively incorporated in the T_2 sites in sample No. 2.23 as a result of the OSDA-free synthesis. The ^{29}Si MAS NMR spectra showed five main signals at approximately −110, −105, −100, −95, and −90 ppm that were assigned to silicon atoms surrounded by 0, 1, 2, 3, and 4 aluminum atoms, respectively. The SiO_2/Al_2O_3 ratios calculated from the integrated intensity ratios of the ^{29}Si MAS NMR spectra were 6.4 and 5.0 for sample No. 2.23 and the seed crystals, respectively, which are in good agreement with the values obtained from the chemical analysis (6.4 and 5.6, respectively). Interestingly, sample No. 2.23 had a relatively high SiO_2/Al_2O_3 ratio compared to that of the seed crystals. In the seed-directed method, the SiO_2/Al_2O_3 ratios of the products are strongly governed by the initial gel compositions, which are similar to those of the products synthesized from the unseeded gels.[200] In this study, the SiO_2/Al_2O_3 ratio of zeolite T (sample No. 2.22) obtained from an unseeded gel was 7.4, as evidenced by the chemical analysis, which is higher than that of the seed crystals ($SiO_2/Al_2O_3 = 5.0$); as a result, the SiO_2/Al_2O_3 ratios of the MAZ-type zeolites obtained using the seed-directed method were higher than those of the seeds. A similar result was reported for the seed-directed, OSDA-free synthesis of MTW-type zeolites using beta zeolite seed crystals, which will be shown in the following section. These results indicate that seed crystals with a lower SiO_2/Al_2O_3 ratio than that of the zeolite synthesized from the seed-free gel are effective in some cases.

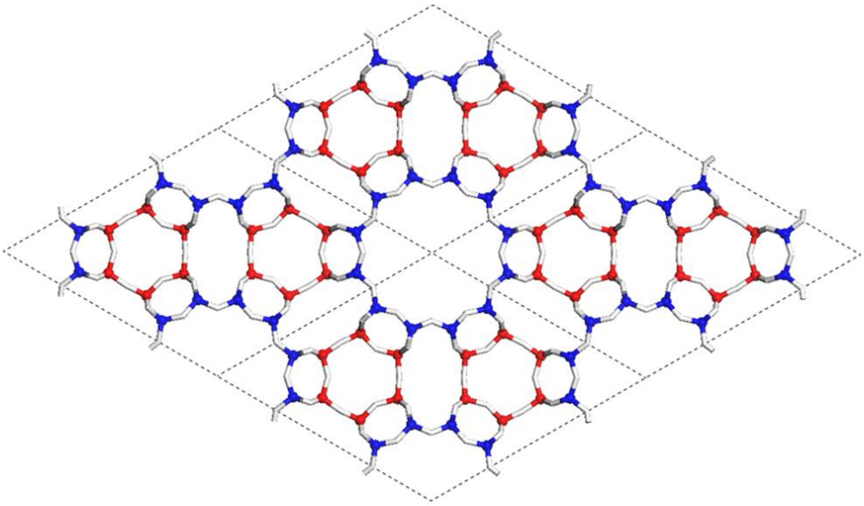

Figure 2.16 Crystal structure of MAZ-type zeolite viewed along [001]. T1 and T2 sites are colored with blue and red, respectively.[221]

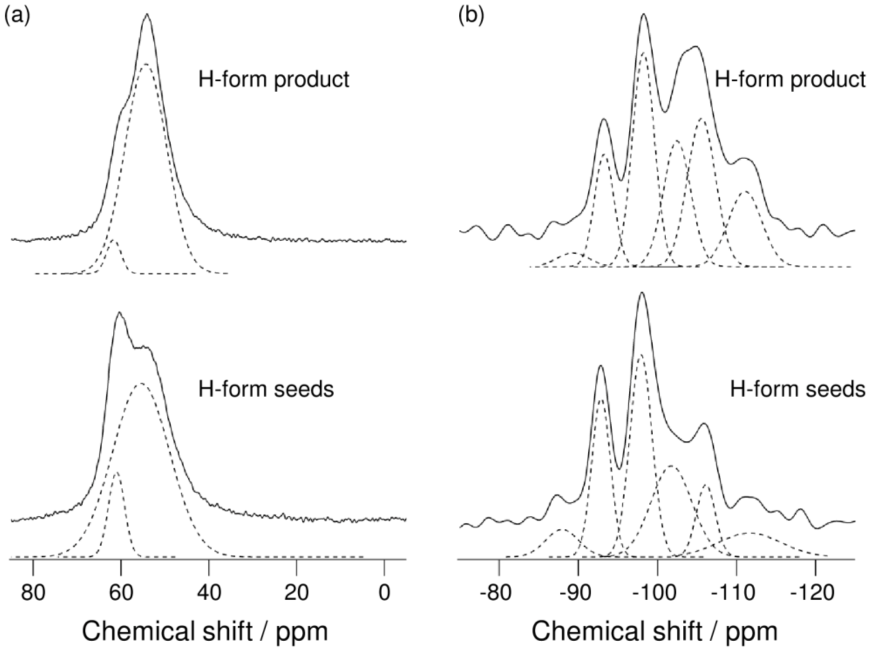

Figure 2.17 (a) ^{27}Al and (b) ^{29}Si MAS NMR spectra of the H-form seeds and sample No. 2.23.[221]

Figure 2.18 shows the nitrogen adsorption–desorption isotherms of H-form of sample No. 2.23 and the omega seed crystals. Both isotherms are classified as IUPAC type I with a hysteresis loop at higher relative pressures due to the presence of interparticle mesopores as their morphology has bundles of small needle type crystals (*cf*. Figure 2.12 (a), Figure 2.13 (b) and Figure 2.15 (b)) that may provide these interparticle mesopores. Sample No. 2.23 possesses a higher Brunauer–Emmett–Teller (BET) surface area (455 m^2 g^{-1}), micropore surface area (392 m^2 g^{-1}), and micropore volume (0.15 cm^3 g^{-1}) than those of the seed crystals (314 m^2 g^{-1}, 236 m^2 g^{-1}, and 0.093 cm^3 g^{-1}, respectively) and previously reported values (422 m^2 g^{-1}, (micropore surface area was not shown), and 0.14 cm^3 g^{-1}, respectively).[218] It can also be seen from the isotherms that the interparticle mesopore surface area of the product (63 m^2 g^{-1}) is smaller than that of the seed crystals (78 m^2 g^{-1}) owing to the larger-sized crystals of the sample. It should be noted that the pore characteristics of the seed crystals are slightly smaller than the reported values,[218] which may be due to the partial collapse of the framework structure during calcination, as evidenced from the XRD patterns.

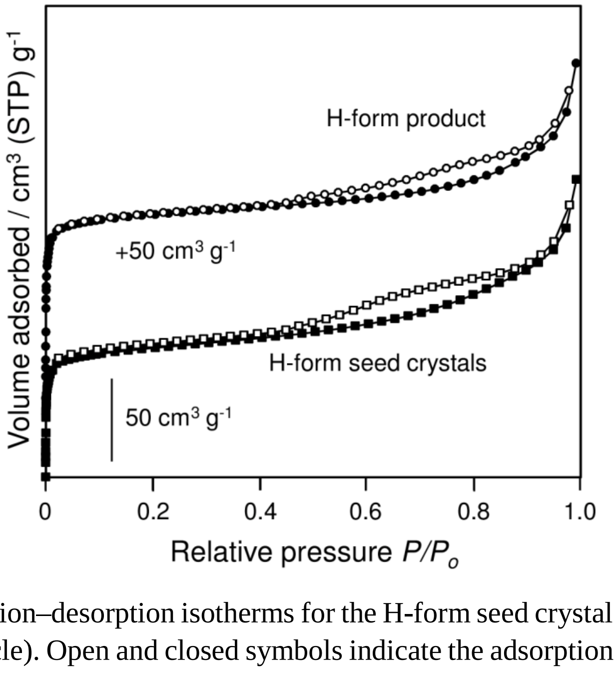

Figure 2.18 N_2 adsorption–desorption isotherms for the H-form seed crystals (square) and H-form sample No. 2.23 (cuircle). Open and closed symbols indicate the adsorption and desorption points, respectively.[221]

Figure 2.19 presents the NH_3-TPD profiles of the H-form of the omega seed crystals and sample No. 2.23. Ammonia desorbed in the temperature range of 100–

300 °C was attributed to the physisorbed ammonia molecules that were either adsorbed on the external surfaces of the zeolite crystals or weak adsorption sites in the MAZ-framework. The desorption of ammonia at higher temperature range was attributed to ammonia molecules strongly adsorbed on the brønsted acid sites in the framework of MAZ-type zeolites. It should be noted from the figure that the ammonia desorbed at higher temperature was relatively higher for sample No. 2.23 indicating that the sample No. 2.23 has got stronger acid sites compared to the omega seed crystals. The total acidity was mainly calculated based on the amount of strongly adsorbed ammonia molecules and the values were found to be 1.14 and 0.93 mmol g^{-1} for sample No. 2.23 and the seed crystals, respectively. The excellent solid acidity and pore characteristics of the MAZ-type zeolite obtained using the OSDA-free synthesis technique suggest that this zeolite has the significant potential for use as catalysts and adsorbents.

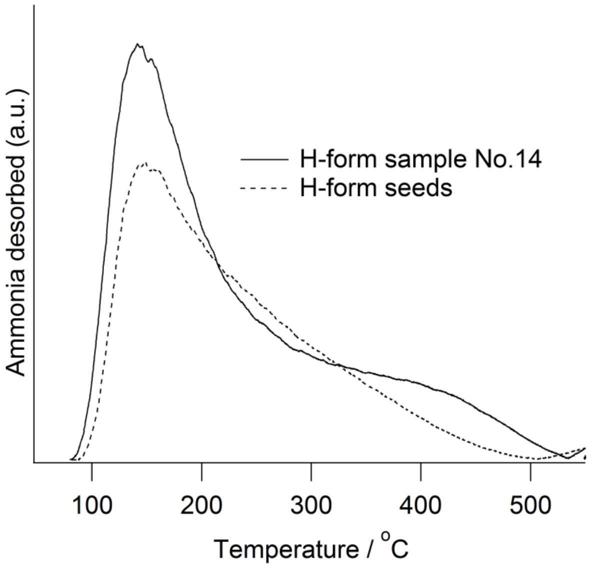

Figure 2.19 NH_3-TPD profiles of H-form sample No. 2.23 (solid line) and the H-form seed crystals (dashed line).[221]

2.3.3. Discussion on the zeolite structures and synthesis conditions

In this chapter, PAU- and MAZ-type zeolites have been synthesized using K-, and (Na,K)-aluminosilicate gels, respectively. These inorganic cations might play important roles in the OSDA-free system. For example, Suzuki et al. in Okubo-group revealed the cooperative effect of sodium and potassium cations on the synthesis of ferrierite (FER-type aluminosilicate zeolite), and discussed about their roles in the precursor formation and the crystallization.[84] They concluded that potassium contributed to the formation of building units of ferrierite, while sodium contributed to the final crystallization to order the building units. Subsequently, Iwama et al. reported that intermediate addition of potassium cation hinders the crystallization of zeolite A (LTA-type aluminosilicate zeolite), but promotes LSX (FAU-type aluminosilicate zeolite with $SiO_2/Al_2O_3 = 2$).[85]

Figure 2.20 shows the XRD patterns of the products synthesized using ECR-18 seed crystals with the variation of $K_2O/(K_2O+Na_2O)$ ratios (other conditions are same as the sample No. 2.6 in Table 2.1). PAU-type zolite was not obtained with the presence of sodium cation, and other zeolites such as Linde W, Na-P1 (GIS-type), and analcime (ANA-type) were obtained in shorter times of hydrothermal treatment (40 h) compare to the K-aluminosilicate systems (72 h). Sodium cation seems to promote sponteneous nucleation or crystal growth of by-products. Moreover, Figure 2.21 represents the XRD patterns of the products synthesized using omega seed crystals with the variation of $K_2O/(K_2O+Na_2O)$ ratios (other conditions are same as the sample No. 2.17 in Table 2.2). Unknown phase appeared without pottassium cations (see Figure 2.21 (c)) and excess amout of pottasium cations promoted nucleation of zeolite L, therefore, clearly, the $K_2O/(Na_2O+K_2O)$ ratio should be optimized to obtain pure MAZ-type zeolite. Both results about synthesis of PAU- and MAZ-type show an important role of pottassium and sodium cations, and their role might be similar to that in the previous works mentioned above. For example, presence of pottasium cation seems to promote formation of double 6-MR units.[85] However, details are not fully understood yet.

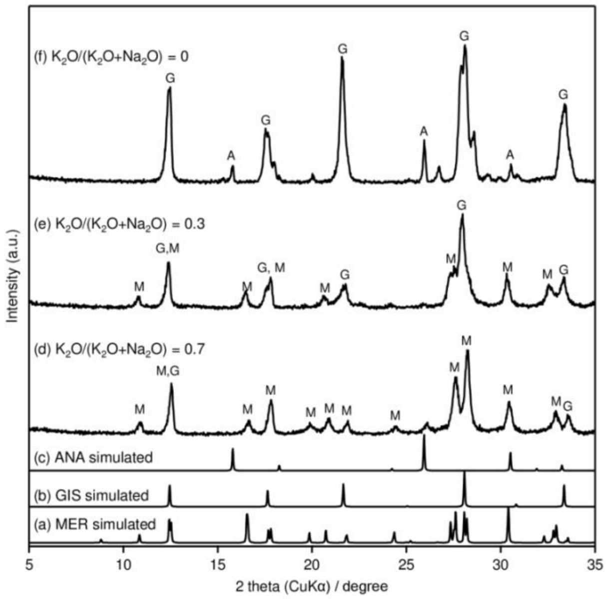

Figure 2.20 XRD patterns of the products synthesized using ECR-18 seed crystals with the variation of $K_2O/(K_2O+Na_2O)$ ratios. $SiO_2/Al_2O_3 = 10$, $H_2O/SiO_2 = 20$, $(K_2O+Na_2O)/SiO_2 = 0.5$, 135 °C × 40 h. M, G, and A indicate Linde W (MER), Na-P1 (GIS), and analcime (ANA), respectively.

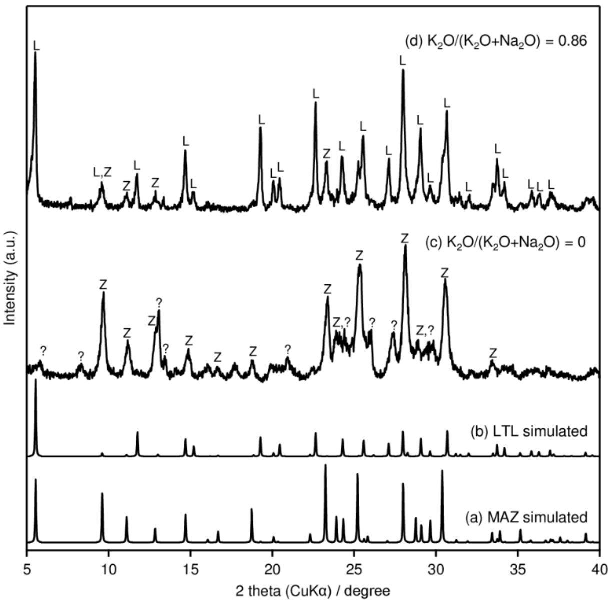

Figure 2.21 XRD patterns of the products synthesized using omega seed crystals with the variation of $K_2O/(K_2O+Na_2O)$ ratios. $SiO_2/Al_2O_3 = 28$, $H_2O/SiO_2 = 20$, $(K_2O+Na_2O)/SiO_2 = 0.35$, 140 °C × 24 h, (seeds: intermediate addition). Z, L, and ? indicate MAZ-type zeolite, zeolite L (LTL), and unknown phase, respectively.

2.4. Conclusion

PAU- and MAZ-type zeolites can be synthesized via the seed-directed, OSDA-free synthesis under a surprisingly short time of hydrothermal treatment compare to the conventional synthesis method using OSDAs. The obtained results clearly demonstrate the validity and the wide applicability of the CBU hypothesis, even for zeolites with cage-type, 4-MR-rich frameworks in the K- and (Na, K)-aluminosilicate systems. Alkaline metal cations play a crucial role in the crystal growth of these zeolites. Moreover, the intermediate addition of seeds and subsequent high-temperature hydrothermal treatment is effective for the production of pure MAZ-type zeolites without spontaneous nucleation and crystal growth of zeolite T.

Chapter 3. Synthesis of MTW-Type Aluminosilicate Zeolite Using Seeds with Different Structures

3.1. Introduction

ZSM-12 is an aluminosilicate zeolite with FTC of MTW, which has a one-dimensional 12-MR channel along the *b* axis[62,226] and has been expected to be a useful catalyst in cracking of hydrocarbons or in other petrochemical processes.[227–229] In addition, Kaliaguine et al. have found that ZSM-12 can be a superior candidate as adsorbents for hydrocarbon trap to reduce cold-start emissions of automotive exhaust due to its high trapping capacity and elevated desorption temperature.[230,231] However, OSDAs such as methyltriethylammonium[232] and TEA[233] have been essential to synthesize ZSM-12. MTW-type zeolite has four CBUs of *bik*, *cas*, *jbw*, and *mtw* according to the IZA-SC,[62] and MFI-type zeolite has common CBU, *cas* as shown in Figure 3.1 (a). Therefore, considering the CBU hypothesis proposed above, MTW-type zeolite should be obtained from a gel that yields ZSM-5 (MFI) when the gel is heated without seeds for a long time.[200]

In this section, MTW-type zeolites have been synthesized without using OSDA via seed-directed hydrothermal treatment. The optimal initial gel compositions and reaction conditions are investigated for the successful synthesis of pure MTW-type zeolites. Obtained products are characterized in detail and their characteristic pore systems are shown. Moreover, MTW-type zeolite can be synthesized using zeolite beta (*BEA) seed crystals, which has different structure from MTW-type, but a similar projection plane. The Correlation of CBUs for MTW, MFI, and *BEA is shown in Figure 3.1 (b).

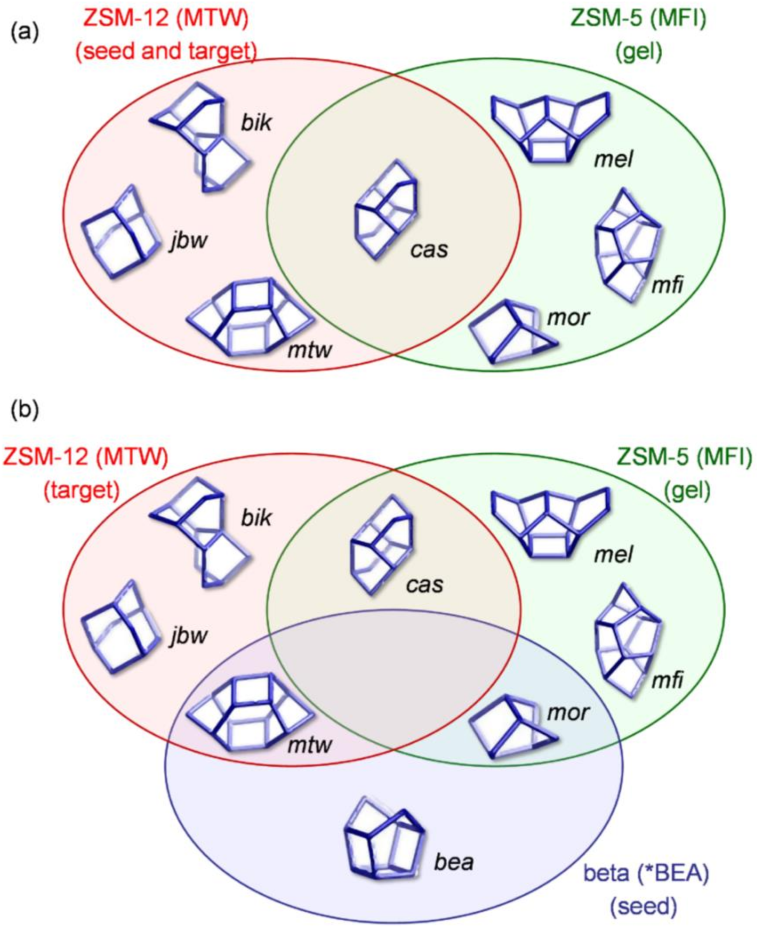

Figure 3.1 Correlation of common CBUs for (a) MFI and MTW and (b) MFI, *BEA, and MTW.[136]

3.2. Experimental

3.2.1. Chemicals

For the synthesis of the zeolite ZSM-12 seed crystals, Ludox® HS-40 (40 wt.% silica in water, Sigma-Aldrich Co.) as the silica source, TEAOH solution (35 wt.% in water, Aldrich) as the OSDA, sodium aluminate ($NaAlO_2$, Wako Pure Chemical Industries, Ltd.) as the aluminum source were used as provided, while Mizukasil® P707 (Mizusawa Industrial Chemicals, Ltd.) was used as the silica source for zeolite beta seed crystals. For the OSDA-free synthesis of MTW-type zeolite, aluminum powder (Al, 99.5%, Wako) was used as the aluminum source. For the OSDA-free synthesis of MTW-type zeolites, sodium hydroxide solution (NaOH, 50 w/v% in water, Wako) and lithium bromide (LiBr, Wako) were used in addition to the above raw materials.

3.2.2. Preparation of ZSM-12 and beta seed crystals

ZSM-12 for seed crystals was prepared using TEAOH as OSDA following a reported procedure.[234] The initial gel composition was 0.79 Na_2O: 6.4 $(TEA)_2O$: 80 SiO_2: Al_2O_3: 1040 H_2O. Sodium aluminate was dissolved in 35 wt.% aqueous TEAOH solution. Colloidal silica was then added to the solution, and the mixture was stirred until homogeneous gel was obtained. The gel was heated at 160 °C for 5 days in a Teflon®-lined autoclave (#4749, Parr Instrument Co.) under static conditions. The product was collected by filtration, washed with distilled water, dried at 60 °C, and calcined at 550 °C for 10 h. Zeolite beta seed crystals were prepared by the hydrothermal treatment of the Na-aluminosilicate gel in the presence of TEAOH with the following chemical composition: 1.25 Na_2O: 6.12 TEA_2O: Al_2O_3: 35 SiO_2: 490 H_2O. Mizukasil was slowly added into the solution of TEAOH and sodium aluminate. A mortar and pestle were then used to mix the solution and obtain a homogenous aluminosilicate gel. Aluminosilicate gel slurry (40 g) was transferred to a stainless-steel autoclave with a volume of 60 mL, and was then subjected to hydrothermal treatment at 165 °C for 96 h under 20 rpm rotation in an oven under autogeneous pressure. The product was then filtered, washed thoroughly with hot distilled water, dried at 60 °C, and calcined at 550 °C for 10 h under dry air flow.

3.2.3. OSDA-free synthesis of MTW-type zeolites

The OSDA-free syntheses of MTW-type zeolites were carried out by the addition of calcined ZSM-12 (SiO_2/Al_2O_3 = 101 analyzed by ICP-AES) and zeolite beta seeds (SiO_2/Al_2O_3 = 24.0) to the (Li, Na)- and Na-aluminosilicate gels having the following chemical compositions: a Li_2O: b Na_2O: c Al_2O_3: SiO_2: d H_2O, where a = 0.075, b = 0.1875, c = 0.0167–0.1, and d = 16 and x Na_2O: y Al_2O_3: SiO_2: z H_2O, where x = 0.125–0.175, y = 0.0083–0.0125, and z = 8.3–11.7, respectively. The Na-aluminosilicate gel was prepared by the following procedure: sodium aluminate and sodium hydroxide solution were mixed in distilled water to obtain a clear solution. To obtain the (Li, Na)-aluminosilicate gels, lithium bromide was added to the solution. Then, calcined seeds and Cab-O-Sil were slowly added together to the clear solution, and the resulting mixture was homogenized using a mortar and pestle to obtain a pasty gel. The added amount of seeds was set to 10 wt.% relative to the silica source, and the total weight of all aluminosilicate gels was adjusted to 18 g. Then, the gel with seed crystals was transferred to a 23 mL Teflon®-lined stainless-steel autoclave (#4749, Parr) and subjected to hydrothermal treatment at 140–165 °C for different heating periods under static conditions with autogeneous pressure. After the treatment, solid products were recovered by filtration, carefully washed with hot distilled water until the pH of the filtrate becomes neutral and thereafter dried at 60 °C overnight.

3.2.4. Characterizations

In the present study, ZSM-12 and beta seeds were characterized in their calcined forms, whereas the products of the seed-directed, OSDA-free synthesis were characterized in their as-synthesized forms unless otherwise noted. The powder X-ray diffraction (XRD) patterns of the seeds and the solid products were collected using an X-ray diffractometer (Mac Science MO3XHF22) with Cu K_α radiation (λ = 0.154 nm, 40 kV, 30 mA) from 5 to 40° in 2θ with scanning steps of 0.02° at a scanning speed of 2°/min. Crystal size and morphology were observed by a field-emission scanning electron microscope (FESEM, Hitachi S-4800) at an accelerating voltage of 1 kV. Elemental analyses were performed by an inductively coupled plasma-atomic emission spectrometer (ICP-AES, Varian Liberty Series II) after dissolving the seeds or the solid products in a hydrofluoric acid or potassium hydroxide solution. Solid-state ^{27}Al MAS NMR spectra were collected with a JEOL CMX-300 spectrometer at a resonance frequency of 78.3 MHz, a pulse width of 1.0 μs, and a recycle delay of 5 s. Samples were spun at 10 kHz in a standard 4-mm zirconia rotor. The chemical shifts were referenced to 1 M aluminum nitrate (δ = 0 ppm). Prior to NMR measurements, all samples were finely ground and hydrated in a desiccator with a saturated ammonium chloride solution for 72 h at room temperature. Nitrogen adsorption‒desorption measurements were carried out using Quantachrome Autosorb-1 at -196 °C. Prior to the measurements, all samples were preheated at 400 °C for 4 h under vacuum. Water adsorption‒desorption measurements were performed by using Hydrosorb 1000 (HS-2 model, Quantachrome Instruments 2001) at 25 °C after preheating the samples at 400 °C for 12 h under vacuum. Temperature-programmed desorption of ammonia (NH_3-TPD) was performed using a BEL-CAT instrument (BEL Japan Inc.) to compare the acidic behavior of the zeolite products. The sample was allowed for NH_3 adsorption at 100 °C (5% NH_3 in He) for 10 min after pre-treatment at 500 °C in a He stream. Then, the desorption behavior was monitored by a thermal conductivity detector (TCD) while heating the sample to 550 °C at a heating rate of 10 K min^{-1}. The ion-exchange of as-synthesized product was carried out in 1 M ammonium chloride solution at 80 °C under stirring for 12 h, and repeated twice. Subsequently, the H-form sample was obtained by the calcination of NH_4-form product (Product No. 3) at 500 °C for 4 h.

3.3. Results and discussion

3.3.1. Synthesis of MTW-type zeolites from (Li, Na)-aluminosilicate gels using ZSM-12 seeds

XRD patterns of the calcined seeds and the products synthesized at different SiO_2/Al_2O_3 ratios are shown in Figure 3.2. Other initial gel compositions and synthesis conditions were fixed to 0.075 Li_2O: 0.1875 Na_2O: SiO_2: 16 H_2O and at 140 °C for 7 days, respectively. The products synthesized at SiO_2/Al_2O_3 = 15, 20, and 40 are identified as MTW-type zeolites without any impurities. However, at SiO_2/Al_2O_3 = 10 and higher Si/Al ratio (≥60), mordenite (MOR) and a layered silicate magadiite were formed, respectively. Therefore, MTW-type zeolites are successfully crystallized in the OSDA-free, (Li, Na)-aluminosilicate system within a certain range of the SiO_2/Al_2O_3 ratios. Zeolite ZSM-5 (MFI) was obtained as a main product with a small amount of MTW coexisted in the absence of lithium cation, while only a layered silicate magadiite was obtained and no zeolite phase was obtained in the absence of the seed crystals. Moreover, the products obtained from the unseeded Na-aluminosilicate gels were X-ray amorphous. Both calcined seed crystals and lithium cation are indispensable for the OSDA-free synthesis of MTW-type zeolites in the present system. The optimum lithium content, i.e., Li/ (Li + Na) ratio in the initial gel, to obtain pure MTW-type zeolite was limited in a narrow range. When Li/(Li + Na) ratio was changed from 0.29 to 0.44, the crystallinity of MTW decreased and lithium disilicate ($Li_2Si_2O_5$) phases appeared.

The solid-state ^{27}Al MAS NMR spectrum of the product synthesized at SiO_2/Al_2O_3 = 20 (Figure 3.3 (a), top) showed a peak at *ca.* 56 ppm, corresponding to the tetrahedrally coordinated framework Al, along with a peak at *ca.* 0 ppm corresponding

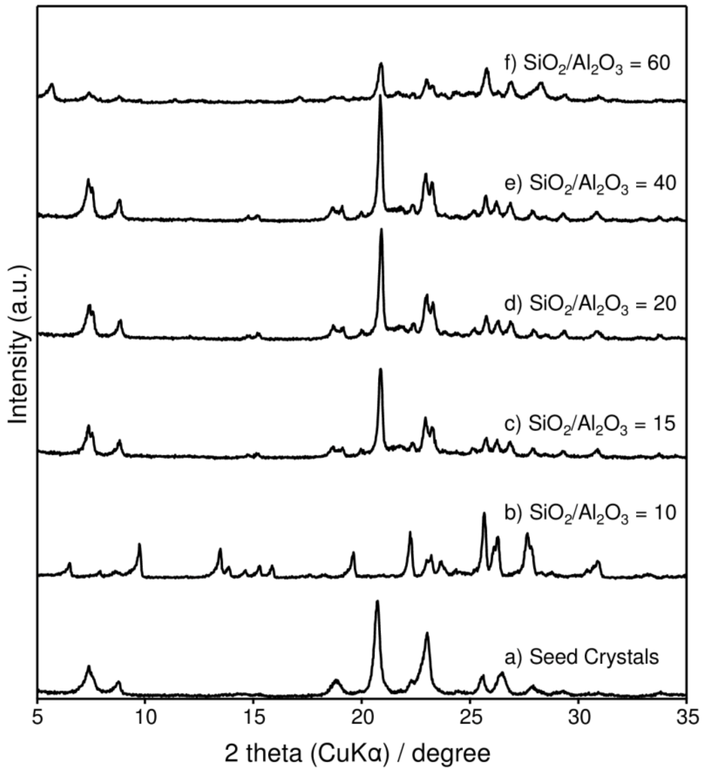

Figure 3.2 Powder XRD patterns of a) seed crystals and b)–f) products synthesized with different SiO_2/Al_2O_3 ratios.[193]

to the octahedrally coordinated Al. This result, together with the XRD data, suggests that amorphous extra-framework Al species coexisted in the as-synthesized products. This impurity phase (*ca.* 5 wt.% calculated from the SiO_2/Al_2O_3 ratio and the integrated intensity ratio of NMR spectrum) was almost completely removed by acid treatment with 2 M hydrochloric acid at 60 °C under static conditions for 2 days (Figure 3.3 (a), bottom). The XRD patterns were not changed even after the treatment (Figure 3.3). Although a small amount of granular matter attached to the rod-like crystals of MTW-type zeolite was observed before acid treatment, they were removed after treatment, as confirmed by SEM (Figure 3.3 (c) and (d)). The SiO_2/Al_2O_3 ratios of the acid-treated products determined by chemical analyses were 58.2, 54.0, and 58.6 for the products synthesized using initial gels with the SiO_2/Al_2O_3 ratios of 15, 20, and 40, respectively. Noteworthy, one of the lowest SiO_2/Al_2O_3 ratios were achieved among the previously reported ZSM-12.[235]

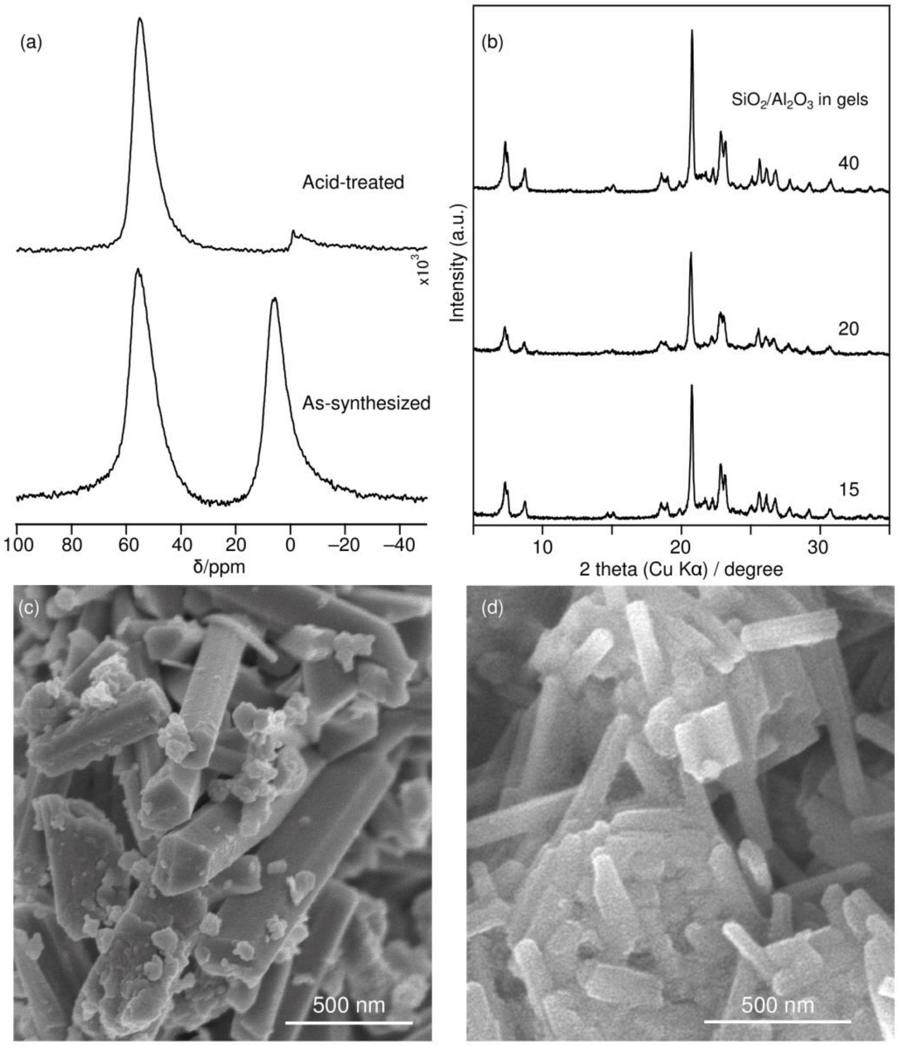

Figure 3.3 (a) ^{27}Al MAS NMR spectrum, (b) XRD patterns (acid-treated samples), and (c, as-synthesized), (d, acid-treated) SEM images of products.[193]

The solid-state ^{29}Si MAS NMR spectrum of the acid-treated product synthesized at SiO_2/Al_2O_3 = 20 (Figure 3.4 (a), bottom) shows peaks at –101, –108, and –111 ppm. These peaks are assigned to the Si(1Al) and two Si(0Al) of MTW-type zeolite, respectively.[236] The SiO_2/Al_2O_3 ratio calculated from integrated intensity ratio of the deconvoluted peaks is 46.4, which is slightly lower than the value of 54.0

obtained by a chemical analysis. The peak at –101 ppm should contain the signal from Q^3 silicon atoms ($(SiO)_3{\equiv}\boldsymbol{Si}{-}OH$) as defect sites of the framework, and ^{29}Si cross-polarization (CP)/MAS NMR spectrum is measured to confirm the presence of Q^3 silicon atoms as shown in Figure 3.4 (a). Clearly, the peak at –101 ppm was enhanced by CP method suggesting that the product contains Q^3 silicon groups.

The nitrogen adsorption–desorption isotherms of as-synthesized and acid-treated product are shown in Figure 3.4 (b). Unfortunately, the BET surface areas of obtained MTW-type zeolites (~100 m^2g^{-1}) were quite lower than the reported values for conventional ZSM-12 synthesized using OSDAs (~400 m^2g^{-1}).[234,235] Although the micropore volume slightly increased by the acid treatment as seen from Figure 3.4 (b), the value did not change any more by further treatment or other treatment such as ion-exchange and treatments with basic solution. This result is characteristic of MTW-type zeolite synthesized without using OSDAs and the reasons will be discussed following section.

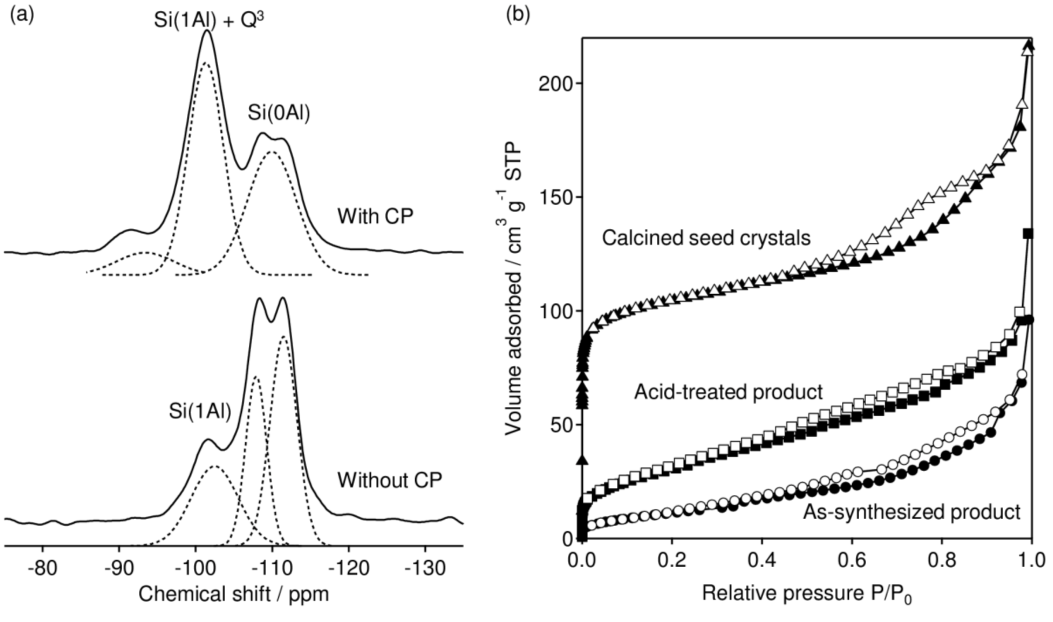

Figure 3.4 (a) ^{29}Si MAS NMR spectra of the acid-treated product and (b) nitrogen adsorption–desorption isotherms of the products and seed crystals.

In addition, Kamimura et al. have recently investigated that MTW-type zeolites could also obtained from Na-aluminosilicate gels using ZSM-12 seed crystals by optimizing gel compositions.[194] The comparison of chemical compositions in Na- and (Li, Na)-aluminosilicate gels for OSDA-free synthesis of MTW-type zeolites are shown in Figure 3.5. MTW-type zeolite can be synthesized at the lower SiO_2/Al_2O_3 regions in the (Li, Na)-aluminosilicate systems than Na-aluminosilicate systems. Contamination of cristobalite can be avoided by synthesizing MTW-type zeolite at Al-rich composition as shown in Figure 3.5. However, considering the ^{27}Al MAS NMR spectrum of the product and other control experiment (data not shown), presence of Li cation caused extra-framework Al. Possible reasons are as follows: (i) partial replacement of Na by Li lowers the effective alkalinity of the solution and decreases the solubility of aluminum species, (ii) amorphous matters with some composition like lithium aluminate are formed.

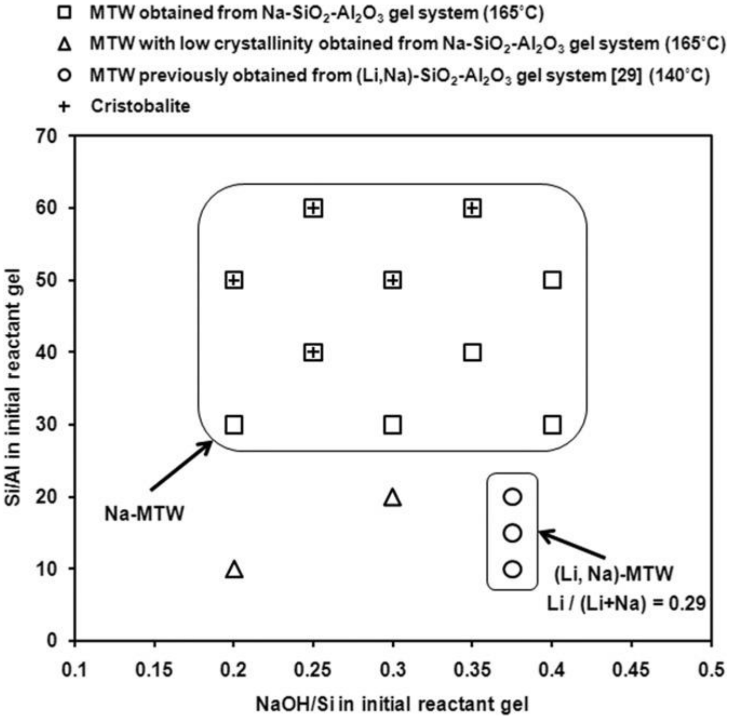

Figure 3.5 Crystallization area of MTW-type zeolites obtained from the hydrothermal treatment of seeded, OSDA-free sodium aluminosilicate gels at 165 °C and this work.[194]

3.3.2. Synthesis of MTW-type zeolites from Na-aluminosilicate gels using zeolite beta seed crystals

The chemical compositions of the initial OSDA-free Na-aluminosilicate gel and the obtained products hydrothermally treated at 165 °C for 96 h are summarized in Table 3.1. Figure 3.6 (a)–(c) present the XRD patterns of MTW by simulation[62], previously obtained ZSM-12 seeds,[194] and Product No. 3.3, respectively. The product is identified as MTW-type zeolite without any detectable impurity. The SiO_2/Al_2O_3 and Na_2O/Al_2O_3 ratios of the products determined by chemical analysis are in the range 31.8–46.4 and *ca*. 1.0, respectively. The solid-state ^{27}Al MAS NMR spectrum of Product No. 3.3 is shown in Figure 3.7. In contrast to the (Li, Na)-aluminosilicate systems, the spectrum exhibits only one signal centered at $\delta = 56$ ppm, which corresponds to tetrahedrally coordinated aluminum. There is no signal in the vicinity of $\delta = 0$ ppm, which confirms the complete absence of octahedrally coordinated extraframework aluminum. Moreover, the peaks in the ^{27}Al MAS NMR spectra of the products obtained under all experimental conditions listed in Table 3.1 correspond to only tetrahedrally coordinated aluminum (data not shown).

Table 3.1 Initial gel compositions of Na-aluminosilicate gels and obtained products hydrothermally treated at 165 °C for 96 h.[195]

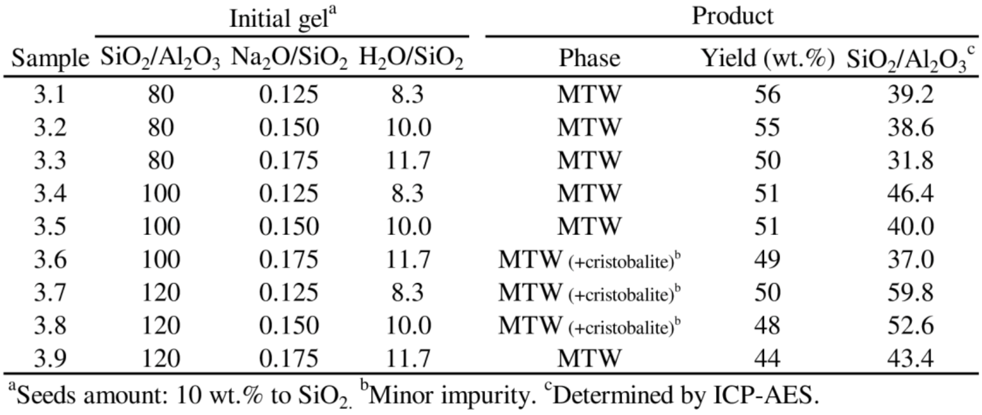

	Initial gel[a]			Product		
Sample	SiO_2/Al_2O_3	Na_2O/SiO_2	H_2O/SiO_2	Phase	Yield (wt.%)	SiO_2/Al_2O_3[c]
3.1	80	0.125	8.3	MTW	56	39.2
3.2	80	0.150	10.0	MTW	55	38.6
3.3	80	0.175	11.7	MTW	50	31.8
3.4	100	0.125	8.3	MTW	51	46.4
3.5	100	0.150	10.0	MTW	51	40.0
3.6	100	0.175	11.7	MTW (+cristobalite)[b]	49	37.0
3.7	120	0.125	8.3	MTW (+cristobalite)[b]	50	59.8
3.8	120	0.150	10.0	MTW (+cristobalite)[b]	48	52.6
3.9	120	0.175	11.7	MTW	44	43.4

[a]Seeds amount: 10 wt.% to SiO_2. [b]Minor impurity. [c]Determined by ICP-AES.

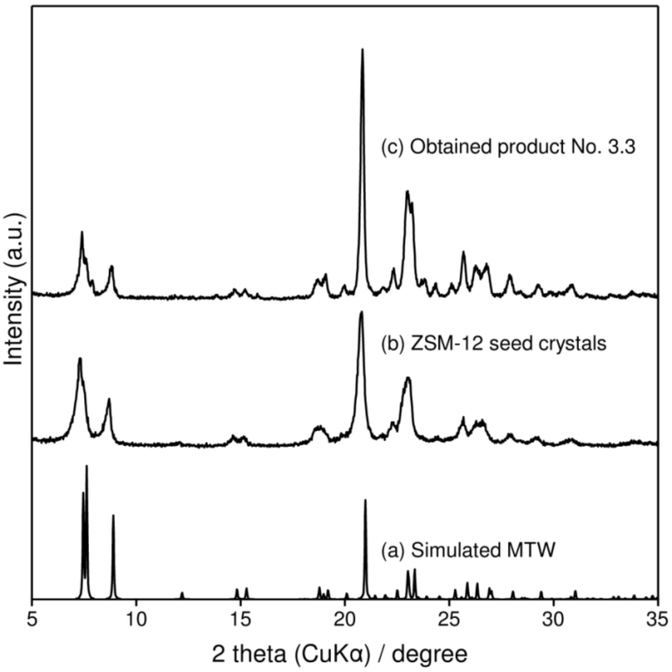

Figure 3.6 Powder XRD patterns of (a) simulated MTW, (b) ZSM-12 seed crystals, and (c) obtained product No. 3.3.[195]

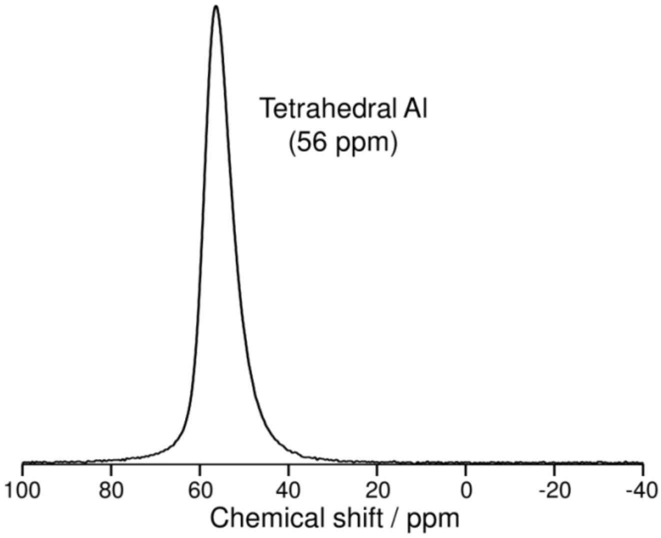

Figure 3.7 Solid-state ^{27}Al MAS NMR spectrum of MTW-type zeolite.[195]

Apparently, crystallization of MTW-type zeolite is accelerated when beta seeds are present in the initial gel by comparing the crystallization behavior of unseeded and seeded gels shown in Figure 3.8 (a) and (b), respectively. These XRD results show that the presence of beta seeds is necessary to induce the crystallization of the MTW-type zeolite prior to the spontaneous nucleation of the MFI phase. Present seeded, OSDA-free system is a rare case, in which the zeolite framework types of target (MTW) and seeds (*BEA) are not the same. Figure 3.9 depicts the framework topologies of ZSM-12 (MTW) and beta (polymorph A, BEA, and polymorph B, BEB, although BEB is not officially used for the FTC in the database of the IZA-SC,[62] here it is just used for the convenience in order to present the similarity in the framework structure of ZSM-12 and beta). ZSM-12 and beta possess very similar topology in which their *a–c* projection viewed along and perpendicular to the 12-MR straight channels is the same as reported by Lobo et al.[237] and Kubota et al.[238] Beta seeds would provide a specific growth surface for the crystallization of the MTW-type zeolite through their structural similarity. Moreover, the crystallization of MTW-type zeolite is induced by not only the structural similarity between seeds and target zeolite but also the chemical composition of the unseeded, OSDA-free gel. The crystallization of MTW-type zeolite favored the unseeded, OSDA-free gel that yields ZSM-5 instead of mordenite as suggested by the XRD results shown in Figure 3.10. MTW- and MFI-type structure has common CBUs named as *cas* as illustrated in Figure 3.1, and this result also supports the working hypothesis mentioned in Chapter 2.

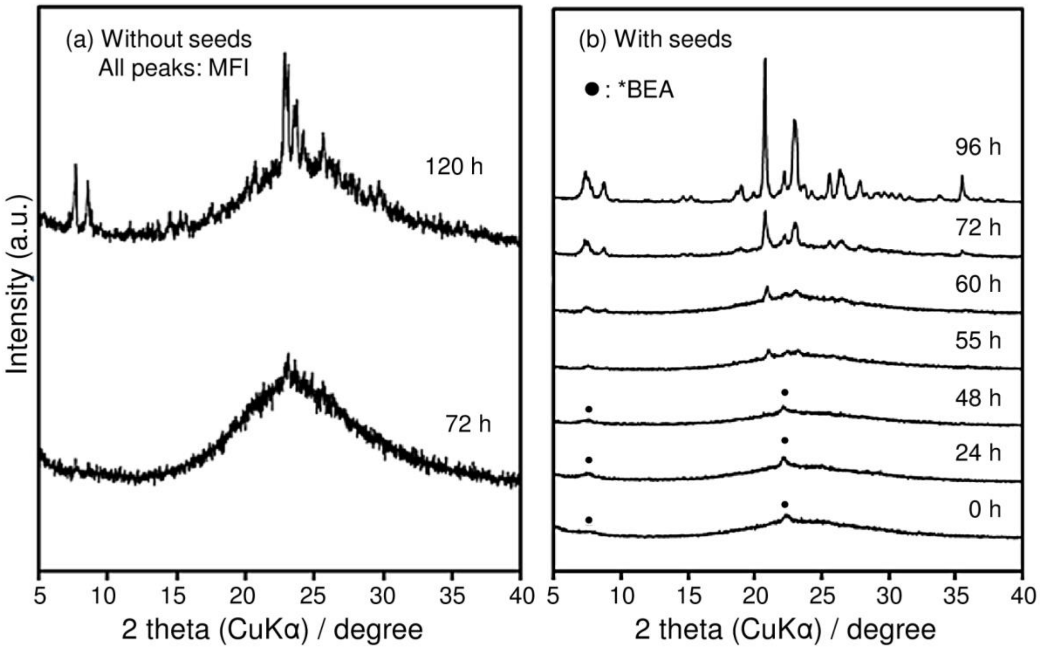

Figure 3.8 Changes in XRD patterns at different heating periods for aluminosilicate products obtained from the (a) unseeded and (b) seeded gel with SiO_2/Al_2O_3 = 80, Na_2O/SiO_2 = 0.175, and H_2O/SiO2 = 11.7 (identical to the synthesis condition of Product no. 3.3 in Table 3.1) at 165 °C.[195]

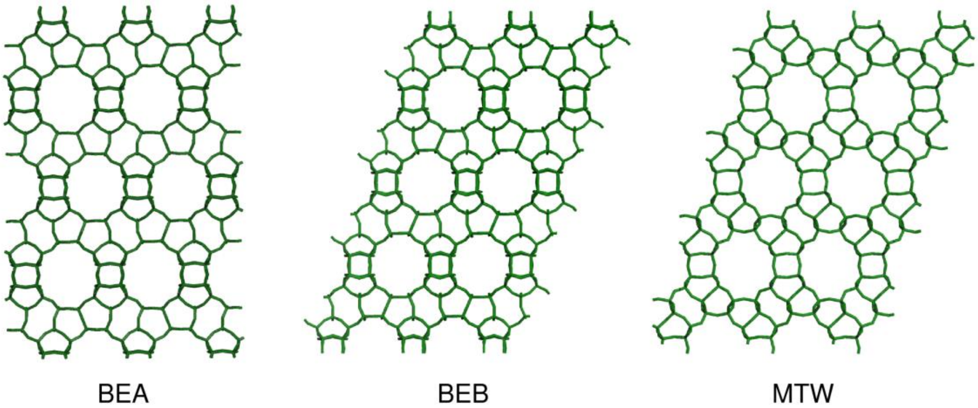

Figure 3.9 Framework topologies of ZSM-12 (MTW) and beta (polymorph A, BEA, and polymorph B, BEB) viewed along the straight 12R channels.[136]

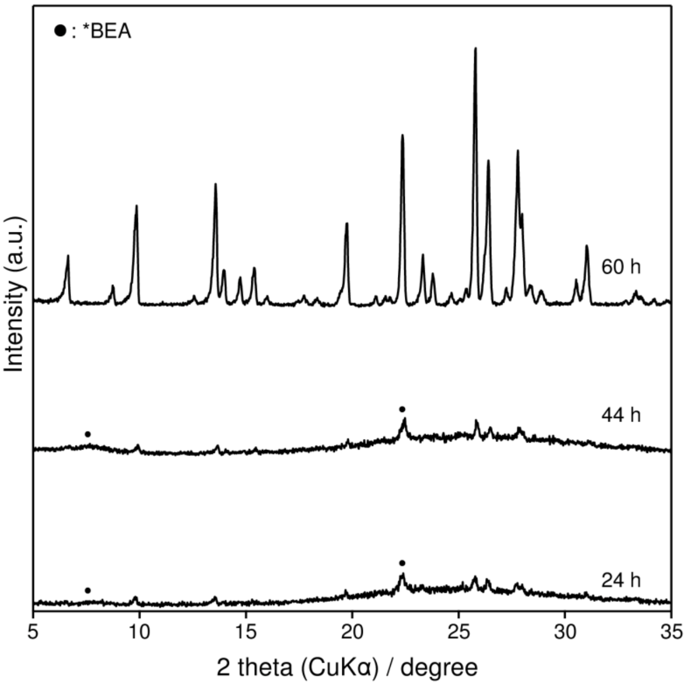

Figure 3.10 Changes in XRD patterns of aluminosilicate products at different heating periods obtained from the OSDA-free gel with SiO_2/Al_2O_3 = 80, Na_2O/SiO_2 = 0.225, and H_2O/SiO_2 = 10 in the presence of calcined beta seeds at 165 °C. Filled circles denote the diffraction peaks attributed to the beta (*BEA) phase.[195]

Figure 3.11 compares the nitrogen adsorption–desorption isotherms of H-form product No. 3.3 (SiO_2/Al_2O_3 = 31.8) and calcined conventional ZSM-12 seed crystals (SiO_2/Al_2O_3 = 94.6) used in the above section. ZSM-12 seed crystals apparently exhibited nitrogen uptake higher than Product No. 3.3. Table 3.2 summarizes the Brunauer–Emmett–Teller (BET) surface areas, micropore surface areas, and micropore volumes of fully crystallized MTW-type zeolites (product Nos. 3.1, 3.3, 3.5, and 3.7), which were calculated by the *t*-plot method. MTW-type zeolites exhibit smaller BET surface areas (81–135 m^2 g^{-1}) and micropore surface areas (8–43 m^2 g^{-1}) as well as smaller micropore volumes (0.004–0.023 cm^3 g^{-1}) compared to those of ZSM-12 (443 m^2 g^{-1}, 217 m^2 g^{-1}, and 0.114 cm^3 g^{-1}, respectively[194]).

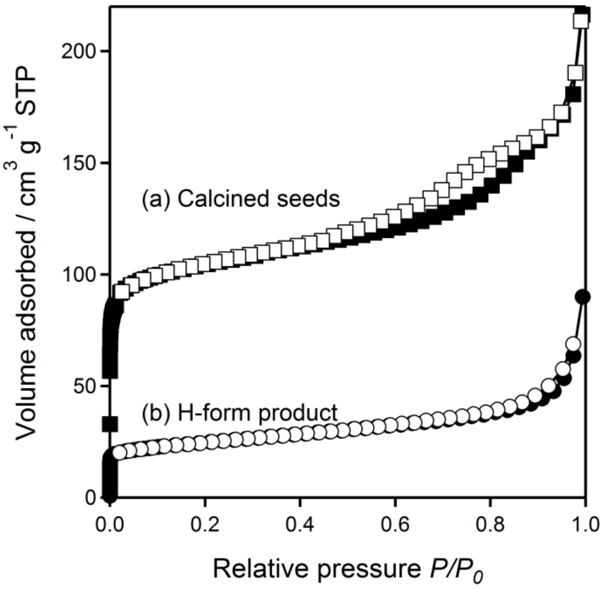

Figure 3.11 Nitrogen adsorption–desorption isotherms for (a, square) calcined ZSM-12 seed crystals and (b, circle) H-form Na-MTW (sample No. 3.3). Filled and open symbols indicate adsorption and desorption points, respectively.[195]

Table 3.2 Pore characteristics of products and ZSM-12 seed crystals.[195]

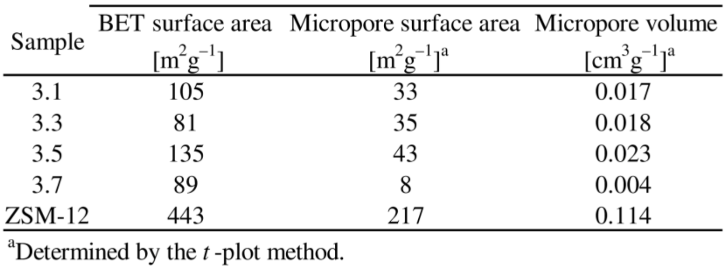

Sample	BET surface area [m^2g^{-1}]	Micropore surface area [m^2g^{-1}]^a	Micropore volume [cm^3g^{-1}]^a
3.1	105	33	0.017
3.3	81	35	0.018
3.5	135	43	0.023
3.7	89	8	0.004
ZSM-12	443	217	0.114

^{a}Determined by the *t* -plot method.

3.3.3. Detailed pore characteristics of MTW-type zeolite

Similar pore characteristics with quite small micropore surface areas and micropore volumes were found in MTW-type zeolite prepared from the (Li, Na)- and Na-aluminosilicate gels in the presence of ZSM-12 and beta as seed crystals, respectively. Here, in the following, these MTW-type zeolites are named as (Li,Na)-MTW (synthesized from initial gel composition of SiO_2/Al_2O_3 = 20,) and Na-MTW (Product No.3.3 in Table 3.1), respectively and characterized in detail about their pore structures. These results were very different from the pore characteristics of zeolite beta obtained from the seed-directed, OSDA-free synthesis[182,184], in which beta products showed significantly larger micropore surface areas and micropore volumes than beta seed crystals by nitrogen adsorption–desorption measurements. Therefore, for some reason, partial pore blocking occurs in MTW-type zeolites, and it hinders the adsorption of nitrogen on the main channels at –196 °C. Partial pore blocking in MTW-type zeolite could be explained by reasons similar to those provided for the case of small- and large-port mordenite, which have different effective apertures *ca*. 0.4 and 0.7 nm, respectively.[239] Small-port mordenite arises because of partial pore blocking caused by the following factors[54]: (i) the presence of amorphous material (extraframework aluminum), (ii) the localization of inorganic cations, and (iii) the presence of structural defects in the main channels. These factors might influence the adsorption behavior of MTW-type zeolites obtained from the seeded OSDA-free system. However, extra-framework aluminum was removed by acid-treatment from (Li,Na)-MTW and there was no extra-framework aluminum in Na-MTW as supported by the ^{27}Al MAS NMR spectrum (Figure 3.7), suggesting that the amorphous material is not completely responsible for pore blocking. In addition, H-form MTW-type zeolite showed no significant differences in the amount of nitrogen adsorbed as compared to that of as-synthesized, (Li,Na)- and Na-form MTW-type zeolites (data not shown). Therefore, it can be concluded that pore blocking of MTW-type zeolite is neither caused by the presence of amorphous materials nor by localization of cations but by structural defects, which may occur during crystal growth along the direction of one-dimensional 12-MR channels [010]. According to the previous paper reported by Sugi and coworkers,[240] the topology of MTW obtained from Na-aluminosilicate gel using OSDA is often affected by the extensive twinning or faulting in the framework, which usually leads to the different stacking sequences of polymorphs (polymorph A and B). Such twinning or faulting may occur in the present MTW-type zeolites obtained from OSDA-free synthesis, which induces the partial pore blocking in the MTW framework.

The adsorption–desorption isotherms of water on Na-MTW and calcined ZSM-12 seed crystals in H-form at 25 °C are expressed in Figure 3.12. Na-MTW exhibits a Type-I isotherm in the IUPAC classification (Figure 3.12 (b)), which is a typical curve for microporous solids. Here, reversible adsorption–desorption isotherm of water with no hysteresis loop was observed. The adsorption amount of water increased steeply in the low relative pressure region due to the micropore filling and exemplifies the hydrophilic character of MTW-type zeolite with $SiO_2/Al_2O_3 = 31.8$, suggesting that the water molecule can access to the intracrystalline voids of MTW-type zeolite. At the relative pressure of $P/P_0 = 0.6$, Na-MTW has enough water adsorption capacity. On the other hand, conventional ZSM-12 shows Type-IV isotherm according to the IUPAC classification (Figure 3.12 (a)) with the hysteresis loop closed at very low relative pressure region. As expected, the adsorption amount of water in the relative pressure region of $P/P_0 < 0.6$ is lower compared to Na-MTW (Figure 3.12 (b)), which is due to the hydrophobic character of ZSM-12 ($SiO_2/Al_2O_3 = 94.6$) stems from less active adsorption sites in the MTW framework. In the relative pressure region of $P/P_0 > 0.6$, the adsorbed amount of water increased steeply caused by the capillary condensation to external surface of zeolite crystals. According to Barrer and Denny,[241] the presence of hysteresis loop in the relative pressure region $P/P_0 < 0.6$ could not be explained by the capillary condensation. They have claimed that the hysteresis loop could be associated with hydration or hydrolysis of aluminate or silicate species included in the framework during crystallization. Similar phenomenon may occur in the present case; however, there are not enough evidences to explain the water desorption behavior in the ZSM-12, and further investigation is necessary.

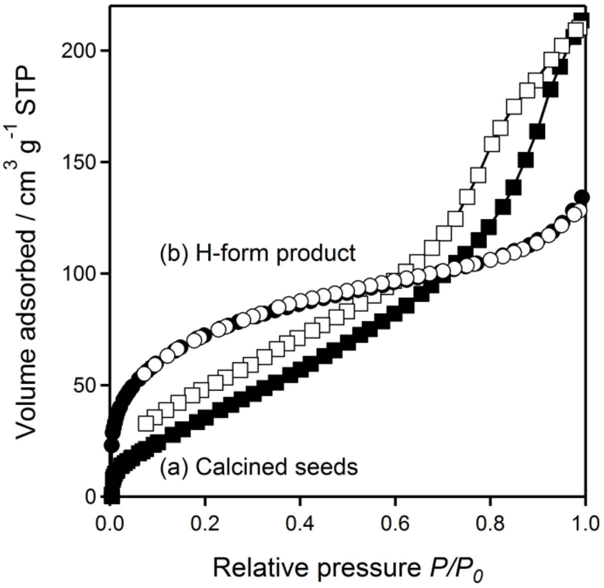

Figure 3.12 Water adsorption–desorption isotherms of (a, square) calcined ZSM-12 seed crystals and (b, circle) H-form Na-MTW (sample No. 3.3). Filled and open symbols indicate adsorption and desorption points, respectively.[195]

Figure 3.13 presents the NH_3-TPD profiles of H-form product No. 3.3 and calcined H-form ZSM-12 seeds. In both samples, two resolved broad desorption peaks were observed between 100–500 °C, which suggest that ammonia desorbs in two stages. The first desorption peak located at 100–230 °C was attributed to the physisorbed ammonia molecules that was either adsorbed on the external surface of zeolite crystals or weak adsorption sites in the MTW framework.[242] The second broad peaks were observed between 260–500 °C, which were attributed to the strongly adsorbed ammonia molecules due to the presence of acid sites in the MTW framework[243,244] with temperatures to give peak maxima of *ca.* 330 °C and 380 °C for calcined H-form ZSM-12 seeds and H-form product No. 3.3, respectively. Notably, the integral area of desorbed ammonia at higher temperature is larger for H-form product No. 3.3 than that of calcined H-form ZSM-12 seeds. As described above, the product has a much amount of framework Al (SiO_2/Al_2O_3 = 31.8), which may contribute to the acidity, compared with conventional ZSM-12 (SiO_2/Al_2O_3 = 94.6). Micropore diffusion through blocked pores or large crystals may affect the desorption temperature[245,246]; therefore, quantitative discussion is avoided here. However, these results suggest that the significant amount of ammonia was adsorbed in the micropores of MTW product No. 3.3.

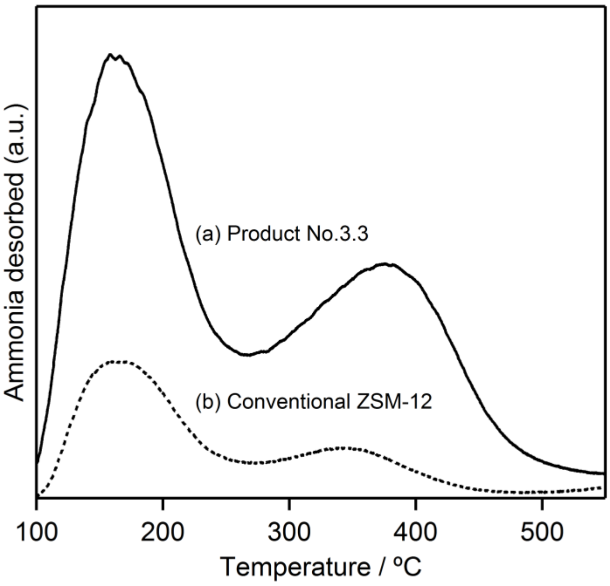

Figure 3.13 NH_3-TPD profiles of (a) product (sample No. 3.3) and (b) conventional ZSM-12.

The results of adsorption–desorption of water (Figure 3.12) and NH_3-TPD measurements (Figure 3.13) of MTW-type zeolite were different from the result of nitrogen adsorption–desorption measurement. On the basis of these results, the present MTW-type zeolite obtained from the seed-directed, OSDA-free synthesis can provide enough adsorption sites for particular adsorbates. However, the generation of open pore in the MTW-type zeolite may be necessary in order to apply it for the adsorption of larger molecules than NH_3 and H_2O. Several research groups[239,247,248] have succeeded in unblocking small-port mordenite by dealumination with acid treatment under suitable conditions. Thus, the dealumination of MTW-type zeolite might be effective to generate open pores and increase the accessibility of other adsorbates to the main channels. Such post synthetic treatment is important from the practical viewpoint of potential industrial applications of MTW-type zeolites. However, the micropore surface areas and micropore volumes did not significantly increase (up to around 50 $m^2\ g^{-1}$ and around 0.02 $cm^3\ g^{-1}$) even after the severe acid treatment with 69 wt.% nitric acid at 160 °C for 4 days.

In Chapter 2 and 4, other zeolites, which also possess 1-dimensional 12-MRs, have been synthesized without using OSDAs but using the alkaline metal cations. Both of these zeolites (MAZ-type zeolite in Chapter 2, and VET-type zeolite in Chapter 4) need to be converted into the H-forms by ion-exchange to open their pores. These results mean that the alkaline metal cations occupied in the zeolite structures block their 1-dimensional pores. In the OSDA-free systems, alkaline metal cations might play structure-directing roles and stabilize zeolite structures like a “support bar” instead of OSDAs. However, hindrances by alkaline metal cations do not explain the pore characteristics of MTW-type zeolite and structural defects might be a significant reason as mentioned above. Therefore, it is worth considering about structural differences between MTW-type zeolite and other two zeolites. Figure 3.14 shows a possible stacking fault model in the MTW-type structure. The black layer in the model can be shifted for (001) direction without changing the [001] projection, and as a result, 12-MRs in blue body are blocked by the shifted layer. Ring sizes of blocked pores are estimated to be similar to 8-MRs, which sometimes hinder nitrogen adsorption but adsorb smaller molecules like water and ammonia. Although this is only one of the possibilities, bond angles and lengths seem to be reasonable, and any stacking fault model could not be made in MAZ- and VET-type structures.

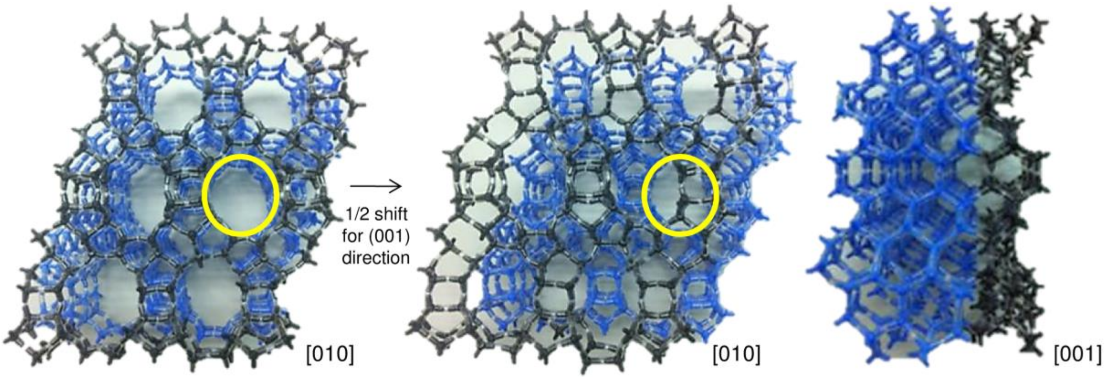

Figure 3.14 Possible stacking fault model in MTW-type structure. Yellow circles indicate 12-MRs.

3.4. Conclusion

The OSDA-free syntheses of MTW-type zeolites were achieved using calcined ZSM-12 and beta seed crystals. The CBU hypothesis was also confirmed in this case between MTW-type and MFI-type structures. Moreover, synthesis of MTW-type zeolite using beta seed crystals suggests that beta seeds provided a specific growth surface similar to the framework structure of MTW-type zeolite. Although octahedral, extra-framework Al species were observed in Li-MTW by ^{27}Al MAS NMR, these can be removed by an acid washing, and Na-MTW did not contain extra-framework Al. The results of nitrogen adsorption–desorption measurements indicated that the obtained MTW-type zeolite has structural defects that hinder the adsorption of nitrogen on the main channels at the liquid nitrogen temperature. On the other hand, the results of water adsorption–desorption and NH_3-TPD measurements showed enough adsorption capacity for water and the existence of an enough amount of the strong acid sites.

Chapter 4. Synthesis of VET-Type Zincosilicate Zeolite and Its Mechanistic Study

4.1. Introduction

Multivalent cations-exchanged zeolites have recently attracted much attention for catalysis and adsorption. For example, Cu(II)- and Fe(II)-exchanged zeolites have proven to be quite promising catalysts for NO_x treatment.[249–253] Isomorphous substitution of Zn(II) for Si(IV) in the zeolite framework generates two anionic charges per zinc atom, while Al(III) generates only one charge. Therefore, zincosilicate zeolites have been considered as efficient stabilizers for multivalent cations. Compared with the aluminosilicate systems, however, the chemistry of zincosilicates has not been investigated sufficiently. The first synthetic, microporous zincosilicate zeolite is VPI-7, reported by Annen et al.,[254] followed by the successful synthesis of VPI-8,[255,256] VPI-9,[257–259] and RUB-17.[260] The FTCs of these zincosilicate zeolites assigned by IZA are VSV, VET, VNI, and RSN, respectively.[62] Zincosilicate analogues of aluminosilicate zeolites are also reported for analcime,[257] sodalite,[261] beta,[262–264] mordenite,[265] and ZSM-5.[266–270] Among these zincosilicate zeolites, those with large pores (12-membered ring (MR)) are VPI-8 and zincosilicate analogues of beta and mordenite. Organic structure-directing agents (OSDAs) have been indispensable to synthesize these large pore zincosilicate zeolites.

VPI-8 is a large pore zincosilicate zeolite with one-dimensional, 12-MR channels. It possesses a unique structure having a “pinwheel” unit, never seen in other zeolites, and 7-MRs, found in only four zeolite structures (MEI, SFG, STT, and VET).[271] This zeolite cannot be prepared in the absence of Zn and Li, which seems to play an important role in the synthesis of VPI-8.[255] VET-type zincoaluminosilicate zeolite named as SSZ-41[272] shows high catalytic activity for the cracking of hydrocarbons.[273] To date, however, VET-type zeolite has never been synthesized without OSDAs such as TEA and *N*,*N*,*N*-trimethyladamantammonium cations.[255,274] OSDA-free synthesis of such a unique zeolite is worth investigating to broaden the applicable scope of OSDA-free synthesis method and enrich the library of available zeolites for practical applications.

Here the successful OSDA-free synthesis of VET-type zinco(alumino)silicate zeolites using the seed crystals is reported. This is a first report on the synthesis of large pore zincosilicate zeolite without using OSDAs. Moreover, investigations on the chemical states and structures of amorphous intermediates and resultant zeolite products provide some insights into the crystal growth behavior, revealing the structural similarities of amorphous intermediates and resultant products, which is thought to be important for the successful synthesis of VET-type zeolites.

4.2. Experimental

4.2.1. Chemicals

The following raw materials for the OSDA-free synthesis were used as provided: colloidal silica (Ludox® HS-40, Sigma-Aldrich Co. LLC) as the silica source, zinc acetate (Aldrich) as the zinc source, and sodium hydroxide solution (NaOH, 50 w/v % in water, Wako Pure Chemical Industries, Ltd.) and lithium hydroxide (LiOH, monohydrate, Wako) as the alkali sources. Commercially available FAU-type zeolites (HSZ-360, 385, and 390HUA, Tosoh Corp., having the SiO_2/Al_2O_3 ratios of 14, 100, and 810, respectively) were used as the silica and aluminum source in the synthesis of VET-type zincoaluminosilicate zeolites. Tetraethylammonium hydroxide (TEAOH, 35 wt. % in water, Aldrich) was used as the OSDA in the synthesis of VPI-8 seed crystals.

4.2.2. Preparation of VPI-8 seed crystals

Zeolite VPI-8 was synthesized according to the procedure mentioned in the earlier report.[255] In a typical synthesis, LiOH and TEAOH were dissolved in distilled water, followed by the addition of zinc acetate to obtain a clear solution. After the addition of colloidal silica, the obtained clear solution was stirred at ambient temperature for 1 day. The final composition of the mix-ture was $0.1\ Li_2O:0.1\ ZnO:1.0\ SiO_2:30\ H_2O:0.2\ (TEA)_2O$. The mixture was transferred to a 23 mL Teflon®-lined stainless autoclave (#4749, Parr Instrument Co.) and was then subjected to hydrothermal treatment at 150 °C for 6 days in an oven under autogenous pressure and static condition. After hydrothermal treatment, the product was separated from mother liquor by centrifugation, washed several times with distilled water, and dried at 60 °C. The obtained VPI-8 was calcined at 550 °C for 10 h in a stream of dry air and thereafter used as seed crystals.

4.2.3. OSDA-free synthesis of VET-type zeolite

Seed-directed syntheses of VET-type zeolites were carried out by adding VPI-8 seeds prepared by the above described procedure to the starting (Na, Li)-zincosilicate gels with chemical compositions of x Na_2O:y Li_2O:z ZnO:SiO_2:20 H_2O (where x = 0.17–0.27, y = 0.02–0.06, z = 0.017–0.033). For the preparation of (Na, Li)-zincosilicate gels, LiOH was dissolved in an aqueous NaOH solution, followed by the addition of zinc acetate to obtain a clear solution. Then, VPI-8 seeds were dispersed in the solution, and colloidal silica was slowly added to the mixture and vigorously stirred until a homogeneous gel was obtained. In the case of zincoaluminosilicate VET, the zeolite HSZ-360, 385, or 390HUA instead of colloidal silica was used and dispersed in the solution. Here the amount of zeolite seeds added was set at 10 wt. % relative to the silica source, and the total weight of (Na, Li)-zincosilicate gel was adjusted to 15 g. Subsequently, the seeded gel was transferred to a 23 mL Teflon®-lined stainless autoclave and subjected to hydrothermal treatment at 140–160 °C for different periods under autogenous pressure and static condition. After hydrothermal treatment, the product was recovered by filtration, thoroughly washed with distilled water, and dried at 60 °C. To obtain the H-form zeolites, three-fold ion-exchange of the products using ammonium chloride was performed at 80 °C for 12 h, and the obtained products were calcined at 500 °C for 3 h. The solid yield of the obtained zeolite was defined as weight ratio percentage (g/g × 100) of the dried solid product to the sum of the dry SiO_2, zinc acetate, lithium hydroxide, and the dry (calcined) seeds in the starting Na, Li-zincosilicate gels.

4.2.4. Characterizations

Powder X-ray diffraction (XRD) patterns of the solid products were collected by using a Rigaku Ultima IV diffractometer and Cu Kα radiation (40 kV, 40 mA) from 3° to 40° in 2θ. Elemental analysis of the zeolite seeds and products was performed by a Thermo iCAP 6300 inductively coupled plasma-atomic emission spectrometer (ICP-AES) after dissolving them in hydro-fluoric acid or a potassium hydroxide solution. The crystal sizes and morphologies were observed by using a Hitachi S-900 field-emission scanning electron microscope (FE-SEM). Nitrogen adsorption−desorption measurements of the zeolite products were performed on a Quantachrome Autosorb-iQ2-MP analyzer at −196 °C. Prior to the measurements, all samples were degassed at 400 °C for 6 h under vacuum. The temperature-programmed desorption of ammonia (NH_3-TPD) was performed by using a BEL-CAT instrument to compare the acidic properties of the zeolite products. Each sample was allowed to adsorb NH_3 at 100 °C (5% NH_3 in He) for 10 min after pretreatment at 500 °C in a He stream. The desorption behavior was then monitored by a thermal conductivity detector while heating the sample to 550 °C at a heating rate of 10 K min^{-1}. Solid-state ^{29}Si magic angle spinning nuclear magnetic resonance (MAS NMR) spectra were obtained on a Chemagnetics CMX-300 spectrometer at 59.7 MHz with a pulse width of 2.0 μs and a pulse delay of 100 s, while ^{27}Al MAS NMR spectra were recorded at 78.3 MHz with a pulse width of 1.0 μs and a recycle delay of 5 s. Diffuse reflectance ultraviolet–visible (DR UV–Vis) spectra were recorded by a JASCO V-670 spectrometer in the wavelength range of 190−500 nm with a scan rate of 100 nm min^{-1}. Raman spectra were obtained by a JASCO NRS-1000 Raman spectrometer equipped with green laser (532 nm). Spectra were recorded over the range of 200–800 cm^{-1} and integrated for 60 s at least twice or more for samples with weak scattering. Samples were carefully dried in a vacuum oven to remove residual water before the measurements. High-energy XRD (HEXRD) measurements were performed, on a pressed zeolite disk weighing 200 mg, at room temperature on a horizontal two-axis diffractometer, optimized for the structural measurements in glass and liquid, built at a BL04B2 high-energy monochromatic bending magnet beamline of SPring-8 (Hyogo, Japan) that operates at 8 GeV. A bent Si(220) crystal, mounted on the monochromator stage fixed at a Bragg angle of 3° in the horizontal plane, provided incident photons at 61.43 keV ($\lambda = 0.2018$ Å). The maximum Q ($Q = 4\pi\sin\theta/\lambda$), Q_{max}, collected in this study was 25 Å^{-1}. The obtained data were subjected to well-established analysis procedures such as absorption, background, and the Compton scattering corrections and then normalized to give Faber–Ziman total structure factor *S(Q)*. These collected data were used to calculate the total correlation function *T(r)* using the following function:

$$T(r) = 4\pi\rho r + \frac{2}{\pi}\int_{Q_{min}}^{Q_{max}} Q[S(Q)-1]\sin(Qr)\,dQ + 1$$

where, ρ is the atomic number of density (0.05783 /Å^3, Li: 56 O: 3 Na: 26 Si: 2 Zn, 2.0 g/cm^3).

4.3. Results and discussion

4.3.1. OSDA-free synthesis of VET-type zincosilicate zeolites

The chemical compositions of the initial gels, reaction conditions, and obtained products are summarized in Table 4.1. Highly crystalline pure VET-type zeolites were obtained from the initial gels having compositions of x Na_2O:y Li_2O:z ZnO:1.0 SiO_2:20 H_2O (where $x = 0.21-0.26$, $y = 0.02-0.04$, and $z = 0.02-0.025$) by hydrothermal treatment at 150 °C for 72–80 h (i.e., sample Nos. 4.3, 4.6, 4.8, and 4.9). For example, the powder XRD pattern of sample No. 4.6 shown in Figure 4.1 (a) is similar to that of the calcined seeds employed and the simulated pattern, corresponding to the VET-type zeolite without any impurity phase. The solid yields and bulk SiO_2/ZnO ratios of the products by the OSDA-free synthesis are 25–40% and 12–14, respectively. Figure 4.1 (b) and (c) show the FE-SEM images of the seeds and the sample No. 4.6, respectively. The seed crystals are aggregates of a bundle of small rod-like crystals with a length of 100–200 nm, whereas, the products by the OSDA-free synthesis are longer rod-like, randomly aggregated crystals with the length of ca. 2–5 μm. The larger crystal size of the product compared to the seeds is one of the evidences of the crystal growth that occurred from the surface of the seed crystals, as shown in the earlier reports,[136,180–200] and the crystals were considered to preferentially grow along one-dimensional pore channels of VET-type zeolite.

On the other hand, some impurity phases were observed in the product synthesized under different conditions. Lower alkalinity and higher temperature result in the contamination with a layered silicate, kenyaite (see sample Nos. 4.1 and 4.7). Both higher and lower SiO_2/ZnO ratios in the initial gels are also unfavorable for the synthesis of VET-type zeolite, causing the decrease in crystallinity and the

Table 4.1 Summary for the OSDA-free synthesis of zincosilicate VET-type zeolites.[275]

	initial gel[a]						reaction condition		product		
sample	SiO_2/ZnO	Li_2O/SiO_2	Na_2O/SiO_2	Li/(Li+Na)	$(Li+Na)_2O/SiO_2$	Li_2O/ZnO	temp.[℃]	time [h]	yield (%)[b]	phase	SiO_2/ZnO
4.1	30	0.033	0.17	0.17	0.20	1.0	150	72	-	VET+kenyaite	-
4.2	30	0.033	0.22	0.13	0.25	1.0	150	96	-	VET (low crystallinity)	-
4.3	40	0.025	0.23	0.10	0.25	1.0	150	80	38.0	VET	13.5
4.4	50	0	0.25	0.00	0.25	0.0	150	72	-	VET (low crystallinity)	-
4.5	50	0	0.25	0.00	0.25	0.0	150	120	-	unkown phase	-
4.6	50	0.020	0.23	0.08	0.25	1.0	150	72	31.9	VET	13.7
4.7	50	0.020	0.23	0.08	0.25	1.0	160	60	-	VET+kenyaite	-
4.8	50	0.020	0.26	0.07	0.28	1.0	150	72	24.5	VET	12.3
4.9	50	0.040	0.21	0.16	0.25	2.0	150	72	31.6	VET	13.6
4.10	50	0.060	0.19	0.24	0.25	3.0	150	72	-	VET+lithium silicate	-
4.11	60	0.017	0.23	0.07	0.25	1.0	150	80	-	VET+kenyaite	-
4.12	60	0.033	0.27	0.11	0.30	2.0	150	96	-	VET (low crystallinity)	-

[a] H_2O/SiO_2=20, seeds: 10wt.% to SiO_2, [b] solid yield

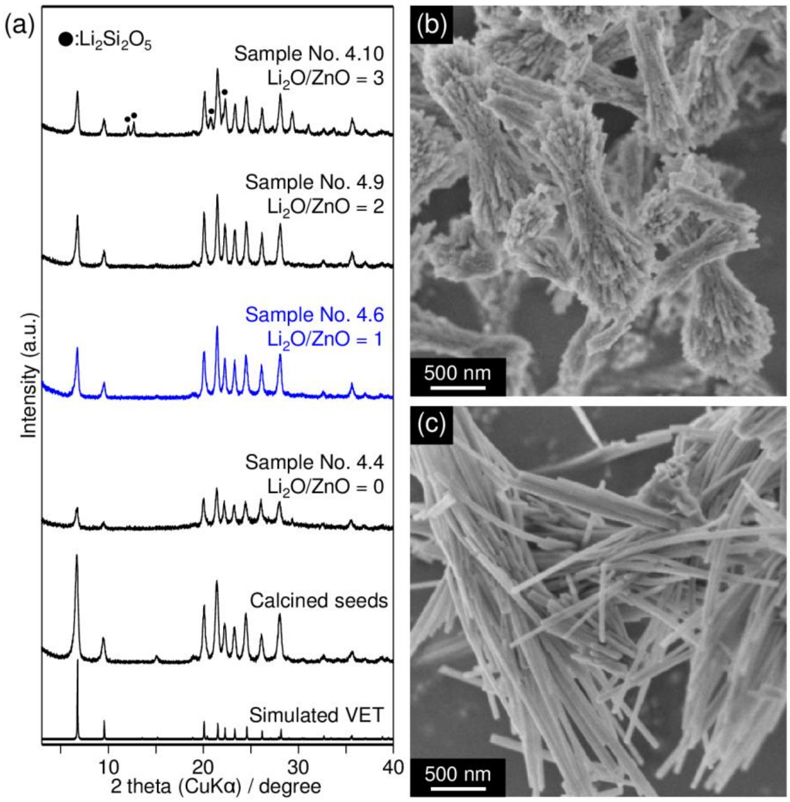

Figure 4.1 (a) Powder XRD patterns of the products synthesized from the initial gels with the different Li_2O/ZnO ratios (SiO_2/ZnO = 50, $(Li+Na)_2O/SiO_2$ = 0.25, 150 °C, 72 h). FE-SEM images of (b) seed crystals and (c) product (sample No. 4.6).[275]

contamination with kenyaite, as can be seen in sample Nos. 4.2, 4.11. Moreover, it is worth noting that lithium cations play a crucial role in the crystallization of VET-type zeolite, as shown in Figure 4.1 (a). The crystallinity of the obtained product decreased without lithium cations (sample No. 4.4), and after prolonged synthesis, unknown phases, probably a mixture of dense silicates, were obtained (sample No. 4.5).

Similar phenomena were also observed in the synthesis of VPI-8 using OSDA. Yoshikawa et al. pointed out the following remarks[255] concerning the roles of LiOH: (i) the use of LiOH lowers the effective OH^- concentration relative to the use of NaOH; (ii) Li^+ appears to serve a function of counterbalancing a portion of charge created by the framework incorporation of Zn; (iii) an important prenucleation complex is formed that may not be provided by other cations. These should also be important factors for the OSDA-free synthesis of VET-type zeolite. In this study, optimal lithium contents are $Li_2O/ZnO = 1-2$, as shown in Figure 4.1 (a), that is, sample Nos. 4.6 and 4.9, and the excess amount of lithium cations causes the formation of a lithium disilicate phase ($Li_2Si_2O_5$, sample No. 4.10). These results indicate that the synthesis conditions for the successful OSDA-free synthesis of the pure VET-type zeolites are limited to the narrow range.

4.3.2. Characterizations of VET-type zincosilicate zeolites

Further characterizations of the product were carried out for the sample No. 4.6 (see Table 4.1). Incorporation of Zn atoms into the frameworks of zeolites is confirmed by ^{29}Si MAS NMR and DR UV–Vis spectra. The deconvolution results of ^{29}Si MAS NMR spectra of the calcined seeds and the obtained VET-type zeolite shown in Figure 4.2 indicate that the spectra are mainly composed of four signals at ca. −95, −100, −105, and −110 ppm. Yoshikawa et al. found that the signal at ca. −95 ppm is assigned to an impurity phase with a SiO_2/ZnO ratio of 3 and denoted it as unknown phase A,[256] which is easily removed by washing with dilute HCl solution. The presence of this unknown phase A is less noticeable for the VET product (Figure 4.2 (b)). The signal at ca. −100 ppm is assigned to Q^4 (1Zn) in the zeolite framework, while the signals at −105 and −110 ppm are assigned to Q^4 (0Zn) at the different crystallographic tetrahedral sites (T-sites) in the zeolite framework. To obtain the actual value of SiO_2/ZnO ratios in the zeolite framework, the SiO_2/ZnO ratios were calculated by the integrated intensity ratios of these three peaks at −100, −105, and −110 ppm. The SiO_2/ZnO ratio of the as-synthesized VET-type zeolite calculated from the NMR spectrum is 18.3, which is slightly higher than the value obtained by the elemental analysis of 13.7 (see Table 4.1), likely due to the slightly presence of the unknown phase A. In contrast, the SiO_2/ZnO ratio of the seed crystals calculated from ^{29}Si NMR (33.2) is much higher than the result from the elemental analysis (13.6) because of the presence of either phase A as reported already[255] or extra-framework Zn. These ^{29}Si NMR results suggest the successful incorporation of Zn into the zeolite framework of product synthesized by the OSDA-free method, yielding a less amount of impurity phase compared with seeds.

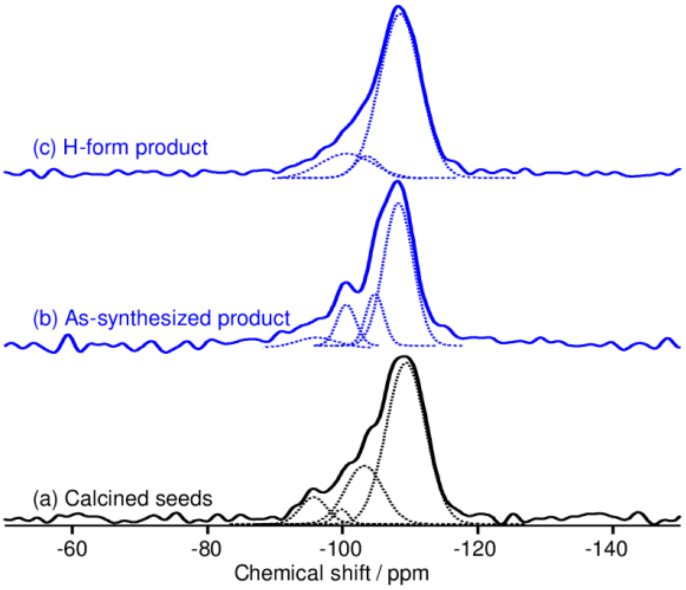

Figure 4.2 ^{29}Si MAS NMR spectra of (a) calcined seeds, (b) as-synthesized product, and (c) H-form product (sample No. 4.6).[275]

The DR UV–Vis spectra are shown in Figure 4.3. It is well known that the zincosilicate zeolite exhibits an absorption band below 300 nm, while ZnO shows a broad absorption band at ca. 360 nm that is assigned to the $O^{2-} \rightarrow Zn^{2+}$ ligand-to-metal charge-transfer transition.[256,270] The spectra of the product show two strong absorption peaks at ca. 250 and 200 nm. Seed crystals exhibit similar spectra but with weaker intensity compared to the product, which, although not quantified, may be attributed to a relatively less amount of incorporation of Zn in the framework, as also evidenced by the ^{29}Si MAS NMR results. Successful incorporation of Zn into the zeolite framework is essentially supported from the spectra, although the state of Zn atom cannot be discussed in detail as the UV absorptions depend on many factors such as particle size and degree of hydration.[256,270]

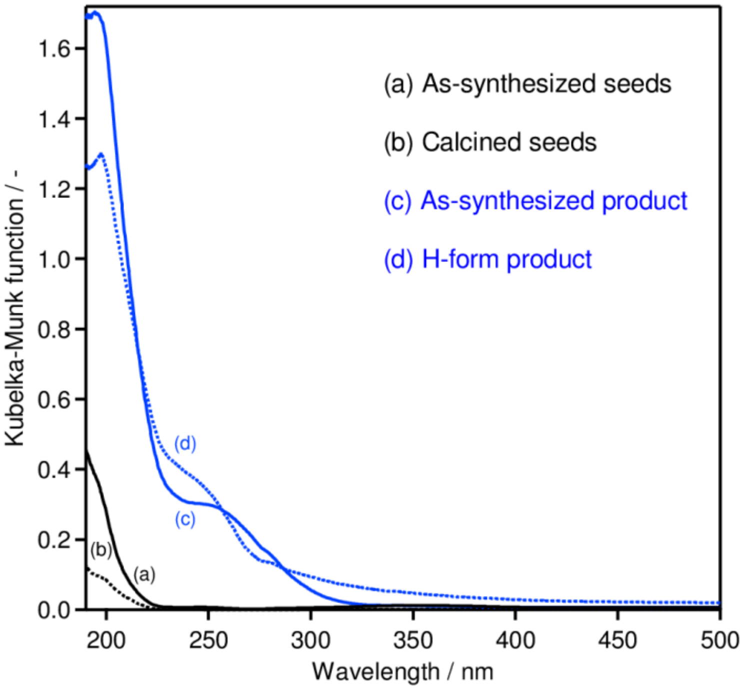

Figure 4.3 DR UV-vis spectra of (a, a red solid line) as-synthesized seeds, (b, a red dushed line) calcined seeds, (c, a blue solid line) as-synthesized product, and (d, a blue dushed line) H-form product (sample No. 4.6).[275]

The as-synthesized product was subjected to NH_4^+ ion-exchange treatment to produce the H-form VET-type zeolite. Note that the NH_4Cl aqueous solution used for ion-exchange has pH 4.4. As shown in Figure 4.4 (a), no loss in crystallinity was observed in the H-form product obtained after ion-exchange and subsequent calcination. The SiO_2/ZnO ratio of the H-form product calculated from the NMR spectrum (23.9) agreed well with the value obtained from the elemental analysis (23.8). This further supports the presence of a small amount of the unknown phase A in the as-synthesized product because, as reported previously,[256] this phase can be simply removed by heating in weak acidic solution (in this case, during ion-exchange). Note that the NH_4^+/Zn ratio of the ion-exchanged sample was estimated from thermogravimetric analysis and ICP-AES to be 2.1, suggesting the completion of ion-exchange. The peaks in the DR UV-Vis spectra remain even after ion-exchange (see Figure 4.3). Nitrogen adsorption–desorption isotherms of the calcined seed crystals, as-synthesized product, and H-form product are shown in Figure 4.4 (b). The micropore volumes derived from a *t*-plot method of the seeds and H-form product are 0.12 and 0.11 $cm^3\ g^{-1}$, respectively. These values are agreed well with the reported values,[4] suggesting a superior porosity of the product. However, the as-synthesized product shows a quite low micropore volume of 0.0020 $cm^3\ g^{-1}$, which can be explained by the hindrance of the nitrogen adsorption by alkaline metal cations located in the one-dimensional channels of as-synthesized product.

Solid acid properties of the H-form product and seed crystals are evaluated by the NH_3-TPD method, as shown in Figure 4.5. Generally, desorption peaks below 200 °C are attributed to the ammonia molecules adsorbed on the weak adsorption sites, whereas desorption peaks at higher temperature are due to the ammonia adsorbed on the

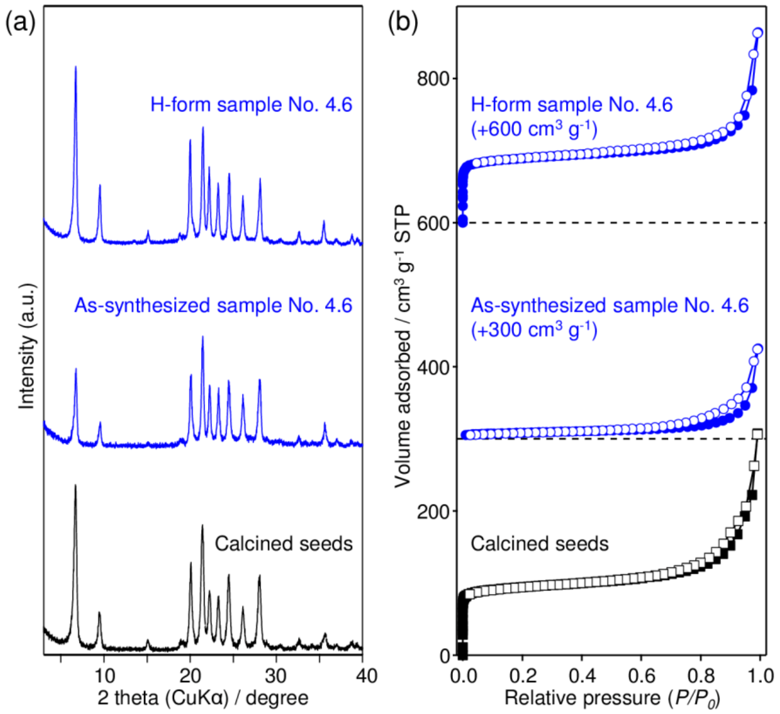

Figure 4.4 (a) Powder XRD patterns and (b) nitrogen adsorption (closed symbol)–desorption (open symbol) isotherms of the calcined seeds, as-synthesized product, and H-form product (sample No. 4.6).[275]

acid sites. The deconvolution of the desorption profiles shows that both product and seed crystals exhibit weak acidities and that the product has relatively a larger amount of acidity (0.14 mmol g^{-1}) compared with that of seed crystals (0.10 mmol g^{-1}) ascribed to its higher content of tetrahedral Zn in the zeolite framework of the product, as also supported by 29Si MAS NMR and DR UV–Vis spectra. However, the zinc species contributed to the acidities are about 20–30% of the framework zinc atoms calculated from the SiO2/ZnO ratio. The low number of acid sites is probably due to the presence of some inaccessible protons trapping inside the building units of VET-type zeolite. Therefore, incorporation of Al atoms along with Zn into the zeolite framework is examined to obtain a product with much more acid sites.

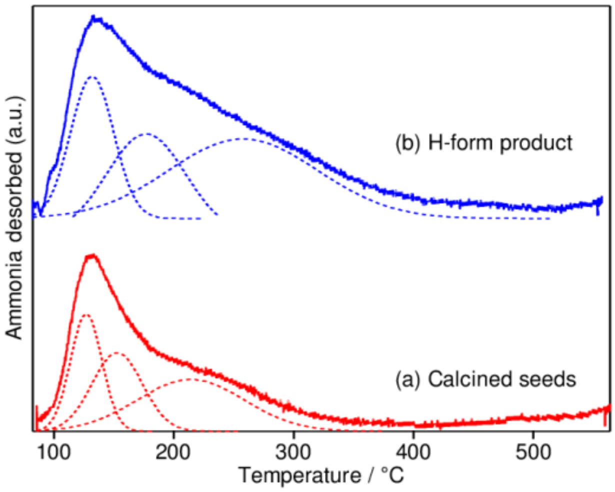

Figure 4.5 NH_3 TPD profiles of (a) calcined seeds and (b) H-form product (sample No. 4.6).[275]

4.3.3. OSDA-free synthesis of VET-type zincoaluminosilicate zeolites

Table 4.2 summarizes the initial gel compositions, reaction conditions, and corresponding products obtained in the synthesis of VET-type zincoaluminosilicate zeolites. Powder XRD patterns of the products are shown in Figure 4.6. When sodium aluminate was added as an Al source to the reactant mixture prepared by a typical procedure similar to that described for the zincosilicate analogue (vide supra), the crystallinity of VET-type zincoaluminosilicate zeolite decreased even with the small amount of Al, as can be seen in sample No. 4.13. The use of HSZ-360HUA (SiO_2/Al_2O_3 = 14) and HSZ-385HUA (SiO_2/Al_2O_3 = 100) as both Al and Si sources induced other zeolite phase (sample No. 4.14) or the VET-type zeolite with low crystallinity (sample No. 4.15). However, highly crystalline VET-type zincoaluminosilicate zeolite was obtained when the HSZ-390HUA (SiO_2/Al_2O_3 = 810) was used (sample Nos. 4.16 and 4.17). The SiO_2/ZnO ratios of obtained products are slightly higher than those of zincosilicate products such as sample No. 4.9, and the SiO_2/Al_2O_3 ratios of sample Nos. 4.16 and 4.17 are 351 and 295, respectively (Table 4.2). Previously, high-silica zeolite Y is also used as a starting material in the synthesis of SSZ-41,a zincoaluminosilicate VET zeolite prepared by using OSDAs,[273] and in the seed-directed, OSDA-free synthesis of zeolite beta.[276] Figure 4.7 (a) shows 27Al MAS NMR spectrum of sample No. 4.16, indicating that all Al atoms are successfully incorporated into the tetrahedrally coordinated framework sites as the signal of extra-framework aluminum at ca. 0 ppm is hardly detected. This is also supported by the fact that the acid amount of sample No. 4.16 is increased up to 0.25 mmol g^{-1} (Figure 4.7 (b)). It is worth mentioning here that Zn is essential for the synthesis of VET-type zeolite regardless of the OSDAs; its only aluminosilicate counterpart has never been obtained so far (data not shown). The catalytic properties of the resultant zincoaluminosilicate VET zeolite are of interest and thus merit investigation in future work.

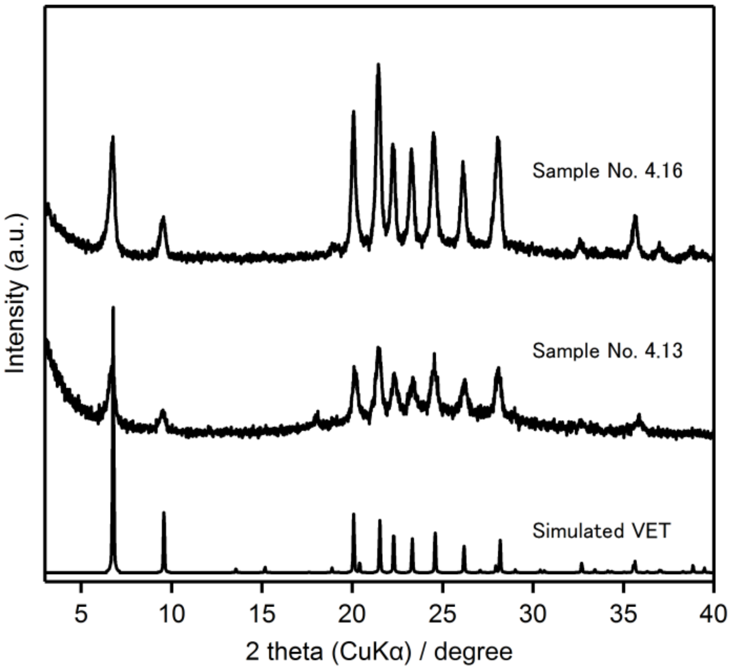

Figure 4.6 Powder XRD patterns of VET-type zincoaluminosilicate zeolite.[275]

Table 4.2 Summary for the OSDA-free synthesis of zincoaluminosilicate VET-type zeolites.[275]

	initial gel[a]		reaction condition		product			
sample	starting material (SiO_2/Al_2O_3)	Na_2O/SiO_2	temp.[℃]	time [h]	yield (%)[b]	phase	SiO_2/ZnO	SiO_2/Al_2O_3
4.9	Ludox	0.21	150	72	31.6	VET	13.6	>1000
4.13	Ludox+sodium aluminate (800)	0.21	150	72	-	VET (low crystallinity)	-	-
4.14	HSZ-360HUA (14)	0.21	150	36	-	MOR	-	-
4.15	HSZ-385HUA (100)	0.21	150	72	-	VET (low crystallinity)	-	-
4.16	HSZ-390HUA (810)	0.21	150	72	36.8	VET	16.6	351
4.17	HSZ-390HUA (810)	0.24	150	72	31.4	VET	14.2	295

[a] $SiO_2/ZnO=50$, $H_2O/SiO_2=20$, $Li_2O/SiO_2=0.04$, seeds: 10wt.% to SiO_2, [b] solid yield

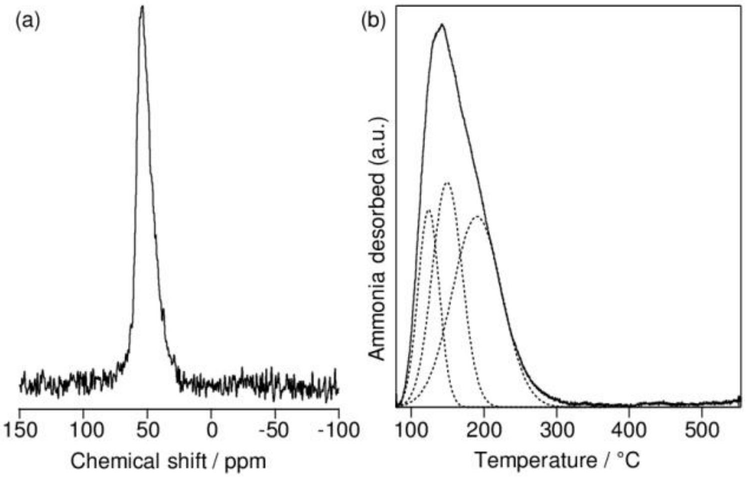

Figure 4.7 (a) ^{27}Al MAS NMR spectra and (b) NH_3-TPD profile of sample No. 4.16.[275]

4.3.4. Crystallization behavior of VET-type zincosilicate zeolite

Figure 4.8 (a) and (b) show the XRD patterns of the products synthesized with different times of crystallization at 150 °C using the same initial gel as that of sample No. 4.6 (see Table 4.1) with or without seed crystals, respectively. It is clearly revealed that seed crystals play a crucial role in the crystal growth of the VET-type zeolite in the OSDA-free system. The XRD pattern for the sample after 12 h of heating in the presence of the seed crystals shows the appearance of phases corresponding to VET-type zeolite, which may mostly be attributed to the diffraction from the undissolved seed crystals as deduced from the low solid yield (23.6 wt.%) of the obtained product. The crystal growth of VET-type zeolite is clearly observed after 24 h of heating, and the maximum peak intensity was attained after 72 h of crystallization in the presence of the seed crystals (Figure 4.8 a)) As can be seen from the SEM images of the intermediate products in Figure 4.9, most seed crystals were embedded with the sphere-shaped amorphous matters after heating the sample for 12 h, and the growing rod-like crystals of VET-type zeolite were observed after 24 h, which is in good agreement with the XRD patterns. Kenyaite, a layered silicate, appeared as a byproduct in the seeded system heated for 120 h, indicating that the crystal growth of the zeolite should be completed before nucleation of the byproduct starts to occur. In the absence of the seed crystals, on the other hand, XRD peaks attributed to another layered silicate, magadiite, were observed after 80−96 h of heating in the absence of the seed crystals, and in this case, no zeolite phase was confirmed (Figure 4.8 (b)). XRD patterns of the samples with prolonged heating revealed that kenyaite seems to be more thermodynamically stable phase under this condition. The results summarized in Table 4.3 show that only magadiite and kenyaite were obtained in the unseeded system (sample Nos. 4.18–4.20). It is inferred from these results that the seeding kinetically accelerates the crystal growth rate of the target VET-type zeolites, but does not influence much on the change of the thermodynamically stable phases (kenyaite or magadiite) under the present reaction conditions.

4.3.5. Structural similarities between VET-type zeolite and magadiite

In Chapter 2, a working hypothesis for the successful OSDA-free synthesis of zeolites has been proposed on the basis of the structural similarity in both seed zeolite and other zeolite obtained when the unseeded gels were heated.[200] This novel hypothesis suggests that the target zeolite should be added as seeds to a gel that usually yields a

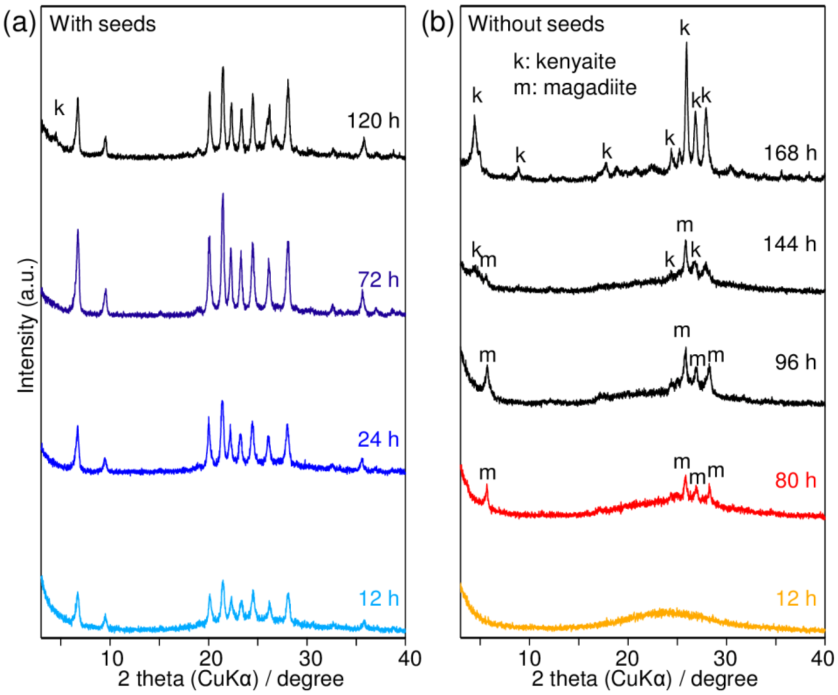

Figure 4.8 Evolution of XRD patterns of the products synthesized in (a) the presence and (b) the absence of the seeds. Other conditions are identical to those of sample No. 4.6. Kenyaite and magadiite phases are marked as k and m, respectively.[275]

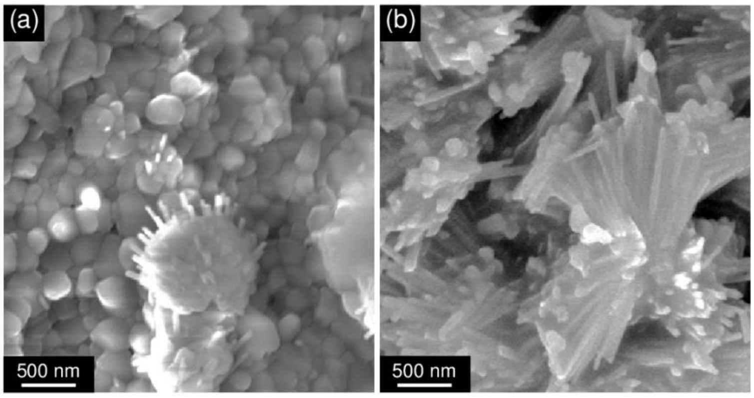

Figure 4.9 FE-SEM images of the intermediate products after (a) 12 h and (b) 24 h of hydrothermal treatment.[275]

Table 4.3 Summary of the OSDA-free synthesis in the unseeded systems.[275]

	initial gel[a]						reaction condition		product
sample	SiO_2/ZnO	Li_2O/SiO_2	Na_2O/SiO_2	Li/(Li+Na)	$(Li+Na)_2O/SiO_2$	Li_2O/ZnO	temp.[℃]	time [h]	
4.18	30	0.033	0.22	0.13	0.25	1.0	150	120	Magadiite
4.19	50	0.020	0.23	0.08	0.25	1.0	150	96	Magadiite
4.20	∞	0.020	0.23	0.08	0.25	∞	150	96	Kenyaite

[a] H_2O/SiO_2=20

zeolite, both containing the common CBU defined by IZA-SC[62]. Applicability of the hypothesis has been confirmed in some aluminosilicate systems (see Chapter 2).

Although magadiite and kenyaite are not zeolites and their crystal structures have not been fully solved,[277] the hypothetical structure of magadiite has been proposed (Figure 4.10 (c)).[278] It should be pointed out that the comparison of the structures of VET-type zeolite and magadiite layered silicate described below should be considered carefully and speculatively because it contains speculation due to the uncertainty of the magadiite crystal structure; however, this structural consideration would be meaningful for understanding the formation of VET-type zeolite under the present conditions. In addition, it is noteworthy that although the proposed structures of magadiite are somewhat different, most of them are 5-MR-rich silicates.[278–280] According to the hypothetical structure, the structure of magadiite is mainly constructed from 5-MRs, and has a structural unit with 8 T-atoms consisting of 5-MRs and liner 3 T-atoms (Figure 4.10 (a)), which is the same structure corresponding to the 5–3 unit categorized as a secondary building unit (SBU, defined by IZA).[62] This unit can also be found in the VET-type structure, as shown in Figure 4.10 (d). By definition, the SBUs are derived by assuming that the entire framework is composed of only one type of SBU (primary building unit is $TO_{4/2}$ tetrahedra).[281] In fact, the 5–3 unit is not an SBU of VET-type zeolite in the structure database [62] because the structure of VET-type zeolite involves one additional T-atom along with 5–3 unit (see Figure 4.10 (d); T-atom in blue color). However, the 5–3 unit is definitely found in the VET framework and thus it can be concluded that VET-type zeolite and magadiite have a common 5-3 building unit. On the contrary, CBUs are not required to build the entire framework structure. The CBU in the VET-type zeolite structure is *cas*, which can be decomposed into a 5–3 unit and 4

T-atoms (Figure 4.10 (b)). Although we are not aiming to describe the crystal growth mechanism by applying the conceptual and structural units, the crystal growth behavior could be reasonably understood when the framework structure of the products is fragmented into smaller common structural units between products obtained with and without seeding.. However, there is no clear evidence until now, and hence, further analyses were performed to support this hypothesis

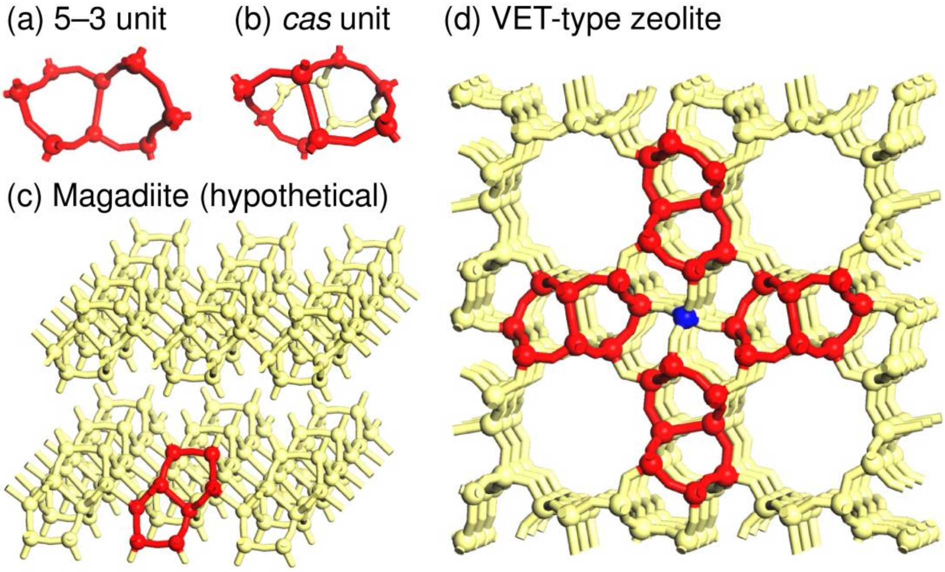

Figure 4.10 (a) 5–3 unit, (b) cas unit, (c) hypothetical structure of magadiite,[278] and (d) structure of VET-type zeolite con-structed from 5–3 unit (red) and single tetrahedral unit (blue). Oxygen atoms are omitted for clarity.[275]

4.3.6. Structural changes in zincosilicate species during hydrothermal treatment

Figure 4.11 shows the changes in the SiO_2/ZnO and the $Li_2O/(Li_2O+Na_2O)$ ratios of the solid products with and without the seed crystals. Zinc and lithium cations were selectively incorporated into the solid phase obtained in the presence of seeds (note that the initial SiO_2/ZnO and $Li_2O/(Li_2O+Na_2O)$ ratios in the gel are 50 and 0.08, respectively). On the other hand, these elements were not easily incorporated into the crystalline phase when the seed crystals were not added. The SiO_2/ZnO ratios showed similar values regardless of the seeding prior to the formation of magadiite and kenyaite; however, the ratio increased with the occurrence of crystal growth of these layered silicates. The SiO_2/ZnO ratio also slightly increased in the seeded system with the formation of kenyaite as impurity. Magadiite and kenyaite are layered sodium silicates, and kenyaite was easily formed without seeds and Zn cations (see Table 4.3, sample No. 4.20). Moreover, $Li_2O/(Li_2O+Na_2O)$ ratios of the products synthesized in the seeded system were clearly higher than those of the unseeded products, suggesting that Li cations were selectively occluded into the VET-type zeolite, while they were hardly incorporated into the layered silicates.

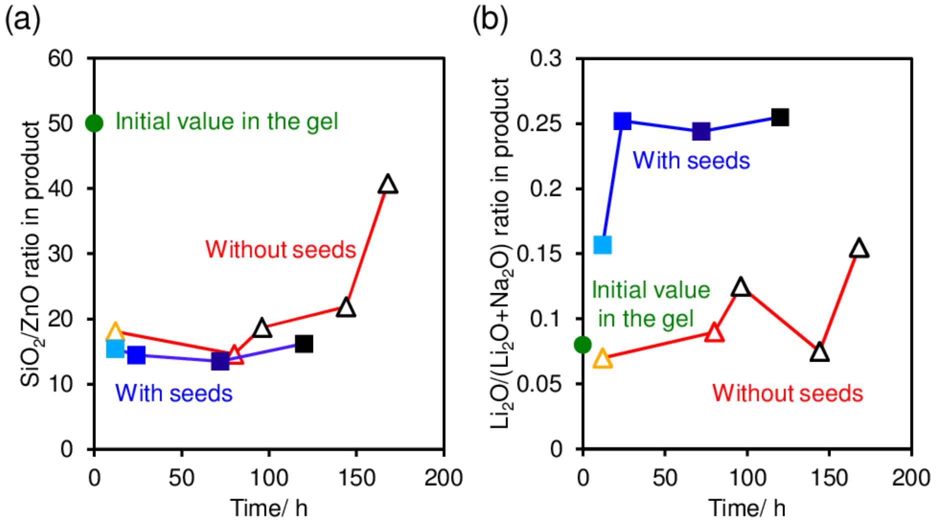

Figure 4.11 Changes in the chemical compositions with time of hydrothermal treatment. (a) SiO_2/ZnO and (b) $Li_2O/(Li_2O+Na_2O)$ ratios in the solid products (solid square: with seeds, open triangle: without seeds, and solid circle: initial value in the gel).[275]

To better understand the structures of the seeded and unseeded zincosilicate products, HEXRD measurements were performed. Figure 4.12 shows the total correlation functions, $T(r)$, of the seeded and unseeded products at different time period of hydrothermal treatment. From the $T(r)$ curves, it is possible to identify the various atomic distances associated with several structural features. The first and second correlation peaks in the *T*(*r*) are assigned to Si–O (*ca.* 1.6 Å) and Zn–O (*ca.* 2.0 Å) correlations, respectively. The peak observed at 2.6 Å is assigned to O–[Si]–O correlation, while Si–[O]–Si (or Zn) and O–[Zn]–O correlations are overlapping at 3.1 Å. No significant difference is observed among these four peaks in the samples (Figure 4.12). It is well known that the incorporation of Zn induces the formation of 3-MRs, and correlation of the second nearest neighbor of T–O (T: tetrahedral atoms, in this case, Si and Zn) in 3-MRs could be seen at *ca.* 3.3 Å in the previous mechanistic study on the synthesis of zincosilicate VPI-7.[282] However, in the OSDA-free synthesis of VET-type zeolite, the peak at 3.3 Å is hardly observed, suggesting that Zn atoms do not promote the formation of 3-MRs even in the intermediate products under this condition. Peaks at 3.7–4.2 Å are mainly due to the second nearest neighbor of T–O in 5-MRs and

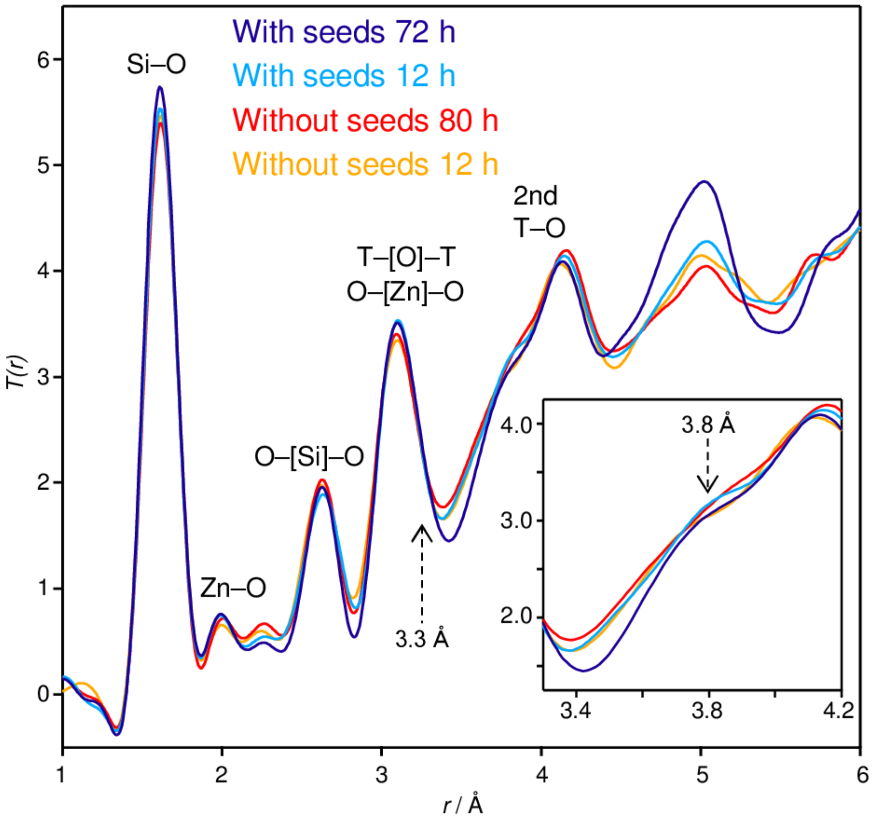

Figure 4.12 Total correlation functions, T(r), (1.0–6.0 Å), of the products synthesized with seeds for 12 h (light blue), and 72 h (dark blue) and without seeds for 12 h (yellow), and 80 h (red).[275]

6-MRs,[184,282] while peaks at *ca*. 5 Å may be due to overlap of various atomic correlations. The presence of the small shoulders at *ca*. 3.8 Å in the $T(r)$ curves of the amorphous products (Figure 4.12 (see incet), light blue and yellow lines) suggests that these products contain a small fraction of 4-MRs,[184,283] and these peaks disappeared as the reaction proceeded. Interestingly, the peaks were barely shifted regardless of the seeding even in this region, and the $T(r)$ curves are quite similar with each other. It is noteworthy that changes in distances between atoms in this system are quite small in comparison with those previously reported, in which the curves dramatically changed in this region as reaction proceeded.[282–284] This result indicates that the seeded and unseeded products, ranging from the intermediate non-crystalline solid to the fully crystallized product in terms of atomic distances, suggesting that crystallization proceeded via the minimal change in the medium-range orders (silicate ring-structures) of non-crystalline networks to form the zeolite framework.

Raman spectra of the obtained products are shown in Figure 4.13. The bands in a 200–600 cm^{-1} region are sensitive to the T–O–T bond angle, the network connectivity, and the size of the ring systems present in the silicate framework.[283] According to the previous reports on the Raman spectra of zeolites, the bands at *ca*. 290–410, 370–430, and 470–530 cm^{-1} are assigned to 6-, 5-, and 4-MRs, respectively.[283,285] The ring distribution of VET-type zeolite shown in Figure 4.14 contains 5-, 6-, 7-, 8-, and 12-MRs. The band intensities of 6-MRs (*ca*. 290 cm^{-1}) and 5-MRs (*ca*. 400 cm^{-1}) in the spectra of the seeded products increased with the progress of crystal growth, which may imply that the numbers of such 6-, and 5-MRs increased somehow during the crystal growth process through the connection of silicate species having 5-MRs or the reconstruction of silicate frameworks. On the other hand, the formation of 6-MRs was not observed in the unseeded product, and only a small peak corresponding to 5-MRs was observed even after 80 h of heating, resembling the seeded product just heated for 24 h. Silicate species with the 5–3 unit or relative 5-MR-rich structures might be spontaneously formed from the reactant gels regardless of the seeding, while 6-MRs are only formed in the framework of the VET-type zeolite by connecting a number of 5–3 units, as shown in Figure 4.15.

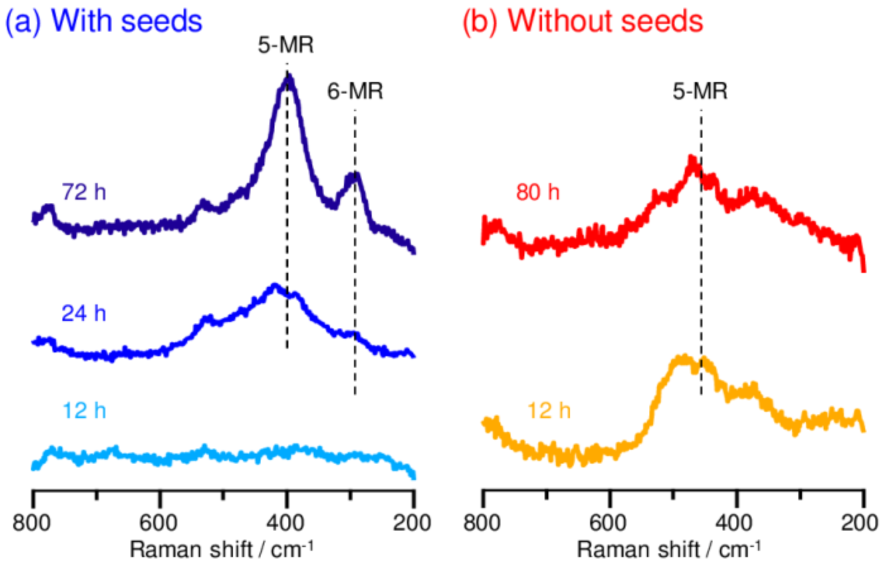

Figure 4.13 Raman spectra of the products synthesized (a) with and (b) without seeds.[275]

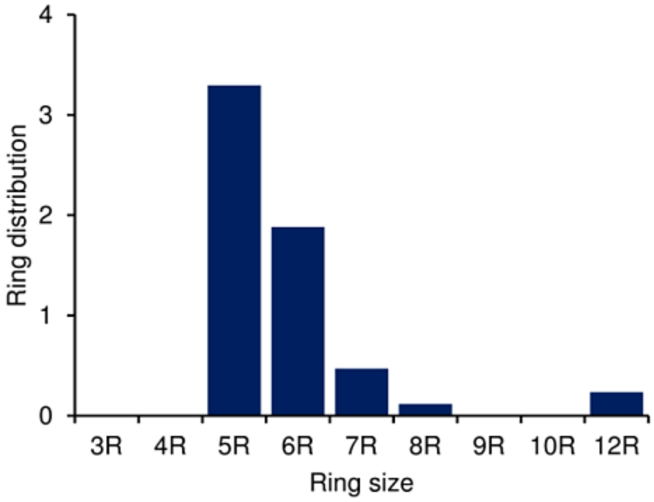

Figure 4.14 Ring distribution of VET-type structure.[275]

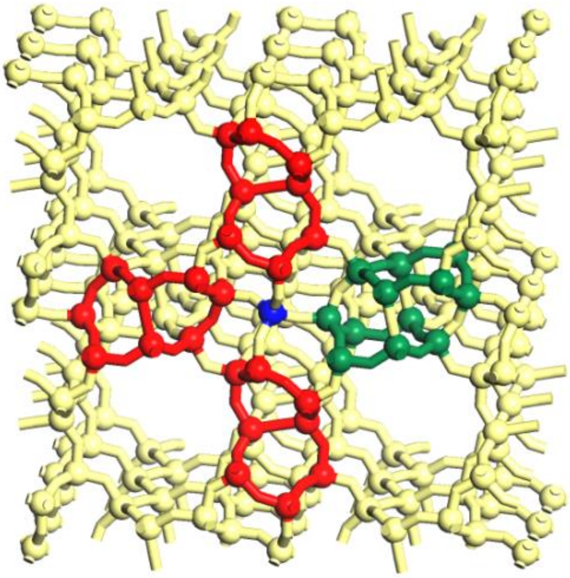

Figure 4.15 Representative two 6-MR in VET-type structure (green). Some of 5-3 units are colored by red with the blue single T-atom same as Figure 4.10.[275]

Changes in the ^{29}Si MAS NMR spectra along with different times of hydrothermal treatment are shown in Figure 4.16. The peak assignment of the fully crystallized product (72 h) is already described in the above section. The products heated for 12 and 24 h with seed crystals show similar but slightly broader spectra to that of the final product (72 h), reflecting the disordered structures. The peaks at *ca.* −100 ppm are the overlapped signals of Q^4 (1Zn) and Q^3 (0Zn) silicon atoms. Additionally, a small signal at −65 ppm, which can be assigned to Q^4 (4Zn), is observed for the product heated for 12 h. This signal suggests the presence of Zn-rich zincosilicate species; however, it disappeared after 24 h of heating as reaction proceeded, and homogeneous amorphous gels were obtained. The spectra of the products synthesized without seeds are slightly different from those of the seeded products. Broader signals are observed at ca. −80 to −120 ppm in the unseeded product heated for 12 h, suggesting the disordered structure of (zinco)silicate species; no signal is observed at −65 ppm. The spectrum is still broad even after 80 h of heating. The spectra observed at ca. −80 to −120 ppm may be a result of overlap between the signals from amorphous zincosilicates (broad peak), and the Q^3 and Q^4 silicons from magadiite (sharp peak).[279]

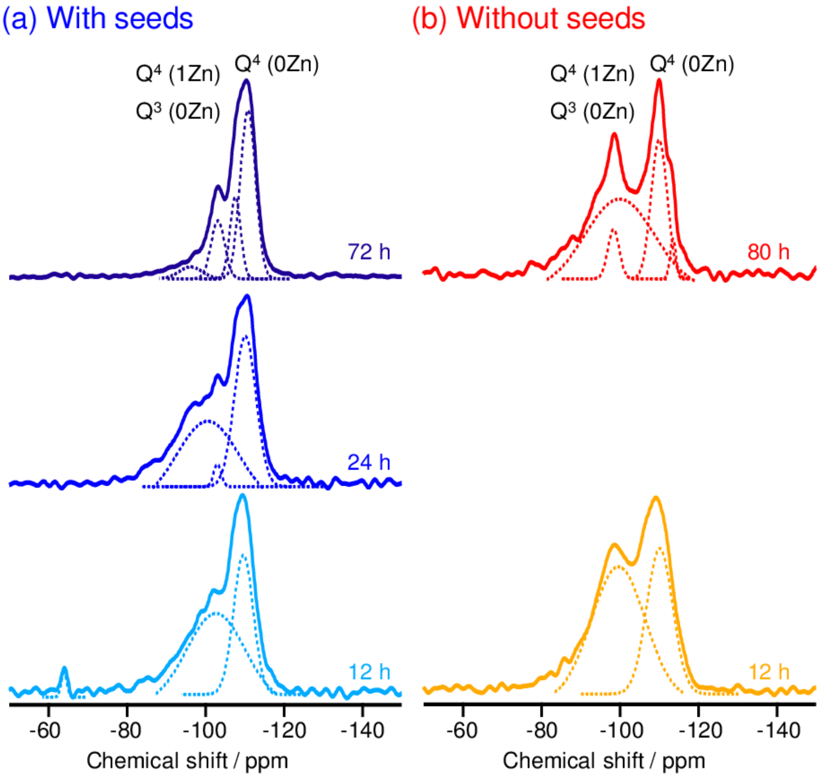

Figure 4.16 ^{29}Si MAS NMR spectra of the products synthesized (a) with and (b) without seeds.[275]

(Zinco)silicate species formed during the reaction can be discussed on the basis of HEXRD, Raman spectroscopy, and ^{29}Si MAS NMR spectroscopy. Prior to the crystal growth, silicates are formed as solid amorphous matters and soluble species via dissolution–reprecipitation processes during hydrothermal treatment. In general, many factors are concerned in these processes, but the presence of seed crystals should not essentially change the structures of solid amorphous matters. Interestingly, these matters might have similar structures to the target VET-type zeolite, as shown in HEXRD results, and possibly magadiite (or specific structural units with 5-MRs might exist in this period), regardless of the seeding. However, even if the amorphous matters have similar structure to the target zeolite, the crystal growth of target zeolite never proceeds without seed crystals, which is thought to provide the active surface for crystal growth. [136,184,200] Moreover, the assembling process of silicate species with cations should be important; therefore, the suitable cations, which were selectively incorporated into the product, should be selected to balance the electric charge (in this case, Zn and Li).

The observation by DR UV–Vis spectroscopy, shown in Figure 4.17, revealed that the chemical states of the zinc-containing species in the solid phases were changed significantly during hydrothermal treatment. As noted above, the detailed assignment of the peaks to the chemical state of Zn species is difficult.[256,270] However, the changes in the spectra during hydrothermal treatment show that the state of Zn species changed throughout the reaction. At the early stage, both seeded and unseeded amorphous matters show similar spectra with mainly two peaks at 255 and 200 nm (Figure 4.17 (a) and (d)). The peak at 360 nm corresponding to the extra-framework ZnO is hardly observed throughout the synthesis. The peak at 255 nm decreased in its intensity and slightly shifted to 250 nm for the seeded product after 24 h heating (Figure 4.17 (b)). The product obtained after 72 h showed further decrease in intensity (Figure 4.17 (c)), suggesting that the state of Zn species continuously changed until the completion of crystallization of VET-type zeolite. In contrast to the spectra of the seeded products, the unseeded product did not provide large change even after 80 h of heating (Figure 4.17 (e)). Interestingly, the spectra of the seeded product heated for 24 h (Figure 4.17 (b)) and the unseeded product heated for 80 h (Figure 4.17 (e)) show similar spectra, suggesting that Zn species in these products are in similar states.

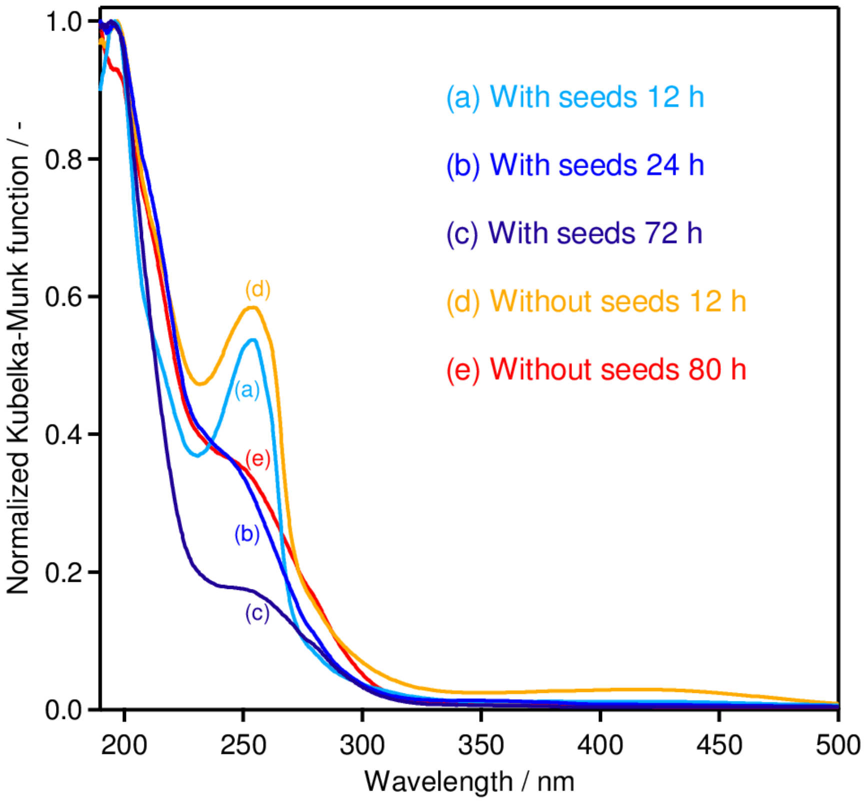

Figure 4.17 DR UV–Vis spectra of the products synthesized with seeds for (a) 12 h, (b) 24 h, and (c) 72 h and without seeds for (d) 12 h, and (e) 80 h.[275]

The state of Zn species during hydrothermal treatment is estimated to be changed as follows. The first change occurring both in seeded and in unseeded products might be caused by the formation of zincosilicate species (i.e., the formation of Si–O–Zn bonds) by heating. The second one observed only in the seeded product with the crystal growth of the VET-type zeolite might be due to the incorporation of Zn atoms into the specific tetrahedral positions of the VET-type structure.

On the basis of all abovementioned measurements, possible pathways for the crystal growth of the VET-type zincosilicate zeolite are illustrated in Scheme 4.1. First zincosilicate species, which might contain the 5–3 units or other 5-MR-rich structural units, are speculated to be the common precursor of the products. The crystal growth of the VET-type zeolite occurs by incorporating the Zn atoms into the specific tetrahedral sites of the framework through the zincosilicate species accompanied by Li cations in the case of the seeded system. On the contrary, magadiite was crystallized through the formation of the 5-3 or other relative structural units from the zincosilicate and silicate species only with the aid of OH^- ions in the unseeded system. Formation of silicate species having medium-range order structures similar to the VET-type framework prior to the crystal growth and successive cation-driven assembly of these species would be critical phenomena for the OSDA-free synthesis of VET-type zeolite in this study. The characteristic of this mechanistic feature is that it involves similarity of intermediate structure of silicates and minimal change of structure in medium-range order, which would not require high activation energy for the crystal growth.

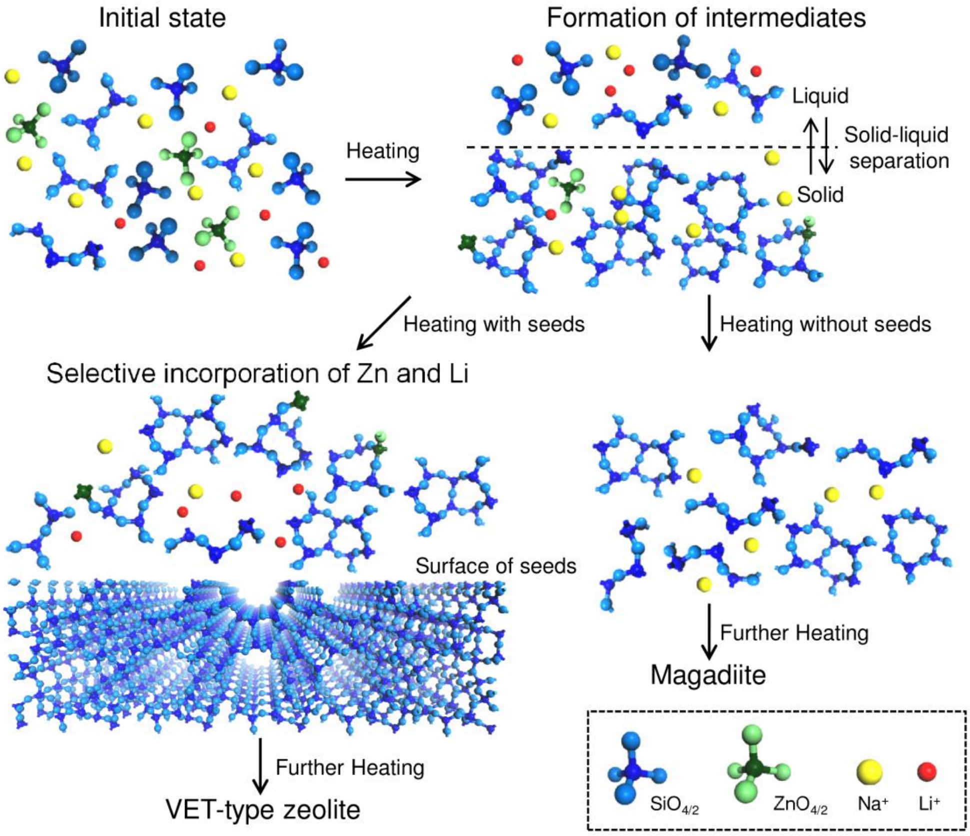

Scheme 4.1 Proposed crystal growth pathways of VET-type zeolite without using OSDAs.[275]

In addition, the framework of the VET-type zeolites has a unique “pin-wheel” building unit constructed from four 5–3 units and one T-atom (see Figure 4.10 (d)). Only one T-atom (blue color in Figure 4.10 (d)) exists per unit cell of VET-type zeolite (containing 17 T-atoms). If one Zn atom is selectively incorporated into this T-site, the SiO2/ZnO ratio of the product should be 16, which is almost agreed well with the experimental data (12.3–16.6 in Table 4.1 and Table 4.2) obtained in this study. Consequently, when the crystal growth of the VET-type zeolite occurs, the specific tetrahedral sites in the framework, in which a Zn atom may be selectively incorporated as described above, are the center site of the “pin-wheel,” surrounded by four 5–3 units. Although details about Zn sites are under investigation, according to the literature, this tetrahedral site has the longest T–O distance and the second narrowest T–O–T angle (1.603 Å and 149.0°, respectively, on average),[271] suitably for the sitting of Zn atoms.

4.4. Conclusion

The successful seed-directed, OSDA-free synthesis of the VET-type zincosilicate zeolite was demonstrated. To the best of our knowledge, this is the first report on the synthesis of large pore zincosilicate zeolite without using OSDA. The results show the applicability and possibility of this novel method to other metallosilicate zeolites beyond aluminosilicates. Magadiite, a layered silicate having the hypothetical structure containing the structural 5–3 unit, common to the VET-type zeolite, was obtained under identical conditions but without seed crystals. Detail investigation of the silicate structures in the solid products by an assay of diffraction and spectroscopy techniques revealed that this common unit or relative 5MR-rich unit might be spontaneously formed during hydrothermal treatment. Furthermore, both Li and Zn cations, which were selectively incorporated into the products, play an important role for the crystal growth of the VET-type zeolite. Possible crystal growth pathways suggested here are the formation of silicate species by minimal change of structure in medium-range order and the crystallization driven by Li and Zn cations. This result gives us some insights into zeolite crystallization, and considerably clearer crystallization scheme of zeolites would be solved through the synthesis of many other zeolites. It is anticipated that the number of zeolites to be synthesized by applying the concept of the common structural units such as the 5–3 unit is much greater than that by applying the concept of the common CBU, proposed previously (see Chapter 2).

Chapter 5. One-Pot Synthesis of *BEA-Type Aluminosilicate Zeolite with Hollow Interior Using Zincosilicate Seeds

5.1. Introduction

There are some difficulties to control the characteristics of the zeolites synthesized by the seed-directed method, such as the SiO_2/Al_2O_3 ratios and the particle sizes. In the all of previous reports,[183–200] the particle sizes of products become larger than those of seed crystals because new zeolite crystals grow on the surface of the residual seeds and secondary nucleation has never been observed. Therefore, the control of particle sizes is especially fundamental issue in seed-directed synthesis of zeolites. It is well known that the large zeolite crystals are not suitable for catalysis, adsorption, and ion-exchange due to the diffusion limitation in micropores.[286] To avoid this problem, hierarchically porous zeolites with mesopores or macropores are attracting many attentions, and these zeolites exhibit remarkably improved catalytic performances.[287–291] Hollow zeolites are also known as one of the hierarchically porous zeolites, and synthesized by various methods such as the use of hard templates like polystyrene beads[292–296] or the selective dissolution of zeolite cores by desilication,[297–299] dealumination,[300] and the removal of other metalosilicates.[301] Self-construction of the core–shell and hollow zeolites by recrystallization route from the surface to core are reported for small pore zeolites such as analcime,[302] zeolite A,[303] and Na-P1.[304] However, all of these methods need organic compounds or post treatment processes.

In this chapter, the one-pot, OSDA-free synthesis of hollow zeolite beta is successfully achieved on the basis of the crystallization strategy: the initial seed-directed crystal growth on the surface of the seeds and the subsequent dissolution of the seed crystals. Zeolite beta is a *BEA-type aluminosilicate zeolite (FTC: *BEA)[62] with 3-dimensional pores with 12-MRs, and has been one of the most important zeolites as practical catalysts and adsorbents in these days.[114] Namely, *BEA-type zincosilicate zeolite called CIT-6[262–264] is used as seed crystals for the OSDA-free synthesis of hollow aluminosilicate zeolite beta. The key factors for the successful seed-directed synthesis of the hollow zeolite beta are the surface structure and the solubility of the CIT-6 crystals. Stability of seed crystals during hydrothermal treatment is a fundamental issue for the seed-directed synthesis, and this new method provides the potential possibility of the seed-directed synthesis for hierarchical zeolites without any organic templates or post treatment processes. Moreover, gallosilicate zeolite with *BEA-type topology (donated as Ga-beta) is also used for the synthesis of aluminosilicate zeolite beta for comparison.

5.2. Experimental

5.2.1. Chemicals

The following raw materials for the OSDA-free synthesis were used as provided: Cab-O-Sil® (Grade M5, Cabot Corp.) as the silica source, sodium aluminate ($NaAlO_2$, Wako Pure Chemical Industries, Ltd.) as the aluminum source, and sodium hydroxide solution (NaOH, 50 w/v% in water, Wako) as the alkali source. For the synthesis of CIT-6 seeds, tetraetylammonium hydroxide (TEAOH, 35 wt.% in water, Sigma-Aldrich Co. LLC), Ludox® (HS-40, Aldrich), zinc acetate (Aldrich), and lithium hydroxide (LiOH monohydrate, Wako) were used as the OSDA, the silica source, the zinc source, and the alkali source, respectively, while gallium nitrate was used for the synthesis of Ga-beta seeds.

5.2.2. Material syntheses

Zeolite CIT-6 seed crystals were synthesized by the following procedure based on the previous report.[262,263] LiOH and TEAOH were dissolved in distilled water, followed by the addition of zinc acetate to obtain a clear solution. After the addition of colloidal silica, the obtained clear solution was kept stirred for 2 h. The total composition of the mixture was as follows: $0.325(TEA)_2O$: $0.025Li_2O$: 0.03ZnO: SiO_2: $30H_2O$. The mixture was transferred to a 23 mL Teflon®-lined stainless steel autoclave (#4749, Parr Instrument Co.) and was then subjected to the hydrothermal treatment at 150 °C for 4 d under autogenous pressure and static condition. After the hydrothermal treatment, the product was recovered by filtration, washed thoroughly with distilled water, and dried at 60 °C. The obtained CIT-6 seed crystals were used both before and after the calcination at 550 °C for 10 h in a stream of dry air.

Ga-beta seed crystals were synthesized by a modified procedure with referring some previous works.[305–307] Gallium nitrate were dissolved in a aqueous TEAOH solution, followed by the addition of fumed silica. The total composition of the mixture was as follows: $0.3(TEA)_2O$: $0.025Ga_2O_3$: SiO_2: $20H_2O$. The mixture was transferred to a 23 mL Teflon®-lined stainless steel autoclave (#4749, Parr Instrument Co.) and was then subjected to the hydrothermal treatment at 150 °C for 8 d under autogenous pressure and static condition. After the hydrothermal treatment, the product was recovered, washed, and dried. The obtained Ga-beta seed crystals were used both before and after the calcination at 550 °C for 10 h in a stream of dry air.

Seed-directed syntheses of zeolite beta were carried out by adding CIT-6 seeds prepared by above described procedure to the starting Na-aluminosilicate gel with a chemical composition of $x$$Na_2O$: $y$$Al_2O_3$: SiO_2: $20H_2O$ (where, x = 0.225-0.35, y = 0.004-0.033). For the preparation of Na-aluminosilicate gel, sodium aluminate was dissolved in distilled water, followed by the addition of aqueous NaOH to obtain a clear solution. Then, a mixture of CIT-6 seeds and Cab-O-Sil® was slowly added to the solution, and vigorously stirred until a homogeneous gel was obtained. Here the added amount of zeolite seeds was 10 wt.% relative to the silica source, and the total weight of the Na-aluminosilicate gel was adjusted to 15 g. Subsequently, the seeded Na-aluminosilicate gel was transferred to an autoclave and subjected to the hydrothermal treatment at 140–150 °C for different periods under autogenous pressure and static conditions. After the hydrothermal treatment, the product was recovered by filtration, washed thoroughly with distilled water, and dried at 60 °C. Obtained products were characterized as their as-synthesized forms unless otherwise noted. In the case of uncalcined seeds were used, the products were calcined at 550 °C for 10 h before N_2

adsorption–desorption measurements. The solid yield of the obtained zeolite was defined as the weight ratio percentage (g/g × 100) of the dried solid product to the sum of the dry SiO_2, $NaAlO_2$, and the dry (calcined) seeds in the starting Na-aluminosilicate gel.

5.2.3. Characterizations

Powder X-ray diffraction (XRD) patterns of the solid products were collected using a Rigaku Ultima IV diffractometer and CuKα radiation ($\lambda = 0.15406$ nm, 40 kV, 40 mA) from 3 to 40° in 2θ. The scanning step was 0.02° at a scanning speed of 2° min^{-1}. Elemental analyses of the zeolite seeds and products were performed by an inductively coupled plasma-atomic emission spectrometer (ICP-AES, Thermo iCAP 6300) after dissolving them in hydrofluoric acid or potassium hydroxide solution. The crystal size and morphology were observed by a Hitachi S-900 field-emission scanning electron microscope (FE-SEM) and a JEOL JEM-2010F transmission electron microscope (TEM). Before TEM observation, samples were embedded in epoxy resin and sliced by an ion slicer. Nitrogen adsorption–desorption measurements of zeolite products were performed on a Quantachrome Autosorb-iQ2-MP at −196 °C. Prior to the measurements, all samples were degassed at 400 °C for 6 h under vacuum. Solid-state ^{29}Si magic angle spinning nuclear magnetic resonance (MAS NMR) spectra were obtained at 59.7 MHz with the pulse width of 2.0 μs and pulse delay of 100 s, while ^{27}Al MAS NMR spectra were recorded at 78.3 MHz, a pulse width of 1.0 μs, and a recycle delay of 5 s on a spectrometer (Chemagnetics CMS-300). Thermogravimetry (TG) and differential thermal analysis (DTA) were performed on a Thermo plus TG 8120 (Rigaku) at the programming rate of 10 K/min in a stream of a mixed gas (O_2: He

= 10%: 90%). Samples (*ca.* 10 mg) were packed into an alumina pan and an empty alumina pan was used as a reference.

5.3. Results and discussion

5.3.1. Characterization of CIT-6 seed crystals

The powder XRD patterns of as-synthesized and calcined CIT-6 seeds in Figure 5.1 (left, XRD patterns) show that obtained CIT-6 crystals are confirmed as *BEA-type structure without any impurity. The SiO_2/ZnO ratio of the seed crystals determined by chemical analysis was 13.1. As shown in Figure 5.1 (right, SEM image), the particle sizes of CIT-6 seed crystals range in 200–600 nm. In order to understand the stability of the seed crystals in alkaline aqueous solution, the crystals were treated in 0.1M NaOH aqueous solution (pH of the solution was *ca.* 13) in an autoclave at 140 °C for 6 h. Changes of the crystallinity by the treatment were calculated from the integrated intensity ratio of the strongest peak ($hkl = 302$) in XRD patterns before and after the treatment. The crystallinity of calcined seeds was dramatically decreased to 21% relative to the non-treated crystals, while that of as-synthesized seeds was slightly decreased to 80%. On the other hand, the crystallinity of aluminosilicate zeolite beta seed crystals ($SiO_2/Al_2O_3 = 24.0$) used for the seed-directed synthesis of zeolite beta in the previous report[182] was not changed after the same treatment regardless of the calcinations or not. Although high-silica seeds are less stable under hydrothermal treatment,[308,309] zeolite beta seed crystals used in the previous study have Al-rich composition and enough stable. CIT-6 seed crystals are less stable in alkaline solution than aluminosilicate beta seed crystals, and the remaining OSDAs in as-synthesized CIT-6 seeds stabilize the seed crystals in alkaline aqueous solution.

5.3.2. Seed-directed, OSDA-free synthesis of hollow zeolite beta

Figure 5.2 a) and b) show the XRD patterns of products synthesized with the

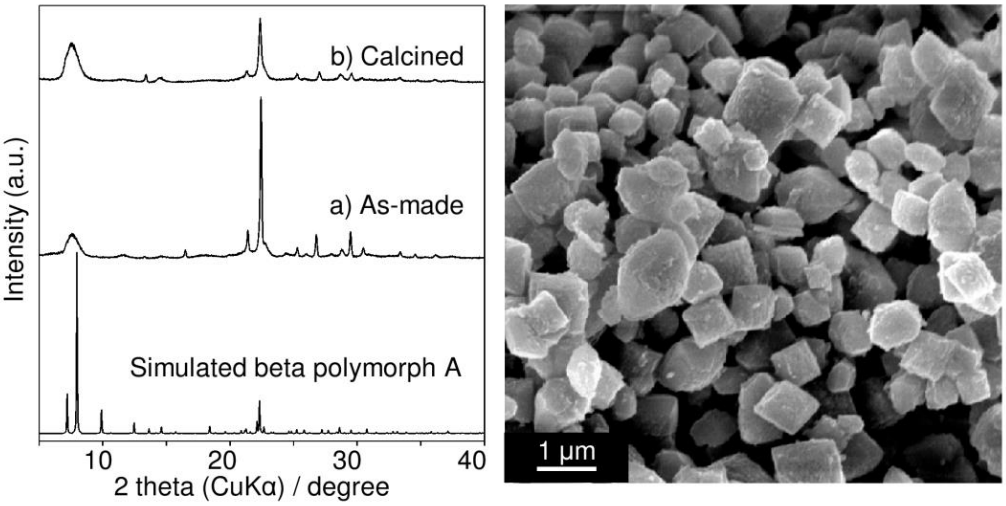

Figure 5.1 (left) Powder XRD patterns of a) as-synthesized and b) calcined CIT-6 seed crystals and (right) SEM image of seed crystals.[187]

addition of as-synthesized and calcined CIT-6 seeds, respectively for different periods of hydrothermal treatment at 140 °C using the same reactant gel for aluminosilicate beta that was already reported ($0.3Na_2O:0.01Al_2O_3: SiO_2:20H_2O$, point A in ref. 200. As in the case of aluminosilicate seeds system, zeolite beta was successfully obtained after 46h of hydrothermal treatment using as-synthesized CIT-6 seeds. However, no crystalline product was obtained in 48 h when calcined CIT-6 seeds were added, and mordenite (MOR-type aluminosilicate zeolite) was obtained after prolonged treatment. The previous reports show that mordenite is obtained from this reactant gel without seed crystals.[182,200] Considering these results and the stability of the seeds, the unstable calcined CIT-6 seed crystals should be completely dissolved prior to the onset of crystal growth during the hydrothermal treatment, and could not act as the active surface for the crystal growth. In addition, in the case of the synthesis with as-synthesized CIT-6 seeds, the organic content of the products were small (~3 wt.% by TG analysis) and the contribution to the crystal growth of that would be negligible.

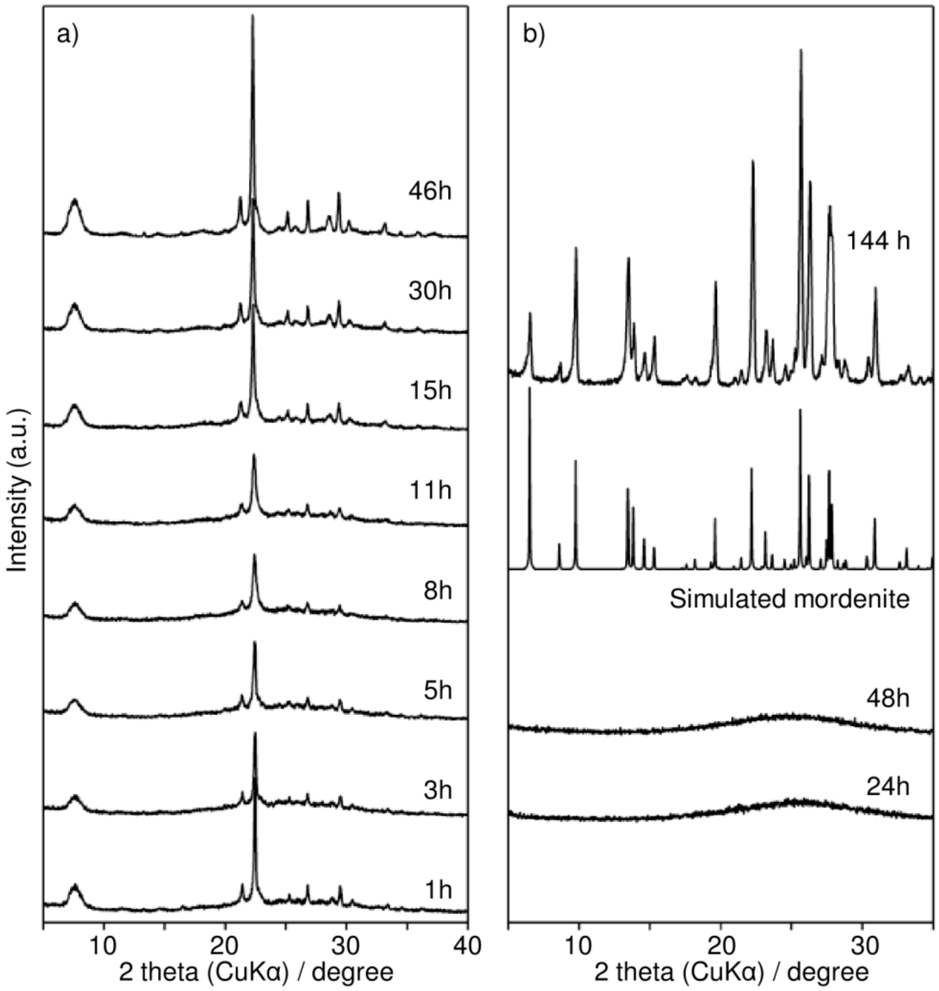

Figure 5.2 Evolution of XRD patterns of the products synthesized using a) as-synthesized and b) calcined CIT-6 seeds.[187]

The SEM images of the obtained zeolite beta are shown in Figure 5.3. Typical truncated octahedral morphologies of OSDA-free synthesized zeolite beta are clearly observed, and the particle sizes range in 0.6–1 μm. The ^{29}Si and ^{27}Al MAS NMR spectra of obtained zeolite beta are shown in Figure 5.4 a) and b), respectively. The ^{29}Si MAS NMR spectrum is similar to that of zeolite beta synthesized using aluminosilicate seeds, and the calculated SiO_2/Al_2O_3 ratio by the deconvolution of the spectra is 12.4, which agrees well with the value (13.1) obtained by chemical analysis. All aluminum species are incorporated in the zeolite framework, and octahedrally-coordinated, non-framework aluminum (at 0 ppm) is hardly observed in the ^{27}Al MAS NMR spectrum. The Na_2O/Al_2O_3 ratio of the product by chemical analysis was 1.0.

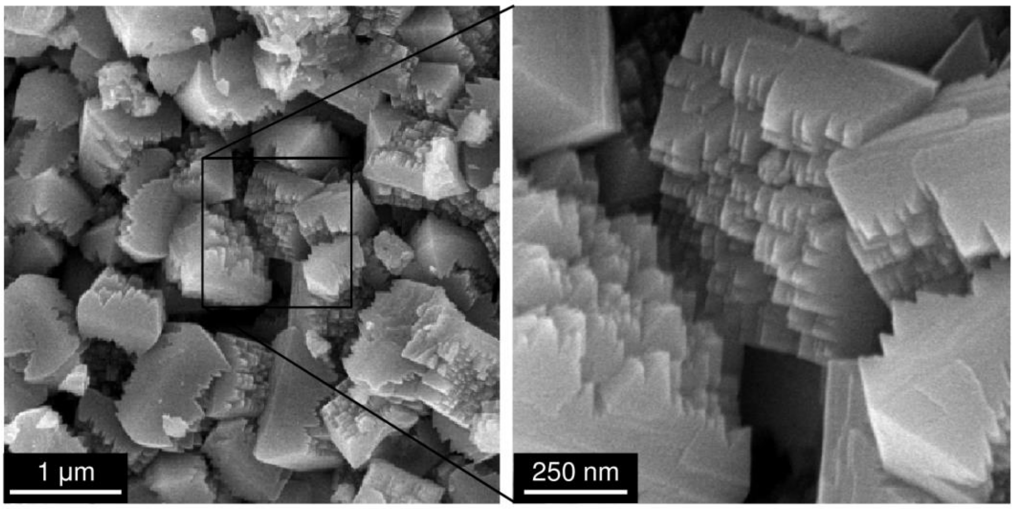

Figure 5.3 SEM images of obtained zeolite beta.[187]

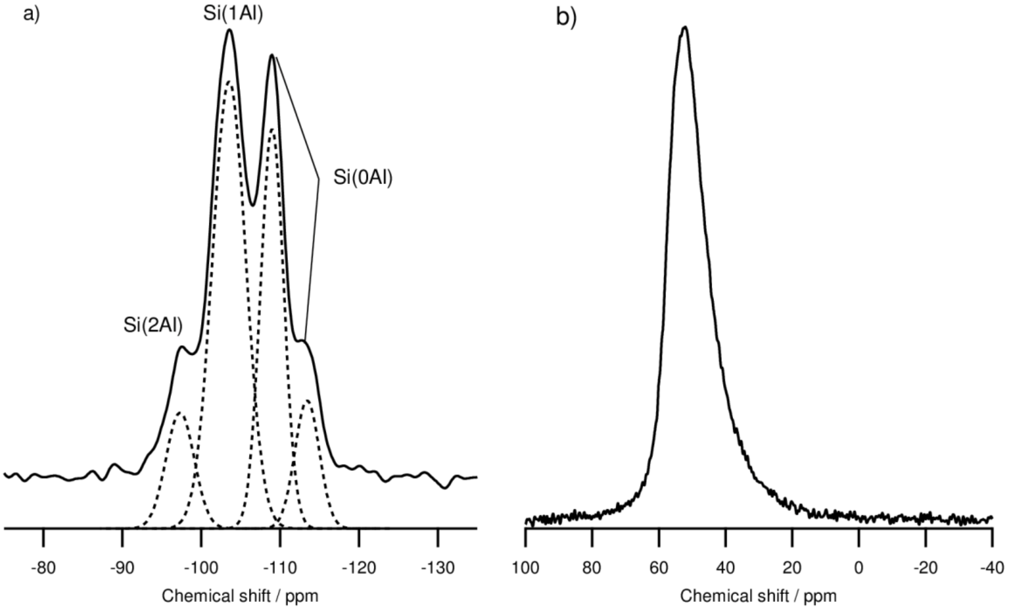

Figure 5.4 a) ^{29}Si and b) ^{27}Al MAS NMR spectra of obtained zeolite beta.[187]

The nitrogen adsorption–desorption isotherms of CIT-6 seeds and the product are shown in Figure 5.5. Both isotherms are classified as IUPAC type I, and a Brunauer–Emmett–Teller (BET) specific surface area and micropore volume derived from a *t*-plot method of the product are 632 $m^2\ g^{-1}$ and 0.22 $cm^3\ g^{-1}$, respectively. These values are almost equal to those of conventional zeolite beta[182] and CIT-6 seeds (614 $m^2\ g^{-1}$ and 0.21 $cm^3\ g^{-1}$). Noteworthy, the isotherm of the product exhibits a specific hysteresis loop, suggesting the presence of intra-crystalline mesopores or voids connected to micropores.[310–313] The hysteresis loop has not been observed in the isotherms of CIT-6 seeds and zeolite beta synthesized using aluminosilicate seeds.[182] It has been reported that the closure point of the hysteresis loop at P/P_0 ~0.45 is characteristic of cavitation-controlled evaporation of nitrogen,[310–313] and similar isotherms are observed in previous reports concerning well-closed hollow crystals of ZSM-5[299] and TS-1.[301] Cavitation (spontaneous nucleation of bubbles) is correlated to bottle-neck type pore structures with smaller neck (< 4 nm) of hollow zeolite crystals, and details are illustrated in Scheme 5.1. The volume of inner void is calculated to 0.032 cm^3/g using the difference between the volume adsorbed at $P/P_0 = 0.54$ and 0.44 in the desorption branch.

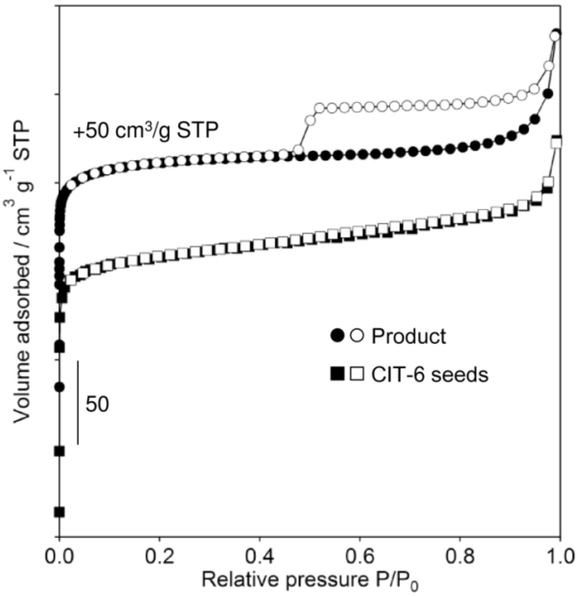

Figure 5.5 Nitrogen adsorption (solid symbols) –desorption (open symbols) isotherms of the product (circule) and CIT-6 seeds (square). For clarity, the isotherm of the product has been shifted by 50 $cm^3\ g^{-1}$.[187]

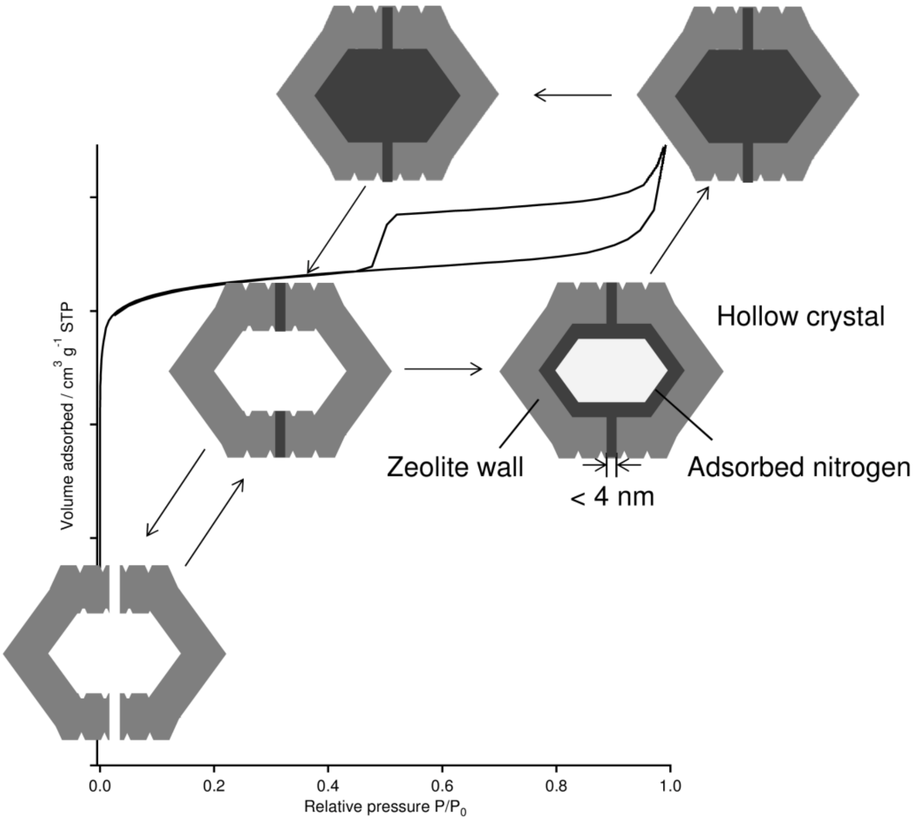

Scheme 5.1 Cavitation phenomena in bottle-neck type pores.[187]

The hollow structure of obtained zeolite beta is confirmed by TEM image of the sliced crystal as shown in Figure 5.6. Interestingly, similar facets are observed both on the outer surface and inner surface of a crystal, suggesting that the crystal growth proceeded toward inside after the complete dissolution of the CIT-6 seed crystal. The diameter of the inner void is *ca.* 500 nm, which is equal to or slightly smaller than the particle size of CIT-6 seed crystals. It is reasonable to consider that CIT-6 seed crystals were completely dissolved during the hydrothermal treatment. The detail mechanism is described and discussed below.

For the comparison, Ga-beta was also used as seed crystals to synthesize aluminosilicate zeolite beta. After same alkaline treatment as CIT-6 and aluminosilicate zeolite beta, the crystallinity of as-synthesized Ga-beta did not change (99%), while that

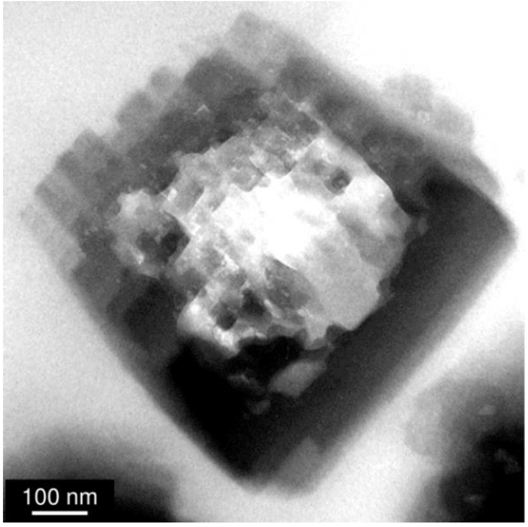

Figure 5.6 TEM image of the sliced crystal.[187]

of calcined seeds was decreased to 66% relative to the non-treated crystals. Ga-beta seed crystals have intermediate stability compared with aluminosilicate zeolite beta and CIT-6 seed crystals. The reactant gel and the reaction conditions are same as the above mentioned sample. Figure 5.7 shows the XRD patterns, the SEM image, and the nitrogen adsorption–desorption isotherm of the product synthesized using Ga-beta seed crystals. Fully crystallized zeolite beta was obtained after 24 h of hydrothermal treatment (Figure 5.7 a)). As in the case with previous studies, mordenite and Na-P1 appeared as byproduct after prolonged treatment, and the time when impurities appeared was slightly earlier than the case using CIT-6 seed crystals. Particle sizes or composition of the seed crystals, namely, external surface areas or dissolution rate, may influence on the nucleation rate of these impurities. Conversely, zeolite beta was not obtained when the calcined seed crystals were used (Figure 5.7 b)). The reason can be similar to the case of calcined CIT-6 seed crystals, and seed crystals are considered to be dissolved completely before the start of crystal growth. Aggregated small particles with a diameter of *ca.* 300 nm can be seen from the SEM image (Figure 5.7 c)). This morphology is similar to that of previously reported zeolite beta synthesized using aluminosilicate seed crystals,[180186] but different from that of the product using CIT-6 seed crystals (see Figure 5.3). Furthermore, the nitrogen adsorption–desorption isotherm was different from that of CIT-6 seeded zeolite beta (Figure 5.7 d)). The hysteresis loop, which is characteristic in the isotherm of CIT-6 seeded product, was not observed in that of Ga-beta seeded product, therefore this product may not possess hollow interior. The SiO_2/Ga_2O_3 ratio of the Ga-beta seeded product was 56.2 (by chemical analysis) suggesting that gallosilicate core was remained in the final product (note that the SiO_2/Ga_2O_3 ratio of seeds were 34.4). It can be concluded that as-synthesized Ga-beta seed crystals are more stable than CIT-6 seed crystals and could not be dissolved. Zeolite beta with hollow interior was not obtained when using stable seed crystals such as Ga-beta.

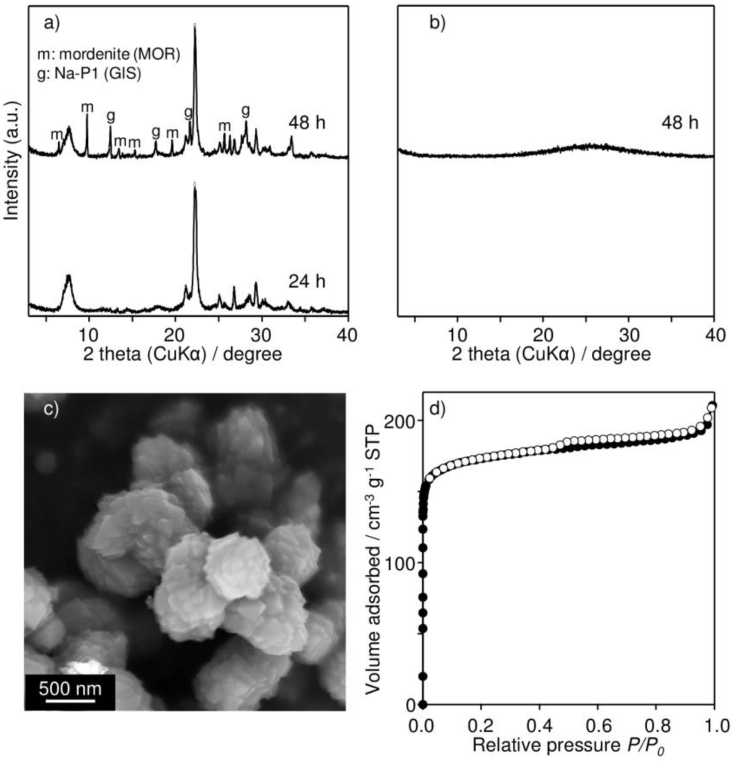

Figure 5.7 XRD patterns of the sample synthesized using a) as-synthesized and b) calcined Ga-beta seed crystals, c) SEM image of the product, and nitrogen adsorption–desorption isotherm of the product (closed and open symbols indicate adsorption and desorption branch, respectively).

5.3.3. Effect of gel compositions on the characteristic properties of the obtained hollow zeolite beta

The various chemical compositions of the initial gel, the reaction conditions, and the characterization results are summarized in Table 5.1 (the sample described above is No. 5.5). The chemical compositions of the initial gels and the reaction conditions in some synthesis batches in Table 5.1 are overlapped with those in the previous work for the OSDA-free synthesis of zeolite beta using aluminosilicate beta seed crystals. [182] Reaction temperature and heating time are optimized for the initial gel compositions, and *BEA-type zeolites with high crystallinity were obtained. However, sample Nos. 5.3 and 5.4 contain small amount of mordenite as minor phase determined by XRD. The spontaneous nucleation of mordenite has occurred before the completion of the crystal growth of beta, and it is difficult to obtain pure *BEA phase in these gel compositions and the synthesis temperature. Hence, the samples to be discussed below were Nos. 5.1, 5.2 and Nos. 5.5–5.10 where pure *BEA phase was obtained. The SiO_2/Al_2O_3 ratios of the obtained products are roughly proportional to the SiO_2/Al_2O_3 ratios of the initial gels; however, those values are limited in extremely lower value range than those of the initial gels. The most highly siliceous product (SiO_2/Al_2O_3 = 21.4, No. 5.10) was obtained using an initial gel with the SiO_2/Al_2O_3 ratio of 250, which was not tried in the previous work.[182] The yields of the products strongly depend on the SiO_2/Al_2O_3 ratios of initial gels, and the yield of highly siliceous product is quite poor, suggesting the most of silicate species were dissolved in the liquid phase. The SiO_2/Al_2O_3 ratios in the products and the yields also depend on the alkaline concentrations (Na_2O/SiO_2 ratio) in the initial gel similarly as in the conventional zeolite syntheses. On the other hand, the values of the SiO_2/ZnO ratios in the products are high enough to suggest the zincosilicate seeds are dissolved during the hydrothermal treatment. Higher alkaline concentration should promote the dissolution of the seeds; therefore comparing the SiO_2/ZnO ratios in the products with the same SiO_2/Al_2O_3 ratios in the initial gels, the higher NaO_2/SiO_2 ratios in the initial gels, the higher SiO_2/ZnO ratios in the products were obtained (compare No. 5.2 to No. 5.1, and No. 5.8 to No. 5.7 in Table 5.1). Additionally, the effect of the SiO_2/Al_2O_3 ratios in the initial gels on the SiO_2/ZnO ratios in the product can be confirmed in the case of the same Na_2O/SiO_2 ratio in the initial gels, and the SiO_2/ZnO ratios decrease according to the increase of the SiO_2/Al_2O_3 ratios in the initial gels (compare No. 5.5 to 5.7, and No. 5.6 to No. 5.8–5.10). This is explained as follows; in the same alkaline concentration, residual zincosilicate species are considered to be the same, and the SiO_2/Al_2O_3 ratios in initial gels affect the amount of newly grown zeolite beta. Therefore, the SiO_2/ZnO ratios in the products are determined by the yields of aluminosilicate zeolite beta.

Except for the presence of the hysteresis loop in the nitrogen adsorption–desorption isotherms, the pore characteristics such as BET and micropore surface areas, and micropore volumes of all the products are almost the same as those of the seed crystals. The intra-particle void volumes depend on the gel compositions, and the nitrogen adsorption–desorption isotherms with the smallest and the largest void volumes are shown in Figure 5.8 (samples Nos. 5.2 and 5.9 in Table 5.1). Obviously, the two different points are observed in these two isotherms; the rising trend of the adsorption isotherms at $P/P_0 > 0.8$, and the magnitude of the hysteresis loops that correspond to the intra-crystalline void volumes.

Table 5.1 Summary of the results in various initial gel compositions.[187]

	Initial gel[a]		Reaction condition		Product							
Sample	SiO_2/Al_2O_3	Na_2O/SiO_2	Temp.[℃]	Time [h]	Yield (%)[b]	Phase	SiO_2/Al_2O_3	SiO_2/ZnO	S_{BET} [$m^2\ g^{-1}$]	S_{micro} [$m^2 g^{-1}$][c]	V_{micro} [$cm^3\ g^{-1}$][c]	V_{void} [$cm^3\ g^{-1}$][d]
5.1	30	0.225	150	74	61.7	*BEA	11.0	241	648	625	0.24	0.0066
5.2	30	0.250	150	74	56.7	*BEA	10.9	324	646	622	0.24	0.0062
5.3	50	0.275	140	76	34.5	*BEA(+MOR)[e]	12.1	96.7	510	472	0.18	0.012
5.4	70	0.275	140	76	26.6	*BEA(+MOR)[e]	12.4	146	594	551	0.21	0.012
5.5	100	0.300	140	46	15.4	*BEA	13.1	124	632	564	0.22	0.032
5.6	120	0.350	140	48	11.2	*BEA	16.0	178	537	503	0.20	0.029
5.7	150	0.300	140	48	10.2	*BEA	15.7	117	600	564	0.22	0.035
5.8	150	0.350	140	48	10.7	*BEA	16.4	122	575	538	0.21	0.041
5.9	200	0.350	140	36	4.9	*BEA	21.2	53.2	631	581	0.23	0.041
5.10	250	0.350	140	20	4.8	*BEA	21.4	48.4	606	543	0.21	0.041
CIT-6 seeds						*BEA	-	13.1	614	539	0.21	0.000

[a] $H_2O/SiO_2 = 20$, seeds: 10wt% to SiO_2, [b] solid yield, [c] determined by the *t*-plot method, [d] calculated from desorption branch, [e] minor impurity

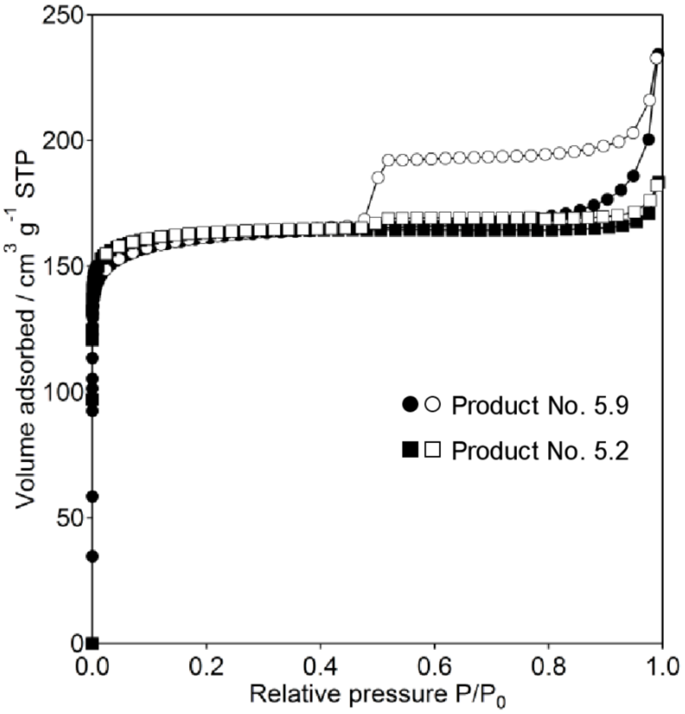

Figure 5.8 Nitrogen adsorption (solid symbols) –desorption (open symbols) isotherms of products synthesized from different initial gels.[187]

Figure 5.9 shows the SEM images of samples Nos. 5.2 and 5.9, and the particle sizes of these two samples are quite different. The difference in the magnitude of hysteresis loops corresponding to the intra-crystalline void volumes is due to the difference of the zeolite wall thickness (note that the numbers of the crystal particles synthesized by seed-directed methods are considered to be the same, and the yields of these crystal particles are quite different as shown in Table 5.1). If the voids are ideally formed by dissolution of the seed crystals, and the crystal growth on the surface of the seeds equally proceeded in all samples, the actual void volumes should be the same in all samples; therefore, the specific void volumes should be affected by the thickness of the zeolite wall of each product. In other words, the sample with larger particle size (No. 5.2, high yield) has the thicker zeolite wall and the lower specific void volume, and the sample with smaller particle size (No. 5.9, low yield) has the thinner zeolite wall and the higher specific void volume. This explanation is confirmed by the comparison of the void volumes of other samples synthesized with the same Na_2O/SiO_2 ratio of a coupled sample Nos. 5.5 to 5.7 and Nos. 5.6 to 5.8. The yield of the sample No. 5.5 (15.4%) is higher than that of the sample No. 5.7 (10.2%), and the void volume of the sample No. 5.5 (0.032 cm^3 g^{-1}) is slightly smaller than that of the sample No. 5.7 (0.035 cm^3 g^{-1}). It is also confirmed in one more coupled sample No. 5.6 (11.2% and 0.029 cm^3 g^{-1}) and No. 5.8 (10.7% and 0.041 cm^3 g^{-1}). On the other hand, the void volumes of the samples Nos. 5.9 and 5.10 with the lowest yields are not so high compare to that of higher yield sample No. 5.8. This is considered to be due to the presence of nonclosed voids. As described above and illustrated in Scheme 5.1, the void volumes mentioned here are the volumes of the intra-crystalline voids covered by well-closed zeolite walls. However, the yields of the samples Nos. 5.9 and 5.10 are quite low, and it is suggested that there are some voids that is not fully covered. In order to discuss detailed effects of the initial gel compositions and synthesis condition on the intra-particle void volume, kinetic investigations of the competitive processes such as dissolution of the seeds and crystal growth of zeolite beta are needed.[187]

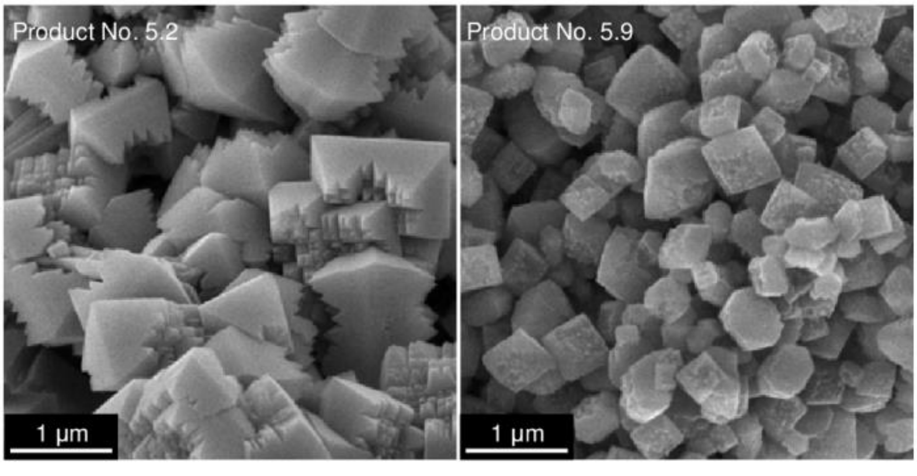

Figure 5.9 SEM images of products synthesized from different initial gels.[187]

5.3.4. Crystallization scheme

The crystallization behavior was investigated to understand the details of the formation of the hollow structure in the case of No. 5.5 in Table 5.1. Figure 5.10 shows the change of the integrated intensity ratio of the strongest peak (*hkl* = 302) in the XRD patterns (relative crystallinity to the sample after hydrothermal treatment of 46 h) and the micropore volumes of the corresponding products. Both curves show similar behavior, suggesting that, after the partial dissolution of the seeds during for initial 3 h of hydrothermal treatment, beta crystals grow period along with the treatment.

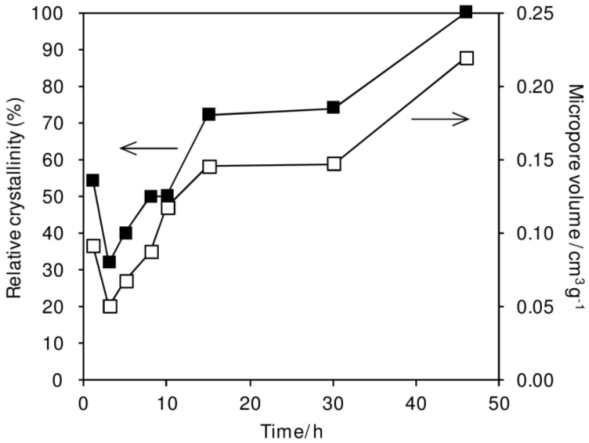

Figure 5.10 Change of the relative crystallinity (solid symbols) and the micropore volume (open symbols) of the product No. 5.5.[187]

Figure 5.11 shows changes of the SiO_2/Al_2O_3 and SiO_2/ZnO ratios in the solid product and the mother liquid along with the time. As shown in Figure 5.11 a), the SiO_2/Al_2O_3 ratio in the mother liquid sharply increases from the early stage of the crystallization, and reaches to the maximum value corresponding to the detection limit in the quantitative analysis of aluminum after 11 h, suggesting that the almost aluminium and aluminosilicate species are incorporated in the solid phase. The decrease in the SiO_2/Al_2O_3 ratio of the solid product basically corresponds to the incorporation of aluminum species as described above as shown in Figure 5.11 b). The SiO_2/ZnO ratio in the mother liquid shown in Figure 5.11 a) greatly decreases from the maximum value corresponding to the detection limit in the quantitative analysis of zinc at the early stage of the crystallization to lower value of 217, and the ratio of the final solid product increases to 124 as shown in Figure 5.11 b) (the SiO_2/ZnO ratio of the seed crystals is 13.1 as seen in Table 5.1). These results suggest that most of zinc and zincosilicate species from CIT-6 seed crystals dissolve into the liquid phase during the hydrothermal treatment, and the SiO_2/Al_2O_3 ratio of the product is determined by the chemical composition of the initial gel.[200]

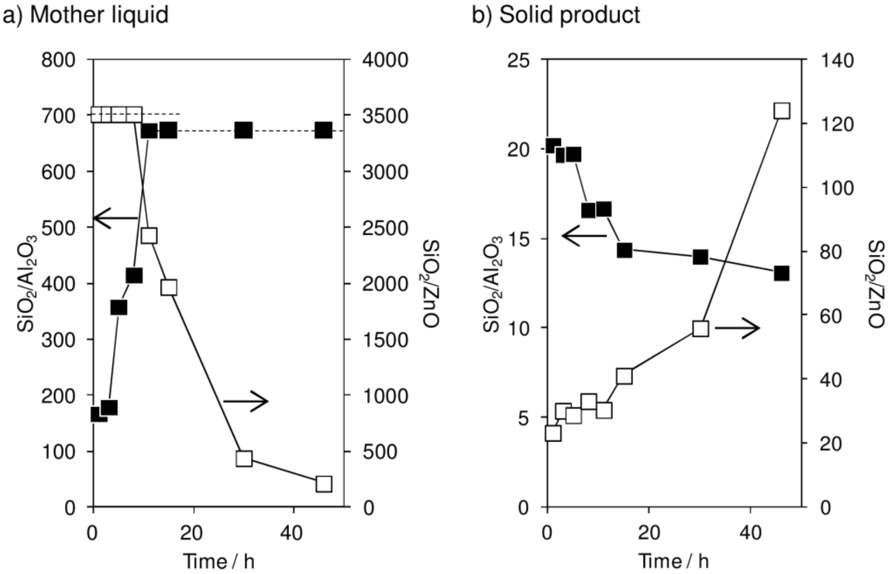

Figure 5.11 Change of the SiO_2/Al_2O_3 ratios (solid symbols) and the SiO_2/ZnO ratios (open symbols) in a) mother liquid and b) solid product in the reaction condition of No. 5.5 in Table 5.1. Dashed lines indicate the detection limits of quantitative analysis for Al and Zn.[187]

The chemical states of the zinc species remaining in the solid products are characterized using diffuse reflectance UV-vis spectra shown in Figure 5.12. There is no absorption peak in the region of 350–400 nm that is attributed to non-framework zinc oxide. On the other hand, the absorption peaks in the range of 200–300 nm is due to the zinc species in the zeolite framework. These peaks slightly change according to the time of hydrothermal treatment, suggesting that the chemical environments of zinc species were affected by some factors such as distortion of the framework. However, significant change or other absorption peaks corresponding to other zinc species are hardly observed.

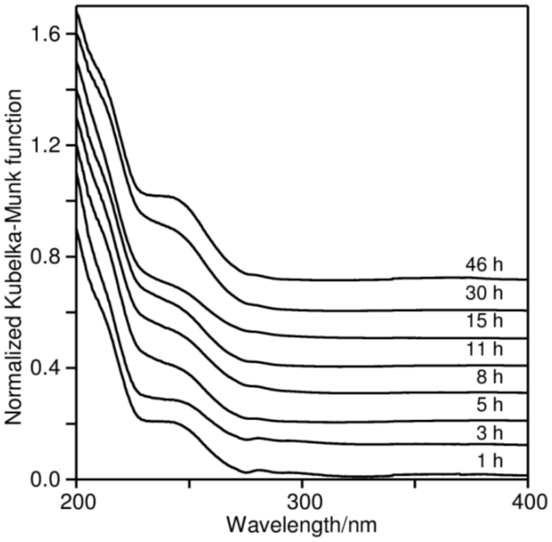

Figure 5.12 DR UV-vis spectra of solid products synthesized for different time (reaction condition: No. 5.5 in Table 5.1). To clarify, spectra are shifted 0.1 each for y-axias.[187]

The SEM images of the products at different time periods of hydrothermal treatment are shown in Figure 5.13. At the beginning of the synthesis, seed crystals are embedded in amorphous aluminosilicates and difficult to be observed by SEM (Figure 5.13 a). Then, the square particles with rough surfaces are observed on the surface of the amorphous matters after 8 h (Figure 5.13 b). These particles are considered to be the seed crystals covered by small aluminosilicate zeolite beta crystals newly grown on the surface of the seed crystals. As the reaction proceeds, crystallized particles become larger, and the wall of zeolite beta become thicker (Figure 5.13 c). Although opened macropores can be seen in some particles in this stage, the number of such particles is not so large, and most of the crystal particles have closed surface structure. Finally, at the end of the hydrothermal treatment, the zeolite beta with clear crystal habits is obtained (Figure 5.13 d).

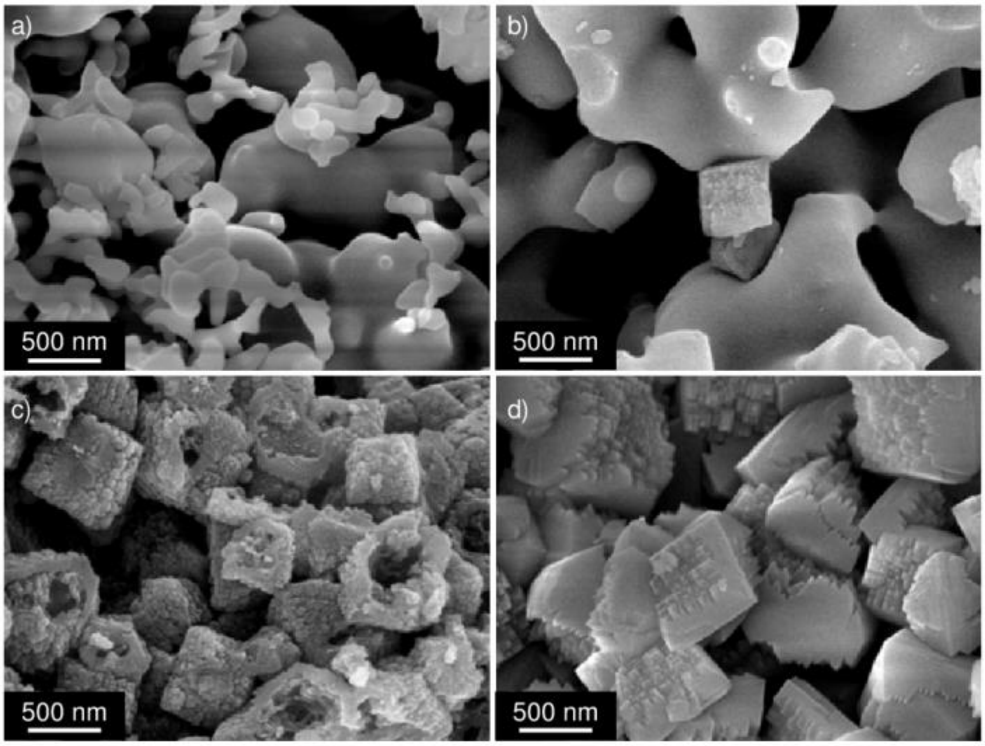

Figure 5.13 SEM images of the products (No. 5.5) hydrothermally treated for a) 2 h, b) 8 h, c) 15 h, and d) 46 h.[187]

The time-dependent change of the nitrogen adsorption–desorption isotherms, and the intra-crystalline void volumes calculated from desorption branch of the isotherms are shown in Figure 5.14 and Figure 5.15, respectively. The void volume was increased during the initial stage of the crystallization until the reaction time of 8–11 h, and then the volume was turned to decrease. Finally the volume increased slightly again. The reason for the decrease in void volume is considered to be the crystal growth toward inside of the hollow crystal particles as seen in Figure 5.6 and the remaining of the small amount of the crystal particles with opened macropores as seen in Figure 5.13. At the completeness of the crystallization, the second increase in the void volume was attributed to the complete closure of the opened macropores on the surface in all crystal particles. The similar behavior is observed in the ratio of the void volume to the micropore volume (Figure 5.15, open symbols). On the other hand, a small amount of mesopores in the zeolite beta wall might exist, because the mother liquid in the internal void after the synthesis was completely removed by washing (note that the Na_2O/Al_2O_3 ratios are around 1.0 in all products). As shown in Scheme 5.1, cavitation-controlled evaporation of nitrogen is caused by bottle-neck structure with smaller pores than the diameter of 4 nm (small mesopores and micropores), and larger pores contribute to the gradual desorption at higher relative pressure. Figure 5.16 shows the change of the pore size distribution calculated from adsorption branch of the isotherms using a method based on nonlocal density functional theory (NLDFT), where nitrogen adsorption was assumed to occur at 77 K in cylindrical siliceous zeolite pores. Mesopores with diameter of 2–6 nm exist through the hydrothermal treatment, and also the final product has mesopores. These mesopores are considered to be inter-particle voids and grain boundaries of the small zeolite beta crystals grown newly. The CIT-6 seed crystals also have mesopores in this region, but the pore sizes are slightly large. It can be concluded that the products obtained by this method have well-closed hollow structure.

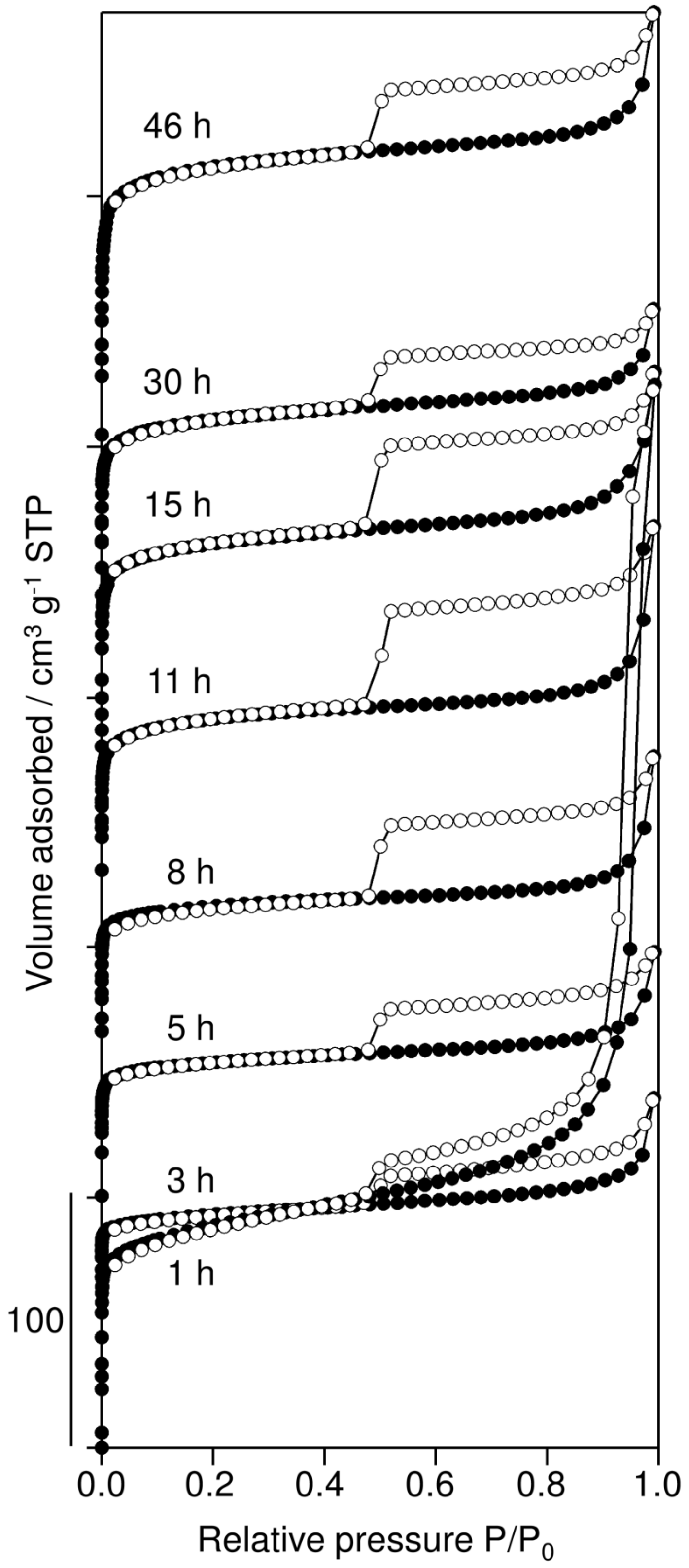

Figure 5.14 Nitrogen adsorption–desorption isotherms of products synthesized for different times. To clarify, isotherms are shifted each 50 cm^3 g^{-1}.[187]

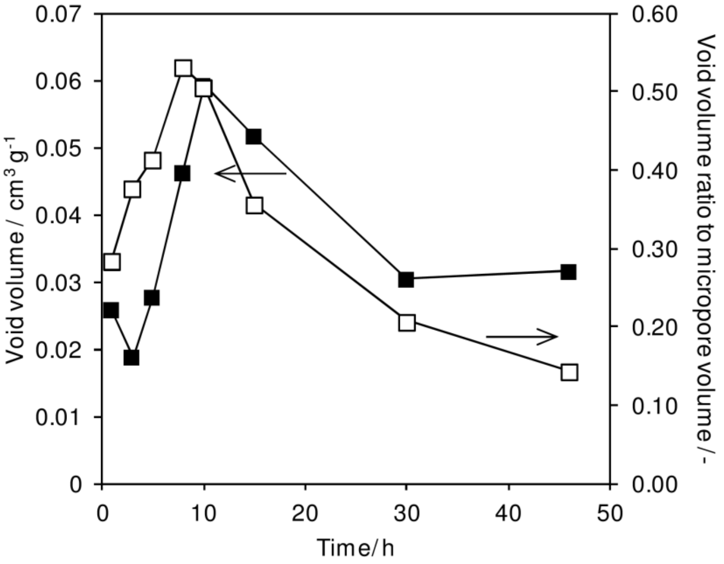

Figure 5.15 Change of the intra-particle void volume (solid symbols) and the ratio of the void volume to the micropore volumes (open symbols) of the product No. 5.5.[187]

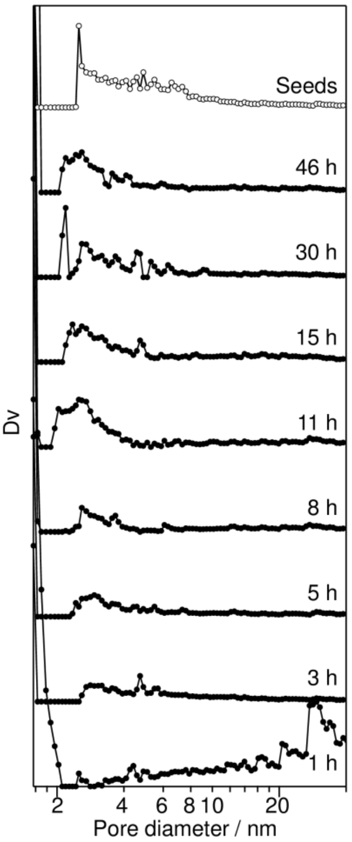

Figure 5.16 Pore size distribution calculated from adsorption branches of product synthesized for different times (solid symbols) and seeds (open symbols).[187]

Considering these results, the formation scheme is proposed in Scheme 5.2. At the beginning of the crystal growth of zeolite beta, small crystals deposit epitaxially on the surface of the seeds and cover them. After or during the covering of the surface, the seed crystals dissolve into the liquid phase through the mesopores formed in the small zeolite beta crystals layer. As a result, the hollow structure has been constructed in the center of zeolite beta crystal particles. Then, the crystal growth proceeds at both outer and inner surface of the crystals, and the outer surface becomes smooth at the end of the hydrothermal treatment.

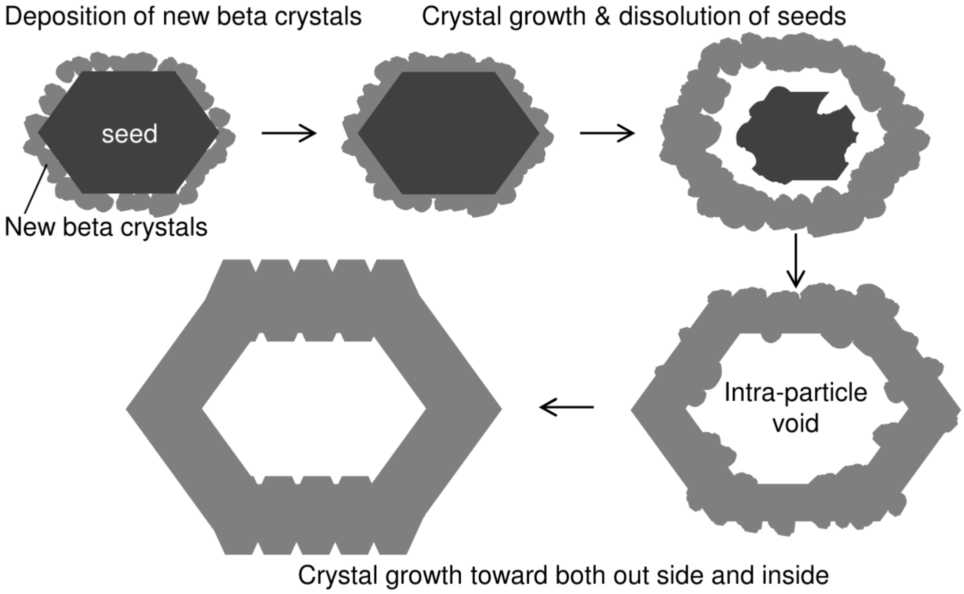

Scheme 5.2 Proposed formation mechanism of hollow zeolite beta.[187]

5.4. Conclusion

The dissolution rates of the seed crystals are an important factor for the seed-directed, OSDA-free synthesis of zeolites, and the rates can be controlled by the inclusion of OSDA. The seeds should not be dissolved before the crystal growth starts; however, moderate dissolution rate of as-synthesized CIT-6 seeds contributed to a success in the synthesis of hollow zeolite beta by one-pot method. Detailed investigation suggests that intra-crystalline voids are formed by dissolution of the seed crystals after crystal growth started. These results provide requirements for the seed crystals and novel strategy for the simple synthesis of hollow zeolites.

Chapter 6. General Conclusion and Future Perspectives

Half a century has passed since the first synthesis of zeolites, and significant progress in the synthesis has enabled the preparation of a large number of new zeolites. However, the synthesis of novel zeolites frequently requires the use of expensive and environmentally malign components such as fluoride ions and OSDAs, which have been a significant hurdle for their practical application. Therefore, it is necessary to fundamentally review the production processes and synthetic methods for the preparation of zeolites; in particular, the OSDA-free synthesis of zeolites has been an important issue. As discussed in this dissertation, various zeolites can be synthesized without using OSDAs through a seed-directed approach. This novel approach has attracted considerable attention as a low-cost, environmentally benign technique for the production of zeolites that previously were thought to require the use of OSDAs (Figure 6.1). With the success of this approach, OSDAs are now perhaps only necessary for the nucleation of zeolites, but not for their crystal growth. The ability to skip the nucleation step, which involves high activation energies, should be highly advantageous.

The first syntheses of PAU-, MAZ-, and MTW-type aluminosilicate zeolites without using OSDAs were described in Chapters 2 and 3. These results show the remarkable applicability of the seed-directed approach to various synthetic systems in

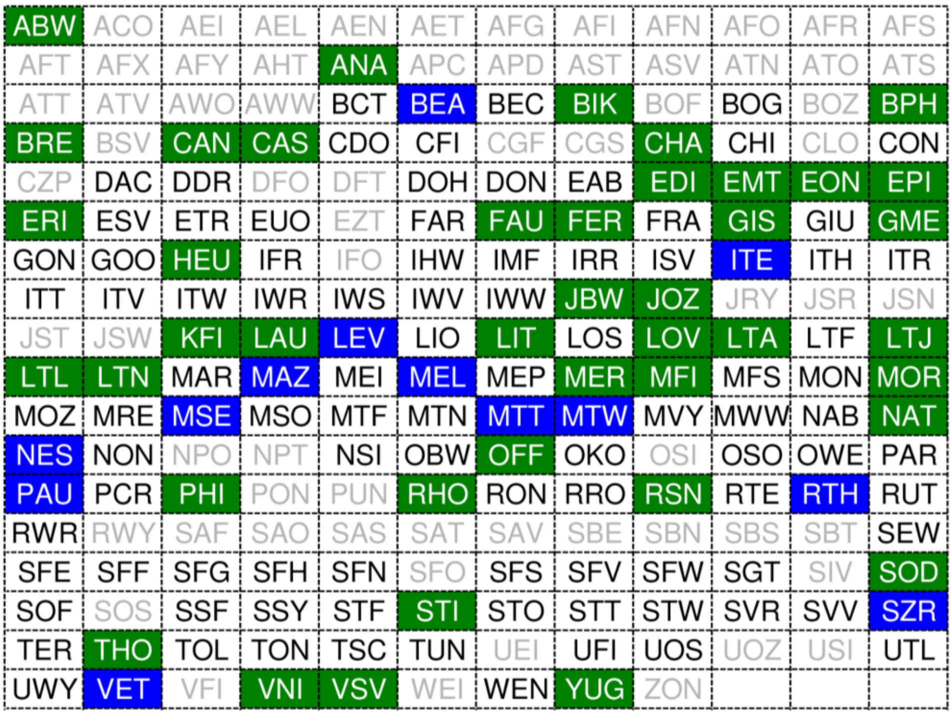

ABW	ACO	AEI	AEL	AEN	AET	AFG	AFI	AFN	AFO	AFR	AFS
AFT	AFX	AFY	AHT	ANA	APC	APD	AST	ASV	ATN	ATO	ATS
ATT	ATV	AWO	AWW	BCT	BEA	BEC	BIK	BOF	BOG	BOZ	BPH
BRE	BSV	CAN	CAS	CDO	CFI	CGF	CGS	CHA	CHI	CLO	CON
CZP	DAC	DDR	DFO	DFT	DOH	DON	EAB	EDI	EMT	EON	EPI
ERI	ESV	ETR	EUO	EZT	FAR	FAU	FER	FRA	GIS	GIU	GME
GON	GOO	HEU	IFR	IFO	IHW	IMF	IRR	ISV	ITE	ITH	ITR
ITT	ITV	ITW	IWR	IWS	IWV	IWW	JBW	JOZ	JRY	JSR	JSN
JST	JSW	KFI	LAU	LEV	LIO	LIT	LOS	LOV	LTA	LTF	LTJ
LTL	LTN	MAR	MAZ	MEI	MEL	MEP	MER	MFI	MFS	MON	MOR
MOZ	MRE	MSE	MSO	MTF	MTN	MTT	MTW	MVY	MWW	NAB	NAT
NES	NON	NPO	NPT	NSI	OBW	OFF	OKO	OSI	OSO	OWE	PAR
PAU	PCR	PHI	PON	PUN	RHO	RON	RRO	RSN	RTE	RTH	RUT
RWR	RWY	SAF	SAO	SAS	SAT	SAV	SBE	SBN	SBS	SBT	SEW
SFE	SFF	SFG	SFH	SFN	SFO	SFS	SFV	SFW	SGT	SIV	SOD
SOF	SOS	SSF	SSY	STF	STI	STO	STT	STW	SVR	SVV	SZR
TER	THO	TOL	TON	TSC	TUN	UEI	UFI	UOS	UOZ	USI	UTL
UWY	VET	VFI	VNI	VSV	WEI	WEN	YUG	ZON			

Figure 6.1 Zeolite structures synthesized by conventional OSDA-free methods (green) and recent seed-directed, OSDA-free methods (blue, unpablished data are also included). Black and gray colored letters indicate silicates and others, respectively.

terms of the target zeolite structure (cage-type or channel-type pore structures) and choice of alkaline cation (or mixed systems). The proposed “CBU hypothesis” was demonstrated to be correct for these aluminosilicate systems. Moreover, with the CBU hypothesis, it can be easily seen that other zeolites with similar crystal structures can be synthesized using the seed-directed approach. In fact, more than 20 zeolite structure types have CBUs in common with these three zeolites. In Chapter 4, for the first time, the seed-directed approach was extended to a zincosilicate system. This result further demonstrates the potential applicability of this novel method for the synthesis of other metallosilicate zeolites beyond aluminosilicates. Although the result was not based on the CBU hypothesis, a common structural unit can be found in the target VET-type zeolite and the unseeded product magadiite. Moreover, a possible crystal growth mechanism was proposed. Notably, based on the results presented in Chapters 2–4, the first aim of this dissertation, expansion of the applicability of the OSDA-free, seed-directed approach to the synthesis of other zeolite types, was achieved. The requirements for seed crystals were investigated in Chapter 5. It was found that zinco- and gallo-silicate zeolites with a *BEA-type structure can direct the crystal growth of aluminosilicate zeolite beta, which possesses the same crystal structure, and zeolite beta with a hollow interior was synthesized for the first time using a simple one-pot procedure. In this chapter, the requirements identified for the successful seed-directed, OSDA-free synthesis of zeolites are summarized based on the results presented in the previous chapters. Moreover, the characteristics of this process and future perspectives are also discussed.

With respect to the requirements for the successful seed-directed, OSDA-free synthesis of zeolites, first it is important that spontaneous nucleation does not occur prior to completion of the crystal growth of the target zeolite. Other zeolites (or silicates) were obtained from unseeded gels after prolonged hydrothermal treatment, even in the presence of seed crystals, for all of the cases described in this dissertation. Generally, nucleation is considered to have a higher activation energy than crystal growth. However, the zeolites obtained from the unseeded gels were thermodynamically stable compared to the target zeolites; in other words, seeding does not change the stability of zeolite phases under the reaction conditions, and the crystal growth of the target zeolites is only advantageous in terms of the kinetic reaction rates. This behavior is characteristic for seed-directed synthesis wherein nucleation of a target zeolite has never been observed without the use of either OSDAs or seed crystals. Therefore, the reaction conditions should be optimized such that spontaneous nucleation does not occur, and crystal growth of the target zeolite is initiated as rapidly as possible.

Parameters such as the reaction temperature, motion (standing/rotation) of the autoclave, and the initial gel composition are also important. The intermediate addition of seeds, i.e., the addition of seeds after preheating of the initial gel, can also be effective for accelerating the crystal growth rate of target zeolites and avoiding spontaneous nucleation, as discussed in Chapter 2.

Second, the surfaces of the seed crystals should be exposed to the liquid phase, and the precursor must access clean seed crystal surfaces; namely, the liquid-mediated supply of small silicate species may be a crucial mechanism for the successful growth of the target zeolite. Seed crystals provide specific surfaces for the newly growing zeolites, as was seen from the results presented in Chapters 3 and 5. Moreover, it was observed that the seed crystals did not affect the structure of amorphous materials (Chapter 4), and crystal growth did not occur when the seed crystals were covered by amorphous matter (Chapter 2). To prevent the latter problem, intermediate addition of the seeds and increasing the reaction temperature and alkaline concentration to promote the dissolution of the amorphous reactant gels are effective. This requirement seems to be the same for conventional seed-assisted syntheses, although it has been infrequently discussed. One possible reason is that conventional seed-assisted methods require only a very small amount of seed crystals, and secondary or spontaneous nucleation of the target zeolites has been observed. Conversely, these nucleation types have not been observed to date in seed-directed syntheses. Moreover, the presence of competing stable phases may narrow the acceptable synthesis time for pure products. Therefore, the requirements for seed crystals may be stricter in seed-directed syntheses. For example, a more limited exposure time and a larger total seed crystal surface area are needed compared to those for seed-assisted syntheses.

Third, during hydrothermal treatment, the zeolite seed crystals should not be completely dissolved prior to the onset of crystal growth. In some previous reports on seed-assisted synthesis, dissolved seed crystals or amorphous aluminosilicates were reported to promote crystallization of the target zeolite. This phenomenon has been considered as secondary nucleation. However, in the present study on seed-directed synthesis, these micro dusts tended to promote nucleation of competing phases, and secondary nucleation of the target zeolite was never observed. Although detailed data are not shown in this dissertation (because they are not “good data”), the requirements for the stability of the seed crystals used in seed-directed syntheses may again be more demanding compared to those for seed crystals used for conventional seed-assisted syntheses. The dissolution rate of the seed crystals can be controlled by optimizing the alkaline concentration in the reactant gels and the composition of the seeds such as the SiO_2/Al_2O_3 ratio. Generally, seed crystals with a high silica content are less stable under hydrothermal conditions. Moreover, as-synthesized seeds containing OSDAs in their pores are considered to be more stable than calcined seeds, as discussed in Chapter 5. Zeolite beta with a hollow interior structure was synthesized using seed crystals with a moderate dissolution rate. CIT-6 seeds, namely, *BEA-type zincosilicate zeolites, were used for the synthesis of hollow aluminosilicate zeolite beta, and the CIT-6 seeds were dissolved along with new crystal growth of the aluminosilicate beta.

Finally, the chemical composition of the reactant gel should be optimized. This requirement was not fully investigated and seems to involve one of the deepest mysteries of zeolite synthesis. Even if the abovementioned requirements are satisfied, optimization of the reactant composition is still required in some cases. For example, there may be hidden requirements for initiation of the crystal growth of zeolites. In conventional zeolite syntheses, crystal growth can occur immediately after nucleation or simultaneously with nucleation; therefore, the effects of chemical composition on crystal growth have been rarely investigated. In seed-directed syntheses, the chemical composition of the reactant gel may influence the formation or assembly of specific precursors, and the structure of the target zeolite is important. Although definitive techniques for investigation of the precursors, which really exist in the reactant mixtures, are not available at this time, a possible mechanism was proposed in Chapter 4. A comparison of the structural similarities of seed zeolites and the other zeolites (or silicates) obtained from unseeded gels provided valuable information that was not previously available. Based on this new information, the CBU hypothesis was proposed, and was demonstrated to be useful for determining appropriate synthesis conditions. It was also shown that to apply the CBU hypothesis effectively to the synthesis of other zeolites, the chemical composition of the initial OSDA-free gel should be carefully controlled. Therefore, systematic studies of the conditions for the OSDA-free synthesis of zeolites are still required.

Moreover, it is important to determine if the zeolites obtained via the OSDA-free approach are truly the same as the zeolites synthesized using OSDAs. The characteristic properties of zeolites are easily changed by factors such as their composition, particle size, and the presence of defects. The characteristics of the seed-directed, OSDA-free process would thus be expected to influence these parameters. The unique features of zeolites prepared using the seed-directed method can be summarized in three main points as follows.

First, the SiO_2/Al_2O_3 ratios of zeolites obtained using the seed-directed approach are nearly the same as those of corresponding zeolites obtained from unseeded gels and tend to be lower than those of the corresponding seeds synthesized using OSDAs. These Al-rich zeolites have hydrophilic properties, and, in this study, the lowest SiO_2/Al_2O_3 ratios were obtained for PAU- and MTW-type zeolites. Both hydrophilic and hydrophobic zeolites have been required and utilized in different industries; therefore, the synthesis of zeolites with various SiO_2/Al_2O_3 ratios is an important issue. Generally, alkaline cations such as Na^+ have high charge densities, and electrostatic interactions between aluminosilicate species that form aluminum-rich rings are dominant in the OSDA-free system; therefore, aluminum-rich zeolites tend to be obtained without the use of OSDAs. On the other hand, the charge densities of OSDAs are low, and hydrophobic interactions between silicate species are dominant. Therefore, the SiO_2/Al_2O_3 ratios of the products seem to be in accordance with the same law for conventional zeolite synthesis. However, it should be noted that the SiO_2/Al_2O_3 ratios of the products are not always lower than those of the seeds. When seeds are added to initial gels that yield zeolites with higher SiO_2/Al_2O_3 ratios than those of the seeds, the products have silica-rich compositions (Chapter 2 and 3).

Second, the particle sizes of the zeolites obtained via seed-directed synthesis are larger than those of the seeds because new zeolite crystals are grown from the surfaces of the seed crystals, and it is thought that secondary nucleation does not occur. In addition, the crystal habits of the products have been clearly observed to be similar to those of natural zeolites. For example, the truncated octahedral morphology of beta produced using the seed-directed method is analogous to that of its natural counterpart tschernichite, while zeolite beta synthesized using OSDAs typically comprises aggregates of small, round particles (Chapter 5). Although nucleation tends to dominate the crystal morphology when OSDAs are used, it appears that crystal growth dominates the crystal morphology in the seed-directed method.

Third, zeolites synthesized using the seed-directed method do not require calcination, which often causes dealumination or partial collapse of the framework; therefore, these zeolites exhibit excellent pore characteristics compared to those of the seed crystals (Chapter 2). Moreover, no extra-framework Al species were detected in the seed-directed products judging from the ^{27}Al MAS NMR spectra. In addition, an MTW-type zeolite synthesized without OSDAs adsorbed a much smaller amount of nitrogen than conventional ZSM-12 (Chapter 3). Although further investigation is required, based on these initial results, it is possible to conclude that the effective pore diameter is decreased compared to that of the 8-MRs; the obtained MTW-type zeolite was found to adsorb small molecules such as water and ammonia, and extra-framework aluminum and amorphous silicates were barely detected. This result is also considered to be evidence that crystal growth is dominant in the seed-directed system.

In summary, the seed-directed, OSDA-free synthesis approach developed in this dissertation is a promising route to zeolites, and this crystal growth-dominated synthesis is different from conventional zeolite synthesis, which is dominated by nucleation. Therefore, further development of this methodology will contribute to the industrial production of various zeolites with unique features.

Moreover, it is expected that the seed-directed method will be useful for the synthesis of aluminoslicate zeolites with other structures with application of the CBU hypothesis for determination of the best synthesis conditions, as discussed in Chapters 2 and 3. Undoubtedly, the requirements mentioned in this dissertation should be satisfied. The synthesis of high-silica aluminosilicate zeolites without using OSDAs is also a worthwhile challenge. Thus, to tackle this issue, the structures of target zeolites must be carefully considered, because aluminum species have a significant influence on the formation of ring structures and building units. Generally, even-membered rings such as 4-, 6-, and 8-MR tend to formed with Al-rich compositions. On the other hand, as discussed in Chapter 4, 5-MR-based building units can be formed without aluminum species. In brief, it should be possible to form structures with lower aluminum content, and structures that contain 5-3 units shown in Chapter 4 are likely candidates. Beyond aluminosilicates, the synthesis of other metallosilicate zeolites such as gallosilicates shows promise. The processes for formation of the required building units and their assembly must be considered, along with charge compensation of the framework charge by alkaline cations, as discussed in Chapter 4. Moreover, seed-directed syntheses may produce composite materials with core–shell structures in one-pot systems; namely, materials with seed crystals (core) and newly grown phases (shell) that have quite different compositions than those of zeolites obtained using the conventional seed-assisted method. Not only different SiO_2/Al_2O_3 ratios but also the incorporation of different framework metals is possible, as discussed in Chapter 5. The synthesis of hollow zeolite beta as demonstrated in Chapter 5 may be an extreme case where the core phase was completely dissolved.

From a more fundamental view point, investigation of crystal growth mechanisms can be quite important. As described repeatedly, addition of seed crystals can avoid complex nucleation steps, and crystal growth behaviors may be clearly observed. In addition, the importance of dividing zeolite synthesis into two steps and the crystal growth-dominated synthesis of zeolites can be expanded beyond OSDA-free syntheses. In some cases, OSDAs are still necessary such as in the synthesis of pure-silica and titanosilicate zeolites, which have no framework charge except defect sites. To synthesize these zeolites without using OSDAs, a new approach other than the seed-directed method may be needed. However, even in these systems, it may be possible to develop a more efficient, fluoride-free route to zeolites with novel compositions.

Presently, although zeolite synthesis is not truly designed, further progress in this field is expected and the designed synthesis of zeolites should be possible in the future. The novel approach presented in this dissertation has broad applicability and can enable the simple synthesis of zeolites (Figure 6.2). To look for simplicity but not to be limited by stereotypes is essential–while standing on the shoulders of giants (Barrer, Breck, Corma, Davis, Zones, Itabashi, and many others).

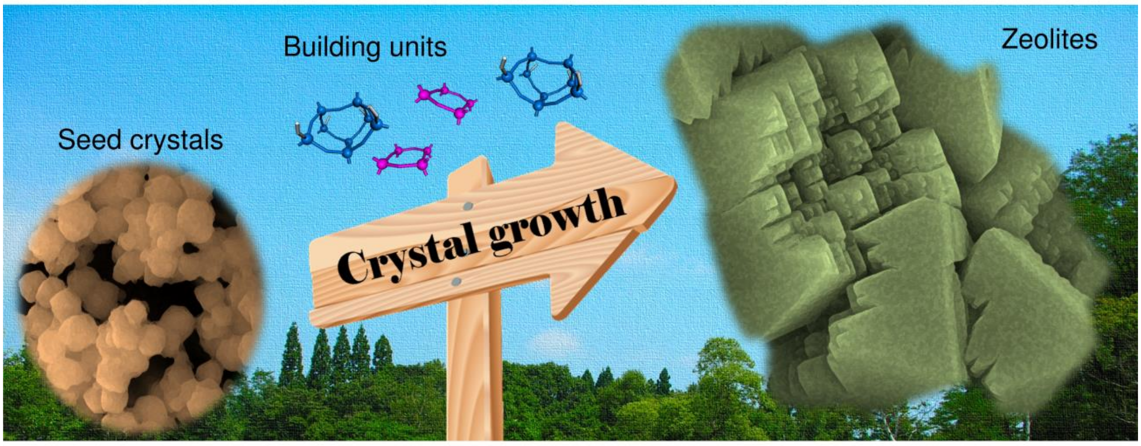

Figure 6.2 Seed-directed synthesis of zeolites.[136]

References

1. M. E. Davis, Nature 417 (2002) 813–821.
2. G. A. Ozin, Adv. Mater. 4 (1992) 612–649.
3. C. R. Martin, Science 266 (1994) 1961–1966.
4. A. Corma, Chem. Rev. 97 (1997) 2373–2419.
5. A. Stein, Adv. Mater. 15 (2003) 763–775.
6. M. Tiemann, Chem. Eur. J. 13 (2007) 8376–8388.
7. R. E. Morris, P. S. Wheatly, Angew. Chem. Int. Ed. 47 (2008) 4966–4981.
8. S. Wang, Microporous Mesoporous Mater. 117 (2009) 1–9.
9. Y. Hoshikawa, H. Yabe, A. Nomura, T. Yamaki, A. Shimojima, T. Okubo, Chem. Mater. 22 (2010) 12–14.
10. K. S. W. Sing, D. H. Everett, R. A. W. Haul, L. Moscou, R. A. Pierotti, J. Rouquerol, T. Siemieniewaka, Pure Appl. Chem. 57 (1985) 603–619.
11. J. L. Figueiredo , M. F. R. Pereira, M. M. A. Freitas, J. J. M. Órfão, Carbon 37 (1999) 1379–1389.
12. T. Kyotani, Carbon 38 (2000) 269–286.
13. T. Kyotani, Z. Ma, A. Tomita, Carbon 41 (2003) 1451–1459.
14. K. Nueangnoraj, H. Nishihara, K. Imai, H. Itoi, T. Ishii, M. Kiguchi, Y. Sato, M. Terauchi, T. Kyotani, Carbon 62 (2013) 455–464.
15. J. Lee, J. Kim, T. Hyeon, Adv. Mater. 18 (2006) 2037–2094.
16. S. Iijima, Nature 354 (1991) 56–58.
17. S. Iijima, T. Ichihashi, Nature 363 (1993) 603–605.
18. N. B. McKeown, S. Makhseed, P. M. Budd, Chem. Commun. (2002) 2780–2781.
19. N. B. McKeown, S. Hanif, K. Msayib, C. E. Tattershall, P. M. Budd, Chem. Commun. (2002) 2782–2783.

20. N. B. McKeown, B. Gahnem, K. J. Msayib, P. M. Budd, C. E. Tattershall, K. Mahmood, S. Tan, D. Book, H. W. Langmi, A. Walton, Angew. Chem. Int. Ed. 45 (2006) 1804–1807.
21. A. P. Cote, A. I. Benin, N. W. Ockwig, M. O'Keeffe, A. J. Matzger, O. M. Yaghi, Science 310 (2005) 1166–1170.
22. F. J. Uribe-Romo, J. R. Hunt, H. Furukawa, C. Klöck, M. O'Keeffe, O. M. Yaghi, J. Am. Chem. Soc. 131 (2009) 4570–4571.
23. X.-H. Liu, C.-Z. Guan, S.-Y. Ding, W. Wang, H.-J. Yan, D. Wang, L.-J. Wan, J. Am. Chem. Soc. 135 (2013) 10470–10474.
24. Y. Yamauchi, A. Sugiyama, R. Morimoto, A. Takai, K. Kuroda, Angew. Chem. Int. Ed. 47 (2008) 5371–5373.
25. Y. Kuroda, K. Kuroda, Angew. Chem. Int. Ed. 49 (2010) 6993–6997.
26. S. Guo, E. Wang, Nano Today 6 (2011) 240–264.
27. P. Yang, T. Deng, D. Zhao, P. Feng, D. Pine, B. F. Chmelka, G. M. Whitesides, G. D. Stucky, Science 282 (1998) 2244–2246.
28. O. D. Velev, E. W. Kaler, Adv. Mater. 12 (2000) 531–534.
29. X. Chen, S. S. Mao, Chem. Rev. 107 (2007) 2891–2959.
30. T. Yanagisawa, T. Shimizu, K. Kuroda, C. Kato, Bull. Chem. Soc. Jpn. 63 (1990) 988–992.
31. S. Inagaki, Y. Fukushima, K. Kuroda, J. Chem. Soc., Chem. Commun. (1993) 680–682.
32. C. T. Kresge, M. E. Leonowicz, W. J. Roth, J. C. Vartuli, J. S. Beck, Nature 359 (1992) 710–712.
33. J. S. Beck, J. C. Vartuli, W. J. Roth, M. E. Leonowicz, C. T. Kresge, K. D. Schmitt, C. T.-W. Chu, D. H. Olson, E. W. Sheppard, S. B. McCullen, J. B. Higgins, J. L. Schlenker, J. Am. Chem. Soc. 114 (1992) 10834–10843.
34. Y. Wan, D. Zhao, Chem. Rev. 107 (2007) 2821–2860.
35. K. Ariga, A. Vinu, Y. Yamauchi, Q. Ji, J. P. Hill, Bull. Chem. Soc. Jpn. 85 (2012) 1–32.
36. T. Asefa, M. J. MacLachlan, N. Coombs, G. A. Ozin, Nature 402 (1999) 867–871.
37. S. Inagaki, S. Guan, T. Ohsuna, O. Terasaki, Nature 416 (2002) 304–307.
38. S. Fujita, S. Inagaki, Chem. Mater. 20 (2008) 891–908.

39. N. Mizoshita, T. Tani, S. Inagaki, Chem. Soc. Rev. 40 (2011) 789–800.

40. S. Kitagawa, M. Kondo, Bull. Chem. Soc. Jpn. 71 (1998) 1739–1753.

41. S. Kitagawa, R. Kitamura, S. Noro, Angew. Chem. Int. Ed. 43 (2004) 2334–2375.

42. S. Horike, S. Shimomura, S. Kitagawa, Nature Chemistry 1 (2009) 695–704.

43. H. Li, M. Eddaoudi, M. O'Keeffe, O. M. Yaghi, Nature 402 (1999) 276–279.

44. O. M. Yaghi, M. O’Keeffe, N. W. Ockwig, H. K. Chea, M. Eddaoudi, J. Kim, Nature 423 (2003) 705–714.

45. S. L. James, Chem. Soc. Rev. 32 (2003) 276–288.

46. M. Eddaoudi, D. B. Moler, H. Li, B. Chen, T. M. Reineke, M. O’Keeffe, O. M. Yaghi, Acc. Chem. Res. 34 (2001) 319–330.

47. M. Eddaoudi, J. Kim, N. Rosi, D. Vodak, J. Wachter, M. O’Keeffe, O. M. Yaghi, Science 295 (2002) 469–472.

48. U. Mueller, M. Schubert, F. Teich, H. Puetter, K. S- Arndt, J. Pastré, J. Mater. Chem. 16 (2006) 626–636.

49. A. U. Czaja, N. Trukhan, U. Müller, Chem. Soc. Rev., 38 (2009) 1284–1293.

50. R. Kitaura, K. Seki, G. Akiyama, S. Kitagawa, Angew. Chem. Int. Ed. 42 (2003) 428–431.

51. S. Kitagawa, K. Uemura, Chem. Soc. Rev. 34 (2005) 109–119.

52. O. K. Farha, C. E. Wilmer, I. Eryazici, B. G. Hauser, P. A. Parilla, K. O’Neill, A. A. Sarjeant, S. T. Nguyen, R. Q. Snurr, J. T. Hupp, J. Am. Chem. Soc. 134 (2012) 9860–9863.

53. R. L. Martin, M. Haranczyk, Chem. Sci. 4 (2013) 1781–1785.

54. D. W. Breck, Zeolite Molecular Sieves: Structure, Chemistry, and Use, Wiley–Interscience publication, New York, (1974).

55. Handbook of Zeolite Science and Technology, ed. by S. M. Auerbach, K. A. Carrado, P. K. Dutta, Marcel Dekker, New York, (2003).

56. M. E. Davis, Chem. Mater. 26 (2014) 239–245.

57. M. Moliner, C. Martínez, A. Corma, Chem. Mater. 26 (2014) 246–258.

58. R. M. Barrer, J. Chem. Soc. (1948) 127–132.

59. R. M. Barrer, L. Hinds, E. A. White, J. Chem. Soc. (1953) 1466–1475.
60. R. M. Barrer, C. Marcilly, J. Chem. Soc. A (1970) 2735–2745.
61. C. S. Cundy, P. A. Cox, Chem. Rev. 103 (2003) 663–701.
62. Ch. Baerlocher, L. B. McCusker, Database of Zeolite Structures: http://www.iza-structure.org/databases/
63. J. Weitkamp, Solid State Ionics 131 (2000) 175–188.
64. S. Quintavalla, L. Vicini, Meat Sci. 62 (2002) 373–380.
65. M. Iwamoto, H. Yahiro, K. Tanda, N. Mizuno, Y. Mine, S. Kagawa, J. Phys. Chem. 95 (1991) 3727–3730.
66. A. Fritz, V. Pitchon, Appl. Catal. B 13 (1997) 1–25.
67. V. I. Pârvulescu, P. Grange, B. Delmon, Catal. Today 46 (1998) 233–316.
68. S. J. Schmieg, S. H. Oh, C. H. Kim, D. B. Brown, J. H. Lee, C. H.F. Peden, D. H. Kim, Catal. Today 184 (2012) 252–261.
69. K. Tanabe, W. F. Hölderich, Appl. Catal. A 181 (1999) 399–434.
70. I. Kiricsi, C. Flego, G. Pazzuconi, W. O. Parker, Jr., R. Millini, C. Perego, G. Bellussi, J. Phys. Chem. 98 (1994) 4627–4634.
71. M. Taramasso, J. Perego, B. Notari, UK Patent 2071 071 A (1980).
72. T. Tatsumi, Curr. Opin. Solid State Mater. Sci. 2 (1997) 76–83.
73. A. Corma, L. T. Nemeth, M. Renz, S. Valencia, Nature 412 (2001) 423–425.
74. A. Corma, H. García, Chem. Rev. 103 (2003) 4307–4365.
75. M. Moliner, Y. Román-Leshkov, M. E. Davis, Proc. Natl. Acad. Sci. USA 107 (2010) 6164–6168.
76. Y. Román-Leshkov, M. Moliner, J. A. Labinger, M. E. Davis, Angew. Chem. Int. Ed. 49 (2010) 8954–8957.
77. C. S. Cundy, P. A. Cox, Microporous Mesoporous Mater. 82 (2005) 1–78.
78. M. E. Davis, R. F. Lobo, Chem. Mater. 4 (1992) 756–768.
79. Y. Kubota, M. Helmkamp, S. I. Zones, M. E. Davis, Microporous Mater. 6 (1996) 213–229.

80. R. Martínez-Franco, M. Moliner, Y. Yun, J. Sun, W. Wan, X. Zou, A. Corma, Proc. Natl. Acad. Sci. USA 110 (2013) 3749–3754.

81. R. M. Barrer, E. A. D. White, J. Chem. Soc. (1952) 1561–1571.

82. H. E. Robson, D. P. Shoemaker, R. A. Ogilvie, P. C. Manor, Adv. Chem. Ser. 121 (1973) 106–115.

83. K. Itabashi, T. Fukushima, K. Igawa, Zeolites 6 (1986) 30–34.

84. Y. Suzuki, T. Wakihara, K. Itabashi, M. Ogura, T. Okubo, Top. Catal. 52 (2009) 67–74.

85. M. Iwama, Y. Suzuki, J. Plévert, K. Itabashi, M. Ogura, T. Okubo, Cryst. Growth Des. 10 (2010) 3471–3479.

86. H. Robson ed., Verified syntheses of zeolitic materials 2nd ed., Elsevier, Amsterdam, (2001).

87. M. Ogura, Y. Kawazu, H. Takahashi, T. Okubo, Chem. Mater. 15 (2003) 2661–2667.

88. S. I. Zones, R. J. Darton, R. Morris, S.-J. Hwang, J. Phys. Chem. B 109 (2005) 652–661.

89. M. Maldonado, M. D. Oleksiak, S. Chinta, J. D. Rimer, J. Am. Chem. Soc. 135 (2013) 2641–2652.

90. A. Navrotsky, Proc. Natl. Acad. Sci. USA 101 (2004) 12096–12101.

91. E.-P. Ng, D. Chateigner, T. Bein, V. Valtchev, S. Mintova, Science 335 (2012) 70–73.

92. E.-P. Ng, J.-M. Goupil, A. Vicente, C. Fernandez, R. Retoux, V. Valtchev, S. Mintova, Chem. Mater. 24 (2012) 4758–4765.

93. E. G. Derouane, S. Detremmerie, Z. Gabelica, N. Blom, Appl. Catal. 1 (1981) 201–224.

94. B. M. Lowe, Zeolites 3 (1983) 300–305.

95. P. A. Cox, J. L. Casci, A. P. Stevens, Faraday Discuss. 106 (1997) 473–487.

96. G. O. Brunner, Zeolites 12 (1992) 428–430.

97. T. Brar, P. France, P. G. Smirniotis, J. Phys. Chem. B 105 (2001) 5383–5390.

98. N. Ren, B. Subotić, J. Bronić, Y. Tang, M. D. Sikirić, T. Mišić, V. Svetličič, S. Bosnar, T. A. Jelič, Cham. Mater. 24 (2012) 1726–1737.

99. P.-P. E. A. de Moor, T. P. M. Beelen, R. A. van Santen, J. Phys. Chem. B 103 (1999) 1639–1650.

100. T. M. Davis, T. O. Drews, H. Ramanan, C. He, J. Dong, H. Schnablegger, M. A. Katsoulakis, E. Kokkoli, A. V. Mccormick, R. L. Penn, M. Tsapatsis, Nat. Mater. 5 (2006) 400–408.

101. N. D. Hould, R. F. Lobo, Chem. Mater. 20 (2008) 5807–5815.

102. N. Hould, M. Haouas, V. Nikolakis, F. Taulelle, Raul Lobo, Chem. Mater. 24 (2012) 3621–3632.

103. W. Xu, J. Dong, J. Li, W. Li, F. Wu, J. Chem. Soc., Chem. Commun. (1990) 755–756.

104. M. Matsukata, M. Ogura, T. Osaki, P. R. H. P. Rao, M. Nomura, E. Kikuchi, Top. Catal. 9 (1999) 77–92.

105. L. Ren, Q. Wu, C. Yang, L. Zhu, C. Li, P. Zhang, H. Zhang, X. Meng, F.-S. Xiao, J. Am. Chem. Soc. 134 (2012) 15173−15176.

106. D. M. Bibby and M. P. Dale, Nature 317 (1985) 157−158.

107. R. E. Morris, S. J. Weigel, Chem. Soc. Rev. 26 (1997) 309−317.

108. E. R. Cooper, C. D. Andrews, P. S. Wheatley, P. B. Webb, P. Wormald, R. E. Morris, Nature 430 (2004) 1012–1016.

109. E. R. Parnham, R. E. Morris, Acc. Chem. Res. 40 (2007) 1005–1013.

110. R. M. Barrer, P. J. Denny, J. Chem. Soc. (1961) 971–982.

111. G. T. Kerr, G.T. Kokotailo, J. Am. Chem. Soc. 83 (1961) 4675.

112. R. M. Barrer, Zeolites 1 (1981) 130–140.

113. M. A. Camblor, L. A. Villaescusa, M. J. Díaz-Cabanas, Top. Catal. 9 (1999) 59–76.

114. A. Corma, J. Cat. 216 (2003) 298–312.

115. A. Corma, M. E. Davis, ChemPhysChem 5 (2004) 304–313.

116. A. W. Burton, S. I. Zones, S. Elomari, Curr. Opin. Colloid Interface Sci. 10 (2005) 211–219.

117. R. Simancas, D. Dari, N. Velamazán, M. T. Navarro, A. Cantín, J. L. Jordá, G. Sastre, A. Corma, F. Rey, Science 330 (2010) 1219–1222.

118. J. E. Naber, K. P. de Jong, W. H. J. Stork, H. P. C. E. Kuipers, M. F. M. Post, Stud. Surf. Sci. Catal. 84 (1994) 2197–2219.

119. B. Yilmaz, U. Müller, Top. Catal. 52 (2009) 888–895.

120. C. C. Freyhardt, M. Tsapatsis, R. F. Lobo, K. J. Balkus, M. E. Davis, Nature 381 (1996) 295–298.

121. P. Wagner, M. Yoshikawa, M. Lovallo, K. Tsuji, M. Taspatsis, M. E. Davis, Chem. Commun. 22

(1997) 2179–2180.

122. S. L. Burkett, M. E. Davis, J. Phys. Chem. 98 (1994) 4647–4653.
123. S. L. Burkett, M. E. Davis, Chem. Mater. 7 (1995) 920–928.
124. S. L. Burkett, M. E. Davis, Chem. Mater. 7 (1995) 1453–1463.
125. P.-P. E. A. de Moor, T. P. M. Beelen, B. U. Komanschek, L. W. Beck, P. Wagner, M. E. Davis, R. A. van Santen, Chem. Eur. J. 5 (1999) 2083–2088.
126. C. W. Jones, K. Tsuji, T. Takewaki, L. W. Beck, M. E. Davis, Microporous Mesoporous Mater. 48 (2001) 57–64.
127. H. Lee, S. I. Zone, M. E. Davis, Nature 425 (2003) 385–388.
128. A. N. Parikh, A. Navrotsky, Q. Li, C. K. Yee, M. L. Amweg, A. Corma, Microporous Mesoporous Mater. 76 (2004) 17–22.
129. H. Lee, S. I. Zone, M. E. Davis, J. Phys. Chem. B 109 (2005) 2187–2191.
130. H. Lee, S. I. Zone, M. E. Davis, Microporous Mesoporous Mater. 88 (2006) 266–274.
131. M. Rivallan, I. Yordanov, S. Thomas, C. Lancelot, S. Mintova, F. Thibault-Starzyk, ChemCatChem 2 (2010) 1074–1078.
132. M. E. Roz, L. Lakiss, V. Valtchev, S. Mintova, F. Thibault-Starzyk, Microporous Mesoporous Mater. 158 (2012) 148–154.
133. J. Song, L. Dai, Y. Ji, F.-S. Xiao, Chem. Mater. 18 (2006) 2775–2777.
134. Z. Wu, J. Song, Y. Li, L. Ren, F.-S. Xiao, Chem. Mater. 20 (2008) 357–359.
135. S. I. Zones, Microporous Mesoporous Mater. 144 (2011) 1–8.
136. K. Iyoki, K. Itabashi, T. Okubo, Microporous Mesoporous Mater. 189 (2014) 22–30.
137. G. T. Kerr, J. Phys. Chem. 70 (1966) 1047–1050.
138. G. T. Kerr, J. Phys. Chem. 72 (1968) 1385–1386.
139. H. Kacirek, H. Lechert, J. Phys. Chem. 79 (1975) 1589–1593.
140. H. Kacirek, H. Lechert, J. Phys. Chem. 80 (1976) 1291–1296.
141. S. Ueda, M. Koizumi, Am. Mineral. 64 (1979) 172-179.

142. S. Ueda, H. Murata, M. Koizumi, Am. Mineral. 65 (1980) 1012-1019.

143. S. Ueda, T. Fukushima, M. Koizumi, J. Clay Sci. Jpn. 22 (1982) 18-28.

144. S. Kasahara, K. Itabashi, K. Igawa, Stud. Surf. Sci. Catal. 28 (1986) 185 – 192.

145. L.-Y. Hou, R. W. Thompson, Zeolites 9 (1989) 526 – 530

146. R. D. Edelman, D. V. Kudalkar, T. Ong, J. Warzywoda, R. W. Thompson, Zeolites 9 (1989) 496–502.

147. J. Warzywoda, R. D. Edelman, R. W. Thompson, Zeolites 11 (1991) 318–324.

148. J. Warzywoda, R. W. Thompson, Zeolites 11 (1991) 577–582.

149. E. A. Tsokanis, R. W. Thompson, Zeolites 12 (1992) 369–373.

150. P. K. Dutta, J. Bronic, Zeolites 14 (1994) 250–255.

151. L. Gora, R. W. Thompson, Zeolites 15 (1995) 526–534.

152. L. Gora, K. Streletzky, R. W. Thompson, G. D. G. Phillies, Zeolites 18 (1997) 119–131.

153. L. Gora, K. Streletzky, R. W. Thompson, G. D. G. Phillies, Zeolites 19 (1997) 98–106.

154. V. Valtchev, S. Mintova, V. Dimov, A. Toneva, Zeolites 15 (1995) 193–197.

155. Y. Kalvachev, M. Jaber, V. Mavrodinova, L. Dimitrov, D. Nihtianova, V. Valtchev, Microporous Mesoporous Mater. 177 (2013) 127–134.

156. T. A. M. Twomey, M. Mackay, H. P. C. E. Kuipers, R. W. Thompson, Zeolites 14 (1994) 162–168.

157. V. Nikolakis, E. Kokkoli, M. Tirrell, M. Tsapatsis, D. G. Vlachos, Chem. Mater. 12 (2000) 845–853.

158. N. Ren, J. Bronić, T. A. Jelić, A. Palčić, B. Subotić, Cryst. Growth Des. 12 (2012) 1736–1745.

159. D. P. Serrano, R. Grieken, J. Mater. Chem. 11 (2001) 2391–2407.

160. K. Suzuki, T. Hayakawa, Microporous Mesoporous Mater. 77 (2005) 131–137.

161. U. Díaz, V. Fornés, A. Corma, Microporous Mesoporous Mater. 90 (2006) 73–80.

162. M. Tsapatsis, M. C. Lovallo, T. Okubo, M. E. Davis, M. Sadakata, Chem. Mater. 7 (1995) 1734–1741.

163. M. Tsapatsis, T. Okubo, M. C. Lovallo, M. E. Davis, Mater. Res. Soc. Symp. Proc. 371 (1995) 21.

164. M. C. Lovallo, M. Tsapatsis, T. Okubo, Chem. Mater. 8 (1996) 1579–1583.

165. S. Yamazaki, K. Tsutsumi, Microporous Mater. 4 (1995) 205–212.

166. H. Kita, T. Inoue, H. Asamura, K. Tanaka, K. Okamoto, Chem. Commun. (1997) 45–46.
167. K. Kusakabe, T. Kuroda, A. Murata, S. Morooka, Ind. Eng. Chem. Res. 36 (1997) 649–655.
168. G. Xomeritakis, S. Nair, M. Tsapatsis, Microporous Mesoporous Mater. 38 (2000) 61–73.
169. M. P. Bernal, J. Coronas, M. Menéndez, J. Santamaría, Microporous Mesoporous Mater. 60 (2003) 99–110.
170. Y. Hasegawa, T. Ikeda, T. Nagase, Y. Kiyozumi, T. Hanaoka, F. Mizukami, J. Membr. Sci. 280 (2006) 397–405.
171. J. Caro, M. Noack, Microporous Mesoporous Mater. 115 (2008) 215–233.
172. Y. Dong, Y. Peng, G. Wang, Z. Wang, Y. Yan, Ind. Eng. Chem. Res. 51 (2012) 3646−3652.
173. X. Lin, E. Kikuchi, M. Matsukata, Chem. Commun. (2000) 957–958.
174. G. Li, E. Kikuchi, M. Matsukata, Microporous Mesoporous Mater. 62 (2003) 211–220.
175. M. Matsukata, K. Sawamura, T. Shirai, M. Takada, Y. Sekine, E. Kikuchi, J. Membr. Sci. 316 (2008) 18–27.
176. I. Kumakiri, T. Yamaguchi, S. Nakao, Ind. Eng. Chem. Res. 38 (1999) 4682–4688.
177. Z. Lai, G. Bonilla, I. Diaz, J. G. Nery, K. Sujaoti, M. A. Amat, E. Kokkoli, O. Terasaki, R. W. Thompson, M. Tsapatsis, D. G. Vlachos, Science 300 (2003) 456–460.
178. L. Tosheva, V. P. Valtchev, C. R. Chimie 8 (2005) 475–484.
179. L. Tosheva, V. P. Valtchev, Chem. Mater. 17 (2005) 2494–2513.
180. B. Xie, J. Song, L. Ren, Y. Ji, J. Li, F.-S. Xiao, Chem. Mater. 20 (2008) 4533–4553.
181. G. Majano, L. Delmotte, V. Valtchev, S. Mintova, Chem. Mater. 21 (2009) 4184 – 4191.
182. Y. Kamimura, W. Chaikittisilp, K. Itabashi, A. Shimojima, T. Okubo, Chem. Asian J. 5 (2010) 2182 – 2191.
183. B. Xie, H. Zhung, C. Yang, S. Liu, L. Ren, L. Zhang, X. Meng, B. Yilmaz, U. Muller, F.-S. Xiao Chem. Comm. 47 (2011) 3945–3947.
184. Y. Kamimura, S. Tanahashi, K. Itabashi, A. Sugawara, T. Wakihara A. Shimojima, T. Okubo., J. Phys. Chem. C 115 (2011) 744–750.
185. K. Honda, A. Yashiki, M. Itakura, Y. Ide, M. Sadakane, T. Sano Microporous Mesoporous Mater. 142

(2011) 161–167.

186. H. Zhang, L. Chu, Q. Xiao, L. Zhu, C. Yang, X. Meng, F.-S. Xiao, J. Mater. Chem. A 1 (2013) 3254–3257.

187. K. Iyoki, K. Itabashi, T. Okubo, Chem. Asian J. 8 (2013) 1419–1427.

188. T. Yokoi, M. Yoshioka, H. Imai, T. Tatsumi, Angew. Chem. Int. Ed. 48 (2009) 9884–9887.

189. M. Yoshioka, T. Yokoi, M. Liu, H. Imai, S. Inagaki, T. Tatsumi, Microporous Mesoporous Mater. 153 (2012) 70–78.

190. D. Nukaga, Master Thesis, The University of Tokyo (2013).

191. A. Yashiki, K. Honda, A. Fujimoto, S. Shibata, Y. Ide, M. Sadakane, T. Sano, J. Crystal Growth, 325 (2011) 96 – 100.

192. H. Zhang, C. Yang, L. Zhu, X. Meng, B. Yilmaz, U. Muller, M. Feyen, C. Li, F.-S. Xiao, Microporous Mesoporous Mater., 155 (2012) 1 – 7.

193. K. Iyoki, Y. Kamimura, K. Itabashi, A. Shimojima, T. Okubo, Chem. Lett. 39 (2010) 730–731.

194. Y. Kamimura, K. Itabashi, T. Okubo, Microporous Mesoporous Mater. 147 (2012) 149–156.

195. Y. Kamimura, K. Iyoki, S. P. Elangovan, K. Itabashi, A. Shimojima, T. Okubo, Microporous Mesoporous Mater. 163 (2012) 282–290.

196. W. Zhang, Y. Wu, H. Zhau, J. Wang, Mater. Res. Bull. 46 (2011) 1451–1454.

197. Q. Wu, X. Wang, X. Meng, C. Yang, Y. Liu, Y. Jin, Q. Yang, F.-S. Xiao, Microporous Mesoporous Mater. 186 (2014) 106–112.

198. G. Majano, A. Darwiche, S. Mintova, V. Valtchev, Ind. Eng. Chem. Res. 48 (2009) 7084–7091.

199. H. Zhung, Q. Guo, L. Ren, C. Yang, L. Zhu, X. Meng, C. Li, F.-S. Xiao, J. Mater. Chem. 21 (2011) 9494–9497.

200. K. Itabashi, Y. Kamimura, K. Iyoki, A. Shimojima, T. Okubo, J. Am. Chem. Soc. 134 (2012) 11542–11549.

201. W. B. Kamb, W. C. Oke, Am. Mineral. 45 (1960) 79–91.

202. D. E. W. Vaughan, K. G. Strohmaier, Microporous Mesoporous Mater. 28 (1999) 233–239.

203. S. V. Krivovichev, Microporous Mesoporous Mater. 171 (2013) 223–229.

204. V. Y. Shevchenko, S. V. Krivovichev, Struct. Chem. 19 (2008) 571–577.

205. C. P. Hem, E. Makovicky, T. Balić-Žunić, Am. Mineral. 95 (2010) 1429–1438.

206. G. D. Ilyushin, V. A. Blatov, Crystallogr. Rep. 56 (2011) 75–83.

207. D. J. Kim, C.-H. Shin, S. B. Hong, Microporous Mesoporous Mater. 83 (2005) 319–325.

208. A. E. Lapshin, O. V. Magdysyuk, O. Y. Glubeva, E. A. Nikolaeva, Glass Phys. Chem. 37 (2011) 72–77.

209. O. Y. Glubeva, E. A. Nikolaeva, A. E. Lapshin, Glass Phys. Chem. 37 (2011) 426–432.

210. R. M. Barrer, D. E. Mainwaring, J. Chem. Soc. Dalton Trans. 12 (1972) 1254–1259

211. A. A. Belhekar, A. J. Chandwadkar, S. G. Hegde, Zeolites 15 (1995) 535–539

212. B. M. Skofteland, O. H. Ellestad, K. P. Lillerud, Microporous Mesoporous Mater. 43 (2001) 61–71.

213. D. McQueen, B. H. Chiche, F. Fajula, A. Auroux, C. Guimon, F. Fitoussi, P. Schulzy, J. Catal. 161 (1996) 587–596.

214. S. P. Mirajkar, B. S. Rao, M. J. Eapen, V. P. Shiralkar, J. Phys. Chem. B 105 (2001) 4356–4367.

215. J. F. Allain, P. Magnoux, P. Schulz, M. Guisnet, Appl. Catal. A 152 (1997) 221–235.

216. R. Aiello, R. M. Barrer, J. Chem. Soc. A (1970) 1470–1475.

217. A. J. Perrotta, C. Kirby, B. R. Mitchell, E. R. Tucci, J. Catal. 55 (1978) 240–249.

218. A. M. Gossens, E. J. P. Feijen, G. Verhoeven, B. H. Wouters, P. J. Grobet, P. A. Jacobs, J. A. Martens, Microporous Mesoporous Mater. 35 (2000) 555–572.

219. B. D. Witte, J. Patarin, J. L. Guth, T. Cholley, Microporous Mater. 10 (1997) 247–257.

220. H. Xu, P. Dong, L. Kiu, J.-G. Wang, F. Deng, J.-X. Dong, J. Porous Mater. 14 (2007) 97–101.

221. A. Ogawa, K. Iyoki, Y. Kamimura, S. P. Elangovan, K. Itabashi, T. Okubo, Microporous Mesoporous Mater. 186 (2014) 21–28.

222. A. Palčić, J. Bronić, Đ. Brlek, B. Subotić, CrystEngComm 13 (2011) 1215–1220.

223. J. Wang, X. Cheng, J. Guo, X. Xu, Y. Long, Microporous Mesoporous Mater. 96 (2006) 307–313.

224. H. Zhou, J. Gu, Y. Wu, J. Wang, J. Porous Mater. 20 (2013) 523–530.

225. B. H. Wouters, T. Chen, A. M. Goossens, J. A. Martens, P. J. Grobet, J. Phys. Chem. B 104 (1999)

8093–8096.

226. R. B. LaPierre, A. C. Rohrman Jr., J. L. Schlenker, J. D. Wood, M. K. Rubin, W. J. Rohrbaugh, Zeolites 5 (1985) 346–348.

227. B. H. Chiche, R. Dutartre, F. Di Renzo, F. Fajula, A. Katovic, A. Regina and G. Giordano, Cat. Lett. 31 (1995) 359–366.

228. C. W. Jones, S. I. Zones, M. E. Davis, Appl. Catal. A 181 (1999) 289–303.

229. W. Zhang, P. G. Smirniotis, J. Cat. 182 (1999) 400–416.

230. A. Iliyas, M. H. Zahedi-Niaki, M. Eić, S. Kaliaguine, Microporous Mesoporous Mater. 102 (2007) 171–177.

231. Z. Sarshar, M. H. Zahedi-Niaki, Q. Huang, M. Eic, S. Kaliaguine, Appl. Catal. B 87 (2009) 37–45.

232. S. Ernst, P. A. Jacobs, J. A. Martens, J. Weitkamp, Zeolites 7 (1987) 458–462.

233. K. Yoo, R. Kashfi, S. Gopal, P. G. Smirniotis, M. Gangoda, R. N. Bose, Microporous Mesoporous Mater. 60 (2003) 57–68.

234. S. Gopal, K. Yoo, P. G. Smirniotis, Microporous Mesoporous Mater. 49 (2001) 149–156.

235. A. S. Araujo, A. O. S. Silva, M. J. B. Souza, A. C. S. L. S. Coutinho, J. M. F. B. Aquino, J. A. Moura, A. M. G. Pedrosa, Adsorption 11 (2005) 159–165.

236. J. C. Trewella, J. L. Schlenker, D. E. Woessner, J. B. Higgins, Zeolites 5 (1985) 130–131.

237. R. F. Lobo, M. Tsapatsis, C. C. Freyhardt, I. Chan, C.-Y. Chen, S. I. Zones, M. E. Davis, J. Am. Chem. Soc. 119 (1997) 3732–3744.

238. Y. Kubota, T. Honda, J. Plevert, T. Yamashita, T. Okubo, Y. Sugi, Catal. Today 74 (2002) 271–279.

239. F. Raatz, C. Marcilly, E. Freund, Zeolites 5 (1985) 329–333.

240. S. Ritsch, N. Ohnishi, T. Ohsuna, K. Hiraga, O. Terasaki, Y. Kubota, Y. Sugi, Chem. Mater. 10 (1998) 3958–3965.

241. R. M. Barrer, A. F. Denny, J. Chem. Soc. (1964) 4684–4692.

242. S. P. Elangovan, M. Ogura, S. Ernst, M. Hartmann, S. Tontisirin, M. E. Davis, T. Okubo, Microporous Mesoporous Mater. 96 (2006) 210–215.

243. V. R. Choudhary, S. G. Pataskar, Zeolites 6 (1986) 307–311.

244. V. R. Choudhary, K. R. Srinivasan, A. P. Singh, Zeolites 10 (1990) 16–20.

245. V. Valyon, Gy. Onyestyák, L. V. C. Rees, Langmuir 16 (2000) 1331–1336.

246. S. Kouva, J. Kanervo, F. Schüßler, R. Olindo, Chem. Eng. Sci. 89 (2013) 40–48.

247. P. C. van Geem, K. F. M. G. J. Scholle, G. P. M. van der Velden, W. S. Veeman, J. Phys. Chem. 92 (1988) 1585–1589.

248. S. Moreno, G. Poncelet, Microporous Mater. 12 (1997) 197–222.

249. M. Iwamoto, S. Yokoo, K. Sakai, S. Kagawa, J. Chem. Soc., Faraday Trans. 1 77 (1981), 1629–1638.

250. M. Iwamoto, H. Furukawa, Y. Mine, F. Uemura, S. Mikuriya, S. Kagawa, J. Chem. Soc., Chem. Commun. (1986) 1272–1273.

251. D. W. Fickel, R. F. Lobo, J. Phys. Chem. C 114 (2010) 1633–1640.

252. F. Göltl, R. E. Bulo, J. Hafner, P. Sautet, J. Phys. Chem. Lett. 4 (2013) 2244–2249.

253. F. Gao, J. H. Kwak, J. Szanyi, C. H. F. Peden, Top Catal 56 (2013) 1441–1459.

254. M. J. Annen, M. E. Davis, J. B. Higgins, J. L. Schlenker, J. Chem. Soc., Chem. Commun. (1991) 1175–1176.

255. M. Yoshikawa, S. I. Zones, M. E. Davis, Microporous Mater. 11 (1997) 127–136.

256. M. Yoshikawa, S. I. Zones, M. E. Davis, Microporous Mater. 11 (1997) 137–148.

257. M. J. Annen, M. E. Davis, Microporous Mater. 1 (1993) 57–65.

258. M. A. Camblor, M. E. Davis, J. Phys. Chem. 98 (1994) 13151–13156.

259. L. B. McCusker, R. W. Grosse-Kunstleve, C. Baerlocher, M. Yoshikawa, M. E. Davis, Microporous Mater. 6 (1996) 295–309.

260. C. Rohrig, H. Gies, Angew. Chem. Int. Ed. 34 (1995) 63–65.

261. M. A. Camblor, R. F. Lobo, H. Koller, M. E. Davis, Chem. Mater. 6 (1994) 2193–2199.

262. T. Takewaki, L. W. Beck, M. E. Davis, Top. Catal. 9 (1999) 35–42.

263. T. Takewaki, L. W. Beck, M. E. Davis, J. Phys. Chem. B 103 (1999) 2674–2679.

264. D. P. Serrano, R. van Grieken, M. E. Davis, J. A. Melero, A. Garcia, G. Morales, Chem. Eur. J. 22

(2002) 5153–5160.

265. M. Dong, J. Wang, Y. Sun, Microporous Mesoporous Mater. 43 (2001) 237–243.
266. S. Kowalak, E. Szymkowiak, M. Gierczynska, G. Giordano, Stud. Surf. Sci. Catal. 142 (2002) 351–358.
267. S. Kowalak, E. Janiszewska, M. Gierczynska, V. Dolata, N. Z. Evmiridis, T. Katranas, A. Vlessidis, V. Tsiatouras, F. Roessner, E. Schneider, Stud. Surf. Sci. Catal. 154 (2004) 2200–2207.
268. E. Janiszewska, S. Kowalak, M. Gierczynska, V. Dolata, M. Zielinski, M. Wojciechowska, Catal. Lett. 114 (2007) 64–70.
269. L. Wang, S. Sang, S. Meng, Y. Zhang, Y. Qi, Z. Liu, Mater. Lett. 61 (2007) 1675–1678.
270. Y. Ni, A. Sun, X. Wu, G. Hai, J. Hu, T. Li, G. Li, Microporous Mesoporous Mater. 143 (2011) 435–442.
271. C. C. Freyhardt, R. F Lobo, S. Khodabandeh, J. E. Lewis, Jr., M. Tsapatsis, M. Yoshikawa, M. A. Camblor, M. Pan, M. M. Helmkamp, S. I. Zones, M. E. Davis, J. Am. Chem. Soc. 118 (1996) 7299–7310.
272. S. I. Zones, Y. Nakagawa, G. S. Lee, C. Y. Chen, L. T. Yuen, Microporous Mesoporous Mater. 21 (1998) 199–211.
273. S. I. Zones, US005591421A, (1997).
274. H. Lee, S. I Zones, M. E. Davis, Microporous Mesoporous Mater. 88 (2006) 266–274.
275. K. Iyoki, K. Itabashi, S. P. Elangovan, W. Chaikittisilp, T. Wakihara, S. Kohara, Tatsuya Okubo, Chem. Mater. 26 (2014) 1957–1966.
276. K. Honda, A. Yashiki, M. Itakura, Y. Ide, M. Sadakane, T. Sano, Microporous Mesoporous Mater. 142 (2011) 161–167.
277. N. Takahashi, K. Kuroda, J. Mater. Chem. 21 (2011) 14336–14353.
278. J. M. Garcés, S. C. Rocke, C. E. Crowder, D. L. Hansha, Clays Clay Mineral. 36 (1988) 409–418.
279. T. J. Pinnavaia, I. D. Johnson, M. Lipsicas, J. Solid State Chem. 63 (1986) 118–121.
280. G. G. Almond, R. K. Harris, K. R. Franklin, J. Mater. Chem. 7 (1997) 681–687.
281. H. van Koningsveld, Compendium of Zeolite Framework Types: Building Schemes and Type Characteristics, Elsevier, Amsterdam, (2007).

282. Y. Suzuki, T. Wakihara, S. Kohara, K. Itabashi, M. Ogura, T. Okubo, J. Phys. Chem. C 115 (2011) 443–446.

283. T. Wakihara, S. Kohara, G. Sankar, S. Saito, M. Sanchez-Sanchez, A. R. Overweg, W. Fan, M. Ogura, T. Okubo, Phys. Chem. Chem. Phys. 8 (2006) 224–227.

284. W. Fan, M. Ogura, G. Sankar, T. Okubo, Chem. Mater. 19 (2007) 1906–1917.

285. P. P. Knops-Gerrits, D. E. De Vos, E. J. P. Feijen, P. A. Jacobs, Microporous Mater. 8 (1997) 3–17.

286. J. Kärger, D. Freude, Chem. Eng. Technol. 25 (2002) 769–778.

287. F.-S. Xiao, L. Wang, C. Yin, K. Lin, Y. Di, J. Li, R. Xu, D. S. Su, R. Schlögl, T. Yokoi, T. Tatsumi, Angew. Chem. Int. Ed. 45 (2006) 3090–3093.

288. J. Pérez-Ramírez, C. H. Christensen, K. Egeblad, C. H. Christensen, J. C. Groen, Chem. Soc. Rev. 37 (2008) 2530– 2542.

289. L.-H. Chen, X.-Y. Li, J. C. Rooke, Y.-H. Zhang, X.-Y. Yang, Y. Tang, F.-S. Xiao, B.-L. Su, J. Mater. Chem. 22 (2012) 17381–17403.

290. K. Na, M. Choi, R. Ryoo, Microporous Mesoporous Mater. 166 (2013) 3–19.

291. W. Chaikittisilp, Y. Suzuki, R. R. Mukti, T. Suzuki, K. Sugita, K. Itabashi, A. Shimojima, T. Okubo, Angew. Chem. Int. Ed. 52 (2013) 3355–3359.

292. X. D. Wang, W. L. Yang, Y. Tang, Y. J. Wang, S. K. Fu, Z. Gao, Chem. Commun. 2000, 2161–2162.

293. V. Valtchev, S. Mintova, Microporous Mesoporous Mater. 43 (2001) 41–49.

294. S. P. Naik, A. S. T. Chiang, R. W. Thompson, F. C. Huang, Chem. Mater. 15 (2003) 787–792.

295. L. Han, J. Yao, D. Li, J. Ho, X. Zhang, C.-H. (C.) Kong, Z. M. Zong, X. Y. Wei, H. Wang, J. Mater. Chem. 18 (2008) 3337–3341.

296. Z. Wang, Y. Liu, J. Jiang, M. He, P. Wu, J. Mater. Chem. 20 (2010) 10193–10199.

297. S. Cartlidge, H. U. Nissen, R. Wessicken, Zeolites 9 (1989) 346–349.

298. J. C. Groen, T. Bach, U. Ziese, A. M. P. Donk, K. P. Jong, J. A. Moulijn, J. Pérez-Ramírez, J. Am. Chem. Soc. 127 (2005) 10792–10793.

299. Y. Wang, A. Tuel, Microporous Mesoporous Mater. 113 (2008) 286–295.

300. H. Iwamoto, M. Okamoto, J. H. You, JP2009269788A, (2009).

301. Y. Wang, M. Lin, A. Tuel, Microporous Mesoporous Mater. 102 (2007) 80–85.

302. X. Chen, M. Qiao, S. Xie, K. Fan, W. Zhou, H. He, J. Am. Chem. Soc. 129 (2007) 13305–13312.

303. H. Greer, P. S. Wheatley, S. E. Ashbrock, R. E. Morris, W. Zhou, J. Am. Chem. Soc. 131 (2009) 17986–117992.

304. Y. Huang, D. Dong, J. Yao, L. He, J. Ho, C. (C.) Kong, A. J. Hill, H. Wang, Chem. Mater. 22 (2010) 5271–5278.

305. K. J. Chao, S. P. Sheu, L.-H. Lin, M. J. Genet, M. H. Feng, Zeolites 18 (1997) 18–24.

306. M. L. Occelli, H. Eckert, A.Wölker, A. Auroux, Microporous Mesoporous Mater. 30 (1999) 219–232.

307. W. Chaikittisilp, T. Yokoi, T. Okubo, Microporous Mesoporous Mater. 116 (2008) 188–195

308. J. C. Groen, J. C. Jansen, J. A. Moulijin, J. Pérez-Ramírez, J. Phys. Chem. B 108 (2004) 13062–13065.

309. J. C. Groen, L. A. A. Peffer, J. A. Moulijn, J. PérezRamírez, Chem. Eur. J. 11 (2005) 4983–4994.

310. L. Sarkisov, P. A. Monson, Langmuir 17 (2001) 7600–7604.

311. P. I. Ravikovitch, A. V. Neimark, Langmuir 18 (2002) 9830– 9837.

312. J. C. Groen, J. Pérez-Ramírez, Appl. Catal. A 268 (2004) 121–125.

313. M. Thommes, B. Smarsly, M. Groenewolt, P. I. Ravikovitch, A. V. Neimark, Langmuir 22 (2006) 756–764.

List of publications

Publications related to this dissertation

Chapter 1 (Review)

1. **Kenta Iyoki**, Keiji Itabashi, and Tatsuya Okubo, "Progress in seed-assisted synthesis of zeolites without using organic structure-directing agents," *Microporous and Mesoporous Materials*, 189, 22–30, 2014.

Chapter 2

2. Keiji Itabashi, Yoshihiro Kamimura, **Kenta Iyoki**, Atsushi Shimojima, and Tatsuya Okubo, "A Working Hypothesis for Broadening Framework Types of Zeolites in Seed-Assisted Synthesis without Organic Structure-Directing Agent," *Journal of the American Chemical Society*, 134, 11542−11549, 2012.
3. Akari Ogawa, **Kenta Iyoki**, Yoshihiro Kamimura, Shanmugam Palani Elangovan, Keiji Itabashi, and Tatsuya Okubo, "Seed-Directed, Rapid Synthesis of MAZ-Type Zeolites without Using Organic Structure-Directing Agent," *Microporous and Mesoporous Materials*, 186, 21–28, 2014.

Chapter 3

4. **Kenta Iyoki,** Yoshihiro Kamimura, Keiji Itabashi, Atsushi Shimojima, and Tatsuya Okubo, "Synthesis of MTW-type Zeolites in the Absence of Organic Structure-directing Agent," *Chemistry. Letters*, 39, 730–731, 2010.
5. Yoshihiro Kamimura, **Kenta Iyoki,** Shanmugam Palani Elangovan, Keiji Itabashi,

Atsushi Shimojima, and Tatsuya Okubo, "OSDA-free synthesis of MTW-type zeolite from sodium aluminosilicate gels with zeolite beta seeds," *Microporous and Mesoporous Materials*, 163 282–290, 2012.

Chapter 4

6. **Kenta Iyoki**, Keiji Itabashi, Watcharop Chaikittisilp, Shanmugam P. Elangovan, Toru Wakihara, Shinji Kohara, and Tatsuya Okubo, "Broadening the Applicable Scope of Seed-Directed, Organic Structure-Directing Agent-Free Synthesis of Zeolite to Zincosilicate Components: A Case of VET-Type Zincosilicate Zeolites," *Chemistry of Materials*, 26, 1957–1966, 2014.

Chapter 5

7. **Kenta Iyoki**, Keiji Itabashi, and Tatsuya Okubo, "Seed-assisted, One-pot Synthesis of Hollow Zeolite Beta without Using Organic Structure-Directing Agents," *Chemistry An Asian Journal*, 8, 1419–1427, 2013.

Other publications

1. **Kenta Iyoki**, Ayae Sugawara-Narutaki, Atsushi Shimojima, and Tatsuya Okubo, "Hierarchical porous silica via solid-phase hydrolysis/polycondensation of cubic siloxane-based molecular units," *Journal of Materials Chemistry A*, 1, 671–676, 2013.
2. Yuko Wada, **Kenta Iyoki**, Ayae Sugawara-Narutaki, Tatsuya Okubo, and Atsushi Shimojima, "Diol-Linked Microporous Networks of Cubic Siloxane Cages," *Chemistry A European Journal*, 19, 1700–1705, 2013.

3. Takaaki Ikuno, Atsuro Nomura, **Kenta Iyoki**, Ayae Sugawara-Narutaki, Tatsuya Okubo, and Atsushi Shimojima, “Facile Synthesis of Well-dispersed Hollow Mesoporous Silica Nanoparticles Using Iron Oxide Nanoparticles as Template,” *Chemistry Letters*, 42, 316–317, 2013.
4. Takahiko Moteki, Sye Hoe Keoh, Takafumi Ohmura, **Kenta Iyoki**, Toru Wakihara, and Tatsuya Okubo, “Synthesis of pure-silica ZSM-48 zeolite under mild hydrothermal condition with conventional amphiphilic cation by tuning the reactant gel composition,” *Journal of the Ceramic Society of Japan*, 121, 575–577, 2013.
5. **Kenta Iyoki**, Takuji Ikeda, Tatsuya Okubo, and Atsushi Shimojima, “Highly Stable Molecules Derived from Octasilsesquioxane,” *in preparation*.
6. **Kenta Iyoki**, Keiji Itabashi, Toru Wakihara, and Tatsuya Okubo, “Facile, High Yield Synthesis of Zeolite CIT-6 by Combining Mechanochemical Pretreatment and Seed-Directed Crystal Growth,” *in preparation*.
7. Watcharop Chaikittisilp, **Kenta Iyoki**, Toru Wakihara, and Tatsuya Okubo, “Synthesis and Application of CHA-type Zincosilicate Zeolite,” *in preparation*.
8. Masafumi Takase, **Kenta Iyoki**, Keiji Itabashi, and Tatsuya Okubo, “Organic Structure-Directing Agent-free Synthesis of NES-type Zeolite Directed by EU-1 Seed Crystals,” *in preparation*.

Acknowledgment

This research work hardly attained without enormous help from many kind people, therefore, I would like to thank people mentioned here and others concerned my university life. I am sure that I was blessed with people around me.

First of all, I would like to show my greatest appreciation to my supervisor, Professor Tatsuya Okubo for giving me a chance to work in such an exciting field. He always encouraged, supported, helped and leaded me through the six-year laboratory life. I surely remember his words given me when I was wondering the path, *"If you go on to doctoral course, I will let you skiing abroad."* I decided to go on to the doctoral course after this comment to do my hobby abroad. I could do my research with a dream and freedom owing to his deepest tenderness.

My heartfelt appreciation goes to my teacher, Dr. Keiji Itabashi, who discussed me a lot at any time. All synthesis experiments never been achieved without his valuable advices and secret techniques. Moreover, he taught me a mental attitude as a full-fledged researcher.

I would like to offer my special thanks to Associate Professor Atsushi Shimojima for his encouragement, suggestions, and supports, especially during my master course. I am thankful to Associate Professor Toru Wakihara for his constructive advices and suggestions. Also, I am grateful to Assistant professors, Dr. Ayae Sugawara-Narutaki and Dr. Yasuto Hoshikawa for their helps and companionship.

The committee members, Professor Kazunari Domen, Professor Atsuo Yamada,

Associate Professor Ryuji Kikuchi, and Associate Professor Masaru Ogura are acknowledged for their fruitful comments and discussion.

In Chapter 2 and 3, I would like to thank Ms. Akari Ogawa and Dr. Yoshihiro Kamimura, respectively, who did a part of synthesis experiments and characterizations. I was happy to be able to work with them. NH_3-TPD measurements, HEXRD measurements, and TEM observations in the corresponding chapters were performed in Prof. Masaru Ogura's laboratory by Dr. Shanmugam P. Elangovan, at BL04B2 beamline in SPring-8 with help of Dr. Shinji Kohara, and at the Center for Nano Lithography & Analysis, The University of Tokyo, respectively. In addition, particularly, I would like to thank Dr. Elangovan for his helps in English language review and fruitful discussion on many other points.

I would also like to thank my outstanding seniors, Dr. Ayumu Fukuoka, Dr. Watcharop Chaikittisilp, Dr. Junzheng Wang, Dr. Masaru Kubo, Dr. Riichiro Kimura, Dr. Takahiko Moteki, and Dr. Shujun Zhou for their meaningful discussion and assistance. Mr. Hirotaka Ishii, Mr. Hirotatsu Kou, Mr. Naoya Tamura, Mr. Ryo Hanamura, Mr. Maasa Watanabe, Ms. Emiri Kakazu, Mr. Takehiro Kobayashi, Ms. Dieu Huong Pham, and Ms. Sufang Guo are my colleagues who friendly compete with me and are thanked for their friendship. Discussions and working with other laboratory members engaged in related synthesis fields, Mr. Yuki Suzuki, Mr. Motohiro Isobe, Mr. Shinya Tanahashi, Mr. Takafumi Ohmura, Mr. Daiki Nukaga, Ms. Yuko Wada, Mr. Masafumi Takase, Mr. Takayuki Iida, Mr. Kyosuke Sodeyama, and Mr. Koki Muraoka, were interesting and exciting. I am deeply grateful to all of the members of Okubo–Shimojima and Okubo–Wakihara laboratory for their kindness and helps, especially, our secretaries, Ms. Yoko Ohashi, Ms. Ayako Saito, Ms. Yoshie Hayashi, and Ms. Kazuko Yokoyama.

I want to thank Japan Society for the Promotion of Science and Enago for a financial support and the English language review, respectively.

Finally but not least, I would like to express my gratitude to my parents, my brother and my sister for their moral support, constant understanding, and sincere encouragement.

Kenta IYOKI

伊與木 健太